Investigation of Disturbances in Power line Communications

Von der Fakultät für Ingenieurwissenschaften,

Abteilung Informatik und Angewandte Kognitionswissenschaft

der Universität Duisburg-Essen

zur Erlangung des akademischen Grades

Doktor der Ingenieurwissenschaften (Dr.-Ing.)

genehmigte Dissertation

von

Victor Nomm meinota Papilaya

aus Ambon, Indonesia

1. Gutachter: Prof. Dr.-Ing. A. J. Han Vinck

2. Gutachter: Prof. Dr.-Ing. Khmaies Ouahada

Tag der mündlichen Prüfung: 22.05.2014

Abstract

In this thesis we investigate disturbances in Power Line Communications that influence data throughput of an orthogonal frequency-division multiplexing (OFDM) based transmissions. We found that data throughput is degraded not only because of *low layer problems* such as noise or interferences, but also because of *high layer problems* such as data packet size and the usage of a repeater in between a transmitter and a receiver.

The first low layer problem considered in this thesis is Narrow-band Interference (NBI). We proposed an NBI model that is based on statistical properties. We proposed a QPSK-OFDM coded modulation that performs well to combat the NBI. We also designed a new simple block code, called *permutation code plus* (PC^+), to be concatenated with a Reed-Solomon (RS) code. Our proposed concatenated error-control code has a lower decoding complexity than the concatenation between RS and Convolutional Code (CC), used in the G3-PLC technology – one of the current OFDM based PLC technologies, while providing comparable error rate level (or performance), for hard decision decoding, in combating the NBI.

The second low layer problem of interest in this thesis is impulsive noise (IN). We proposed a way to turn a parametric threshold based IN mitigation scheme into a non-parametric one. We proposed a new simple IN mitigation scheme, called replacement scheme, which delivers a better performance than the known clipping scheme. We also showed that our proposed joint clipping-replacement-nulling scheme delivers the best performance among all simple IN mitigation schemes. Furthermore, we introduced a new idea of combining existing simple IN mitigation schemes. This new combined scheme has a property that cannot be found in the traditional joint IN mitigation scheme, such as the clipping-nulling scheme. It guarantees to deliver the best performance of its individual

combined schemes. Beside non-iterative IN mitigation schemes mentioned before, we proposed modifications on the Mengi-Häring iterative IN mitigation scheme that improve significantly the error rate level.

We investigated G3-PLC technology performance based on a field trial test conducted in Hamburg (Germany), and identified the high layer problems mentioned before, that influence its data throughput. We found that in order to have a good data throughput, big size packet transmission must be used instead of small packet size transmission. We also found that the location of a repeater in between a transmitter and a receiver plays an important role. The lack of knowledge to find a good location for a repeater results in data throughput degradation.

Abstrakt

In dieser Doktorarbeit untersuchen wir Störungen, die den Datendurchsatz einer orthogonal frequency-division multiplexing (OFDM)-basierten Powerline-Kommunikation (PLC) beeinflussen. Wir finden, dass die Schwächung des Datendurchsatzes aus zwei Problemen besteht. Das erste ist das untere Schicht Problem, wie z.B. Geräusche oder Interferenzen. Das zweite ist das hohe Schicht Problem, wie z.B. die optimale Länge eines Paketes und die effiziente Benutzung eines Verstärkers zwischen einem Sender und einem Empfänger.

Das erste untere Schicht Problem das wir berücksichtigen, ist die Schmalband-Interferenz (NBI). Wir stellen ein Model der Frequenzbereich-NBI vor, das auf statistische Eigenschaften basiert. Wir schlagen eine QPSK-OFDM-codierte Modulation vor, die zur Behandlung der NBI geeignet ist. Wir entwerfen einen einfachen Blockcode, genannt *permutation code plus* (PC^+), um mit dem Reed-Solomon (RS) Code zu verketten. Diese Verkettung hat eine niedrige Dekodierungskomplexität vergliechen mit der Verkettung zwischen RS-Code und Convolutional Code (CC). Die Fehlerrate von der Verkettung zwischen RS-Code und CC, mit *hard decision decoding*, ist vergleichbar mit der Fehlerrate von der Verkettung zwischen RS-Code und PC^+.

Das zweite untere Schicht Problem das wir berücksichtigen, ist *Impulsive Noise* (IN). Der Schwerpunkt der Untersuchung der IN liegt auf der Entwicklung von Lösungen, die die IN abschwächen. Wir schlagen nicht-schrittweise und schrittweise Lösungen vor. Die nicht-schrittweise Lösung enthält zwei Varianten: die erste ist ein neues einfaches Schema, genannt Replacement (R) Schema. Sein Verhalten ist besser als das Verhalten des bekannten *Clipping* (C) Schema. Die zweite Variante ist die Änderung des Mengi-Häring-Iterationsschemas, sodass unsere Modifikationsideen eine bessere Leistung als die ursprüngliche Idee bringen. Weiterhin stellen wir eine neue Art der Kombination von

vorhandenen einfachen IN Minderungssystemen vor. Diese Kombination garantiert, dass ihre Ausgabe die beste Ausgabe ist, die man aus den einzelnen IN Minderungssystemen bekommen kann. Diese Garantie wird nicht durch eine traditionelle gemeinsame Regelung, wie z.B. das *Clipping-Nulling* (CN) Schema, zur Verfügung gestellt.

Wir untersuchen die Faktoren, die die Technologie der G3-PLC beeinflussen. Die Untersuchung basiert auf realen Messungen, die in Hamburg (Deutschland) durchgeführt wurden. Wir analysieren die Beziehung zwischen dem erreichten Datendurchsatz und den Parametern, die in den Messverfahren benutzt und abgemessen wurden. Wir finden, dass die Übertragung des grossformatigen Paketes einen besseren Datendurchsatz hat, als der der kleinformatigen Paketübertragung. Wir haben festgestellt, dass der Ort eines Verstärkers zwischen einem Sender und einem Empfänger, eine wichtige Rolle spielt. Der Mangel an Wissen, um den richtigen Ort eines Verstärkers zu finden, verursacht die Verschlechterung des Datendurchsatzes.

List of publications

1. V. N. Papilaya and A. J. H. Vinck, *Improving performance of the MH-iterative IN Mitigation Scheme in PLC Systems*, IEEE Trans. on Power Delivery, **submitted revised version**. [Related work in Chapter 6]

2. V. N. Papilaya, T. Shongwe, A. J. H. Vinck, and H. Ferreira, *Selected sub-carriers QPSK-OFDM transmission schemes to combat frequency disturbances*, in 16th IEEE International Symposium on Power Line Communications and Its Applications (ISPLC), Beijing, China, Mar. 27–30, 2012, pp. 200–205. This paper received the **BEST STUDENT PAPER AWARD**. [Related work in Chapter 2]

3. T. Shongwe, V. N. Papilaya, and A. Vinck, *Narrow-band interference model for OFDM systems for power line communications*, in 17th IEEE International Symposium on Power Line Communications and Its Applications (ISPLC), Johannesburg, South Africa, Mar. 24–27, 2013, pp. 268–272. [Related work in Chapter 3]

4. V. N. Papilaya and A. J. H. Vinck, *Investigation on a new combined impulsive noise mitigation scheme for OFDM transmission*, in 17th IEEE International Symposium on Power Line Communications and Its Applications (ISPLC), Johannesburg, South Africa, Mar. 24–27, 2013, pp. 86–91. [Related work in Chapter 4]

5. V. N. Papilaya, A. J. H. Vinck, K. Ouahada, A. Mengi, M. Weinand, M. Koch, *Analysis of the devolo's 500 kHz G3-PLC Access Technology based on Smart Grid Field Trials*, in 18th IEEE International Symposium on Power Line Communications and Its Applications (ISPLC), Glasgow, United Kingdom, Mar. 30 – Apr. 2, 2014, **accepted**. [Related work in Chapter 7]

Acknowledgements

My most sincere thanks go to ...

- my God and my Saviour, Jesus Christ. Thank You for giving me life and many hands to help me during my PhD study.
- my *Doktorvater*, Prof. Dr.-Ing. A. J. Han Vinck. Thank you for being not only an excellent teacher but also an excellent friend and father. Thank you for giving me chance to learn from you. I am really blessed to know you.
- Prof. Dr.-Ing. Khmaies Ouahada for reviewing this dissertation and providing valuable comments.
- Thokozani Shongwe. You are my "Digital communication" brother. Thank you for a great cooperation in completing the second and the third chapters of this thesis.
- Danica Behrends. Thank you for helping me with administrative processes and German translation of my abstract.
- Digital communication group friends: Dr.-Ing. Tarik Akbudak, Dr.-Ing. Yanling Chen, Dr.-Ing. Anil Mengi, George Hallak, Babak Nikfar, Tobi Sanya, Anna Asmangulyan, Aram Jivanyan, Hovik Khasikyan, Yong Seok and Chao Qi. Thank you for everything I had with you.
- Dr. Theo G. Swart for his latex template.
- IFGF church and PPI Duisburg-Essen families for your support.
- my wife and son, my family in Indonesia and in the Netherlands. Thank you for your endless love, endless support and for always being there when I need you.

Table of Contents

List of Figures

List of Tables

1 Introduction

Power Line Communication (PLC) is a process of sending and receiving data using transmission power lines as a communication channel. PLC is interesting because power-line network, which already exists and is a large network, is used not only for power delivery but also for data transmission. However, the power-line channel is regarded as a hostile channel for data communication, since it is considered as a frequency-selective and a time-varying channel. It also suffers from impulsive noise, non-stationary background coloured noise, narrow-band interference and attenuation. Therefore, researches, including our work, which aim to find effective solutions to the existing communication problems in the PLC, have been conducted until now.

This thesis reports our investigation on the disturbances in the power line communication channel and the proposed solutions to improve the quality of transmission (QoT). The investigation is focused on the orthogonal frequency-division multiplexing (OFDM) based transmission, which also of interest in the current PLC technology such as e.g. G3-PLC and PRIME.

The investigation includes:

1. modelling and handling narrow-band interference (NBI),
2. impulsive noise (IN) mitigation, and
3. investigation of factors that influence G3-PLC technology – one of the current OFDM based PLC technologies – performance. This last investigation is a result of the cooperation between Duisburg-Essen University and Devolo AG – the current leading European company on the market in PLC solutions – in a project sponsored

by the German federal ministry of education and research (BMBF).

1.1 Problem statement

Fig. 1.1 shows a simplified general view of an OFDM based transmission. In this transmission, frequency-domain information S is transformed into its time-domain representation, with the help of the Inverse Discrete Fourier Transform (IDFT), before it is transmitted. At the receiver side, the Discrete Fourier Transform (DFT) transforms back the received data R, which contains not only transmitted information S but also noises N (or interferences), into its frequency-domain representation. From this description, there are two investigated problems, called *low layer problem*, as follows:

1. how to describe or to model the behaviour of the noises N, and
2. how to retrieve the transmitted information S from the noisy received data R.

Our first investigation described in Section 1.1.1 considers these two problems. In our second investigation, as explained in Section 1.1.2, we investigated only the second problem – how to get back the transmitted information S from the noisy received data R – when impulsive noise appears during the transmission of S. Section 1.1.3 describes our investigation on factors that influence data throughput of G3-PLC technology. This investigation is based on the measurement data which is collected and provided by Devolo AG in a field test in Hamburg (Germany).

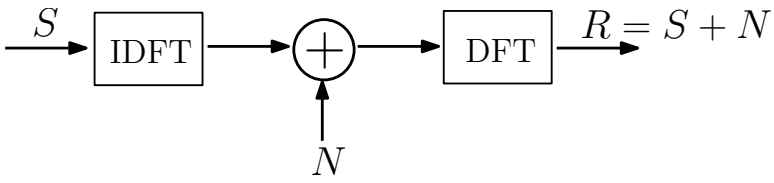

Figure 1.1: A simplified general view of an OFDM based transmission.

1.1.1 Narrow-band Interference (NBI)

The first investigated problem in OFDM based transmission system is Narrow-band interference (NBI). This interference occurs when frequency spectrum component from other

sources appear on the frequency spectrum of the system. To illustrate NBI, let us consider Fig. 1.2, where we assume that an OFDM system contains only two sub-carriers, SC_m and SC_{m+1}, whose center frequencies are f_m and f_{m+1}. An interferer $x(n)$, of certain bandwidth whose spectrum is denoted by $|X(f)|^2$, takes place and its spectrum's power $|X(f_m)|^2$ interferes our system's frequency f_m. In this situation, information contained in the frequency spectrum f_m might be corrupted.

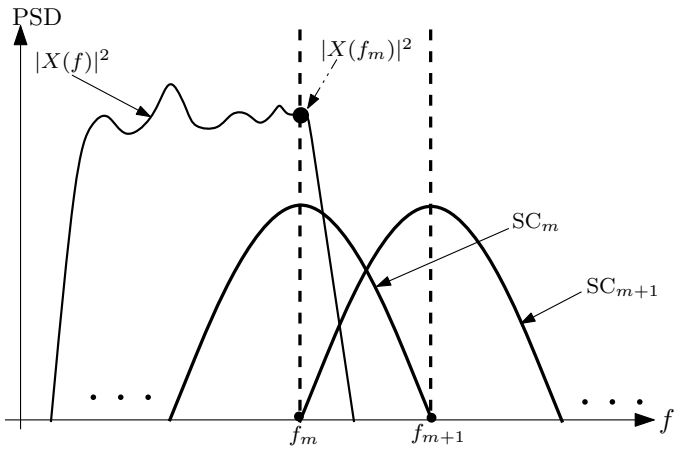

Figure 1.2: An NBI ilustration.

We found that in the literature the NBI still lacks a well defined model which is based on its statistical properties. Therefore, the first investigation, we do related to NBI, is to model it based on these properties. The next investigation is on how to combat NBI. Thus we looked at an error-control coding based solution and a coded modulation solution.

For the error-control coding based solution, we asked ourselves whether it is necessary to have a concatenation between Reed-Solomon (RS) code and binary Convolutional Code (CC), as used in the G3-PLC technology, which is known of having a high decoding complexity. What happens when we replace the CC with a simple block code in order to reduce decoding complexity?

For the coded modulation solution, the question we answer is: can we make use of the idea behind the OFDM-MFSK, as presented in [1], in order to form a coded modulation for QPSK-OFDM based transmission and how does the performance of this coded modulation scheme look like when it is used to combat NBI?

1.1.2 Impulsive noise (IN)

The second investigated problem in this thesis is impulsive noise (IN). The occurrence of IN can produce degradation in the performance of an OFDM system. This is due to the fact that OFDM system spreads IN energy among its sub-carriers as depicted in Fig. 1.3) and which might corrupt the transmitted bits. Therefore, an IN mitigation scheme for OFDM based transmission is needed.

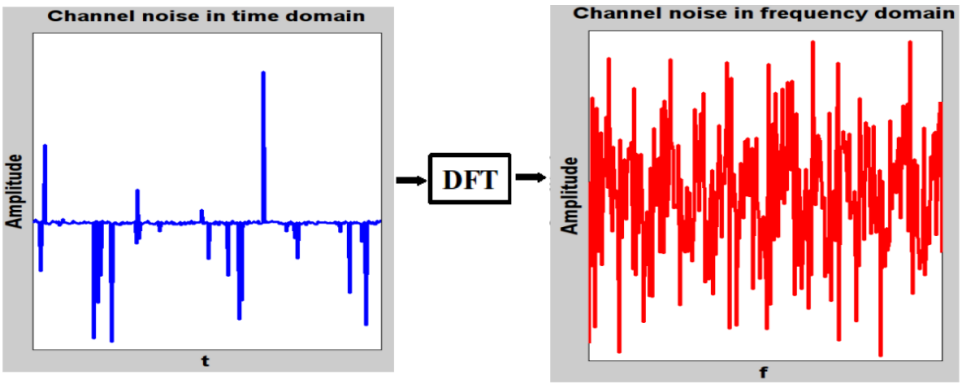

Figure 1.3: Impulsive noise spreading after DFT.

The problems we work on in this topic are:

1. how to further improve the performance of uncoded OFDM based transmissions in an IN channel with the help of threshold based IN mitigation schemes?
2. can we find a practical threshold setting which does not require the knowledge of IN parameters? And
3. can we combine the existing simple IN mitigation schemes to form a combined scheme and expect that the combined scheme can deliver the best performance of its individual combined schemes?

1.1.3 Influencing factors on G3-PLC technology

The last investigation reported in this thesis is on the analysis of the factors that influence the performance of the G3-PLC technology. Devolo AG provided us with information on how they did the measurement, what kind of software they used and the measurement

results themselves which were collected in Hamburg-Germany. The measurement results contain the following information: the achieved data throughput and the internal parameters such as line quality, route cost, number of sub-carriers used for the OFDM and type of modulation used.

Having that provided information, we answer the following question: can the achieved throughput be explained with the help of other given information?

1.2 Outline of the thesis

In this section we give an outline for the rest of the thesis.

Each of the next chapters is an independent chapter. It means that all information needed to understand a chapter is provided within the chapter itself.

Chapter 2 contains our contributions related to the narrow-band interference (NBI). We explained a simple frequency-domain NBI model and provided two solutions to combat NBI. The first solution is a QPSK-OFDM coded modulation, which is a modification of the OFDM-MFSK idea presented in [1]. The second solution is an error-control coding based solution. We concatenate a Reed-Solomon (RS) code and a new simple block code. The new simple block code is called *permutation code plus* (PC^+); it is an extension of a permutation code (PC) by allowing a symbol to appear more than once in a code word. We compared our proposed concatenated codes with the concatenation between RS and a Convolutional Code (CC) which is used in current PLC technology such G3-PLC. The result we found was quite interesting: the concatenation between the RS and the simple block codes brings a comparable performance to the performance of the concatenation between RS code and CC when a hard decision decoding is used. We would like to acknowledge that this chapter is a result of the cooperation between Duisburg-Essen (DUE) University in Germany and University of Johannesburg (UJ) in South Africa which was represented by Thokozani Shongwe. We are so honored that the paper resulting in this chapter was the best paper [2] in the 16^{th} IEEE International Symposium on Power Line Communications and Its Applications (ISPLC) in 2012 held in Beijing-China.

Chapter 3 is the second result of the cooperation between DUE University and UJ University. In this chapter, which has been published in the 17^{th} ISPLC in 2013 held in

Johannesburg, South Africa [3], we extended our simple NBI model in [2]. The extension includes modelling of the probability of a certain number k of interferers on an OFDM system's spectrum and explaining the power contribution of an interferer on a sub-carrier. Furthermore, we discussed two scenarios of setting the amplitude of an interferer: a fixed amplitude and a Gaussian random variable amplitude. We also demonstrated the application of our NBI model.

Chapters 4, 5 and 6 contain our contributions on handling degradation in performance of OFDM based transmission caused by the presence of IN.

There are two known simple impulsive noise (IN) mitigation schemes with only one threshold, the clipping (C) scheme [4] and the nulling (N) scheme [5], [6], before our publication in [7]. Having these schemes, the combined clipping-nulling (CN) scheme can be formed [8]. In Chapter 4, which has also been published in the 17^{th} ISPLC [7], we introduced a new simple IN mitigation scheme, with only one threshold, called replacement (R) scheme. The idea of the R scheme is to replace the magnitude of a received sample which is corrupted by the IN with the average magnitude of the OFDM noiseless samples. We found that the performance of the R scheme is better than that of the C scheme. Furthermore, we found a good location for the replacement threshold T_{rep}, when we form the combined clipping-replacement-nulling (CRN) scheme; it is in between the clipping threshold T_{clip} and the nulling threshold T_{null}. The simulation results show that the performance of CRN scheme is better than the one for the CN scheme.

We discuss also in this chapter an idea to turn a parametric threshold based IN mitigation scheme into a non-parametric threshold based IN mitigation scheme as follows. In a parametric threshold based IN mitigation scheme, the knowledge of IN parameters is required in order to determine the value of the threshold used, whereas in a non-parametric threshold based IN mitigation scheme it is not required. We proposed the usage of the complementary cumulative distribution function (CCDF) of a Rayleigh distribution of the OFDM noiseless samples magnitudes in order to determine the values of the thresholds used. In this way, we can obtain non-parametric threshold based IN mitigation schemes from parametric threshold based IN mitigation schemes.

The idea of combining some threshold based IN mitigations schemes such as the CN or the CRN scheme is a good idea. Simulation results show that when the threshold values used by a combined IN mitigation scheme match the channel parameters – they are well optimized, then the combined scheme will deliver a better performance than that

of its individual combined schemes. However, when the threshold values are not well optimized, then there is a case in which its individual combined schemes deliver a better performance. In Chapter 5, we proposed a new way of combining IN mitigation schemes such that the resulting combined scheme can always deliver the best performance that can be provided by its individual schemes.

The last contributions related to the IN is in Chapter 6, where we improved the performance of the known Mengi-Häring (MH) iterative scheme by proposing two modifications. The first modification is to use the replacement-nulling (RN) scheme instead of the CN scheme as the pre-processing IN mitigation scheme. The second modification is the usage of the output of the pre-processing IN mitigation scheme in all iterations instead of only in the zeroth iteration.

The investigation on the factors that influenced the achieved throughput of the G3-PLC technology based on real measurements is discussed in Chapter 7. We looked at the performance difference between a near and far distance transmission. We also looked at factors that can produce a good data throughput. The important result we found and discussed is that the usage of a repeater in between a transmitter and a receiver provides a reliable transmission with a trade-off on the data throughput degradation. We also found that the throughput of a large packet size transmission is better than that of a small packet size transmission.

Chapter 8 is the last chapter of this thesis. It contains the summary of our researches reported in this thesis and possible future work.

2 QPSK-OFDM based Transmission Schemes to Combat Frequency Disturbances

To combat the impairments caused by frequency disturbances in the power line communications (PLC) channel, a modified conventional QPSK-OFDM transmission scheme is presented. The idea of this scheme is to first group the N sub-carriers of OFDM into groups of M sub-carriers, where $M < N$, and then transmit data by selecting a subset of the sub-carriers in the group. Real and imaginary parts of QPSK symbols are independently assigned to the selected sub-carriers in a group, such that the minimum squared Euclidean distance is maximized. With this kind of symbol assignment to sub-carriers our scheme has no net loss in terms of SNR requirements, in AWGN, in comparison to the conventional QPSK-OFDM, even though it has half the data rate of the conventional QPSK-OFDM. We refer to the conventional QPSK-OFDM as Scheme A. Our scheme displays a superior performance over Scheme A and OFDM-MFSK-like scheme (Scheme B), where in a group of M sub-carriers a QPSK symbol is sent, in the presence of frequency disturbances and also frequency selective fading noise. We further modify Scheme B and come up with additional two new QPSK-OFDM schemes that have better performance than Scheme B in AWGN and impulsive noise. To encode, we apply a (n, k) RS code and a simple permutation code with minimum Hamming distance of two on the conventional QPSK-OFDM scheme, which significantly improves the decoder's performance in the presence of frequency disturbances. A simple narrow band noise model is developed and presented.

2.1 Introduction

Researchers have recently been paying more attention to OFDM modulation scheme as the future choice for PLC data transmission scheme (see [9], [10] and [11]), and several techniques to combat PLC noise when using OFDM transmission have been proposed. Most of the literature on combating PLC noise, when using OFDM transmission focuses on impulsive noise [10]–[13]. Hence there is not much references on combating frequency disturbances in PLC using OFDM.

In [1], Wetz *et al.* presented an OFDM-MFSK scheme employing noncoherent detection, where they showed that it can provide robust transmission over fast fading channels. The OFDM-MFSK scheme in [1] introduces the grouping of IDFT sub-carriers in which the IDFT sub-carriers are grouped into N/M groups, where N is the IDFT size and M is the number of sub-carriers in a group. On every transmission, a sub-carrier from each group is selected by putting a non-zero value on the selected sub-carrier and setting each of the other $M-1$ unselected sub-carriers to zero. Specifically, the non-zero value assigned to the selected sub-carrier in the group is a 1.

The OFDM-MFSK scheme in [1] has been shown to perform well in fast fading channels, but conventional QPSK-OFDM has not been shown to exhibit such good performance in fast fading channels without the help of error control coding (ECC). However, conventional QPSK-OFDM scheme performs well in the presence of AWGN and impulsive noise as the IDFT size gets larger [14].

The first contribution in this chapter is therefore to present an OFDM transmission scheme that combines the strengths of both OFDM-MFSK and QPSK-OFDM schemes. Our proposed scheme is capable of effectively reducing the error floor of the bit error rate curve in the presence of frequency disturbances and frequency selective fading noise, without ECC. Dealing with impulsive noise, our scheme relies on the power of QPSK-OFDM with large N. The second contribution is to extend an OFDM-MFSK-like scheme into two new QPSK-OFDM schemes with better performance than the original OFDM-MFSK-like scheme in AWGN. The OFDM-MFSK-like scheme only differs from the original OFDM-MFSK scheme in [1] by that the non-zero value assigned to the selected sub-carrier is a QPSK symbol instead of just a 1. Thirdly, we present a simple channel model for narrow band noise. Another interesting interference model which our model has some similarities with can be found in [15]. Fourthly, a (n, k) Reed-Solomon (RS) code and a

simple permutation code are employed on the conventional QPSK-OFDM, and the coded system is able to effectively combat frequency disturbances.

The rest of the chapter is organized as follows: Section 2.2, gives a brief background on the OFDM system and M-ary phase shift keying (MPSK), with our discussion limited to BPSK and QPSK. Three main QPSK-OFDM schemes, Scheme A, B and C are discussed in Section 2.3, and a detailed description of our proposed scheme (Scheme C). Also in Section 2.3.4, Scheme B is extended into two new schemes. Coding is discussed in Section 2.3.5. The different types of noise affecting transmission are discussed in Section 2.4, with emphasis on our proposed narrow band noise model in Section 2.4.2. Results are presented in Section 2.5, and finally, concluding remarks in Section 2.6.

2.2 Background information

2.2.1 OFDM system model

OFDM is a multi-carrier transmission scheme, where data is carried in several sub-carriers which are orthogonal to each other to avoid mutual interference. In OFDM system, IDFT (inverse discrete Fourier transform) takes in as input, D data symbols carried in vector X_k, from a phase-shift-keying (PSK) modulation scheme and produces a discrete sequence in the time domain, x_n. The relationship between X_k and x_n is defined as follows:

$$x_n = \frac{1}{\sqrt{N}} \sum_{k=0}^{N-1} X_k e^{j2\pi nk/N}, \tag{2.1}$$

where N is the number of sub-carriers used to carry data, and X_k, is of the same length as x_n. x_n is the complex baseband transmit signal from the output of the IDFT normalized by the factor $\frac{1}{\sqrt{N}}$.

2.2.2 M-ary Phase shift keying system

To describe our contribution, we first give a brief performance comparison between coherent Binary and Quadriphase Shift Keying (BPSK and QPSK) systems for single carrier

modulation. We denote the transmitted signal energy per symbol by E_b and E for the BPSK and QPSK systems, respectively, where E_b is the bit energy. For a BPSK system, symbol and bit energy are the same, while for a QPSK system $E = 2E_b$, which implies that QPSK is 3 dB better due to bit rate. However, BPSK has a minimum Euclidean distance, d_E of $2\sqrt{E_b}$, while QPSK has $d_E = \sqrt{2E}$ (refer to [16]). Therefore, BPSK is 3 dB better than QPSK, where Euclidean distance is concerned. In effect, BPSK and QPSK have similar performances.

2.3 QPSK-OFDM schemes

We give a description of three possible transmission schemes for QPSK-OFDM and compare their performances in the presence of AWGN. To compare these schemes we need to define the following parameters for each scheme: number of bits per sub-carrier, R_b and the minimum Euclidean distance between symbols, d_E or minimum squared Euclidean distance, $d_E^2 = (d_E)^2$.

2.3.1 Scheme A

We refer to the conventional QPSK-OFDM transmission as Scheme A. We shall use this scheme as a reference scheme for the comparison of other schemes because it is the commonly employed OFDM scheme. In the conventional QPSK-OFDM transmission all sub-carriers carrying data are occupied by QPSK symbols chosen according to the transmit data bits. For the QPSK transmission, $R_b = 2$ bits and $d_E = \sqrt{2}$, hence $d_E^2 = 2$.

2.3.2 Scheme B

Scheme B, OFDM-MFSK-like scheme, is similar to OFDM-MFSK transmission scheme introduced in [1]. OFDM-MFSK scheme itself is a modification of the conventional QPSK-OFDM scheme, where it is proposed in [1] that elements of vector X_k are divided into groups of M. In each group, only one element is set to a 1 according to the transmit data, while each of the rest of the group elements are set to a 0. The effect is that only N/M sub-carriers are occupied for each X_k.

To make the comparison with Scheme A straight forward, we adapted the OFDM-4FSK from [1] and employed it as QPSK-OFDM with the properties of the OFDM-4FSK scheme (OFDM-4FSK-like scheme). In this case we still divide OFDM vector X_k into groups of $M = 4$ and only choose one sub-carrier, per group of four, but transmit a QPSK symbol while setting all the other three remaining sub-carriers to zero. The QPSK symbol in the chosen sub-carrier carriers two bits of data and the choice of the sub-carrier to be used among the four conveys two bits of data, and the net data transmitted per group is four bits. For this scheme then, $R_b = 4/4 = 1$ because there are four bits of data in a group of four sub-carriers, and $d_E = \sqrt{2}$ since we are using QPSK, and hence $d_E^2 = 2$.

2.3.3 Scheme C

To describe how the symbols are transmitted, firstly we consider an MPSK-OFDM system with N sub-carriers. In our system the sub-carriers are divided into N/M groups of M as mentioned earlier. M is chosen such that it matches the modulation used in the OFDM system, for example, in QPSK-OFDM, $M = 4$ and in 8PSK-OFDM, $M = 8$. We limited our system to QPSK-OFDM, hence each group has four sub-carriers. The process of assigning symbols in the group of sub-carriers is the same for each group; it is therefore sufficient to give a description of our system for a single group of sub-carriers.

The symbols in a group are assigned as follow: given a QPSK symbol, S to transmit in a group, we use two data bits to assign the real part of S in one of four sub-carriers and another two bits of data to assign the imaginary part of S in one of the four sub-carriers. It should be noted that real and imaginary components of S are assigned to sub-carriers independently, hence it is possible to have them occupying the same sub-carrier, in such a case they are added together forming a QPSK symbol. The remaining sub-carriers in the group carry the components of a QPSK symbol, S' which gives the maximum Euclidean distance between itself and S. This means that for each component of S assigned a sub-carrier, there remains three sub-carriers that are to be filled with the other value in the same dimension with that component (component of S'). For example, filling one sub-carrier with the component of S being j, the three remaining sub-carriers are filled with a $-j$ (imaginary component of S'). If the component of S being used is a 1 then the remaining three sub-carriers will be filled with a -1 (real component of S'). This structured assignment of components to sub-carriers results in the Euclidean distance between the real parts of S and S', and imaginary parts of S and S' being maximized. If

we define QPSK symbols in complex notation as $S = x + yj$ and $S' = -x - yj$, where $x, y \in \{1, -1\}$, the condition for maximum separation between S and S' can simply be stated as follows:
$|\Re(S) - \Re(S')| = |\Im(S) - \Im(S')| = 2$, with $\Re(.)$ and $\Im(.)$ producing the real and imaginary values, respectively.

The following example illustrates the selection of symbols S and S', and how they are assigned sub-carriers.

Example 2.1 Since there are four sub-carriers in a group, for each of the real and imaginary component of S, two data bits are used to select the sub-carrier to carry the components. To illustrate this, let us first define the mapping between data bits and the four sub-carriers in a group, $C_1 \ldots C_4$ are) as follows: $00 \rightarrow C_1$, $01 \rightarrow C_2$, $11 \rightarrow C_3$, $10 \rightarrow C_4$, where the data bits indicate which sub-carrier to carry either the real or imaginary component of S. Assume a portion of the data stream to be modulated is $d = \{01010100 \ldots\}$ and that $S = 1 + j$. The first two bits of d, 01, will assign $\Re(S) = 1$ to C_2 and the next two bits, 01, will assign $\Im(S) = j$ to C_2. This means that both components are in the same sub-carrier, so they appear as $1 + j$ in that sub-carrier. The remaining sub-carriers will be assigned -1 and $-j$ because for our choice of $S = 1 + j$ we have $S' = -1 - j$. If we let $X_k^g \subseteq X_k$ be the vector carrying the QPSK symbols for group g, where $1 \leq g \leq N/M$, then $X_k^1 = \{-1 - j, 1 + j, -1 - j, -1 - j\}$. This scenario is depicted in Fig. 2.1 representing a single group of four OFDM sub-carriers, $C_1 \ldots C_4$, assigned QPSK symbols.

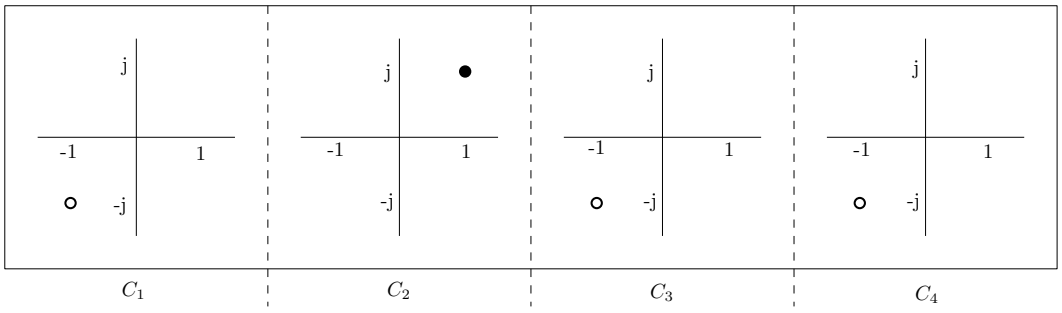

Figure 2.1: QPSK symbols' constellations shown in OFDM sub-carriers $C_1 \ldots C_4$.

For the next group, $g = 2$, data bits five to eight show a slightly different scenario, where bits 01 and 00 will assign $\Re(S) = 1$ to C_2 and $\Im(S) = j$ to C_1, respectively. Since $\Re(S) = 1$ is assigned to C_2, then $\Re(S') = -1$ will be assigned to C_1, C_3 and C_4, while $\Im(S') = -j$ will be assigned to C_2, C_3 and C_4, and $X_k^2 = \{-1 + j, 1 - j, -1 - j, -1 - j\}$.

With this mechanism, our scheme can be seen as a code with $d_{\min} = 2$, which allows for soft decision implementation at the receiver, based on the minimum squared Euclidean distance. Taking each vector X_k^1 and X_k^2, from Example 2.1, as a codeword, we can calculate the minimum squared Euclidean distance as follows. Firstly, the elements of each vector have to be normalized to a magnitude of one, which implies dividing the vectors by $\sqrt{2}$ element-wise, $X_k^1/\sqrt{2}$ and $X_k^2/\sqrt{2}$. The two positions where $X_k^1/\sqrt{2}$ and $X_k^2/\sqrt{2}$ differ, each contributes a Euclidean distance of $\sqrt{2}$ and the overall minimum squared Euclidean distance is $d_E^2 = (\sqrt{2})^2 + (\sqrt{2})^2 = 4$. $R_b = 1$ because there are four bits transmitted per group.

2.3.4 Possible variations of Scheme B

Having presented three schemes, A, B and C, we further propose two more variations of Scheme B. As was shown earlier, in Scheme B, $d_E = \sqrt{2}$ and $R_b = 1$. We propose two cases of transmission: (a) in a group of four sub-carriers, we allow two to carry QPSK symbols and set the remaining two to zero, and (b) in a group of four sub-carriers, we allow three to carry QPSK symbols and set the remaining sub-carrier to zero. We shall refer to schemes in (a) and (b) as Scheme B1 and Scheme B2, respectively. For both Scheme B1 and B2, $d_E = \sqrt{2}$, which is the same as for Schemes A and B.

Scheme B1: For this scheme, the number of transmitted data bits per group is $R_g = \log_2(L) + b$, where $L = \binom{4}{2}$ because out of four sub-carriers we choose two to carry QPSK symbols, and $b = 4$ bits because each of the two QPSK symbols transmits two data bits. $R_g = \log_2(6) + 4 = 6.6$ bits, which results into six bits for the purposes of implementation, and hence $R_b = R_g/4 = 1.5$ bits.

Scheme B2: For this scheme, the number of transmitted data bits per group is $R_g = \log_2(L)+b$, where $L = \binom{4}{3}$ because out of four sub-carriers we choose three to carry QPSK symbols, and $b = 6$ bits because each of the three QPSK symbols transmits two data bits. $R_g = \log_2(4) + 6 = 8$ bits, and $R_b = R_g/4 = 2$ bits.

Table 2.1 gives a summary of the theoretical comparison, in terms of SNR requirements, of all the schemes in the presence of AWGN.

Table 2.1: Comparison between Schemes A, B, B1, B2 and C in terms of SNR requirements in an AWGN channel

	d_E^2	R_b	E_b/N_O at $P_b = 10^{-5}$
Scheme A	2	2	≈ 9.6 dB
Scheme B	2	1	≈ 12.6 dB
Scheme B1	2	1.5	≈ 10.8 dB
Scheme B2	2	2	≈ 9.6 dB
Scheme C	4	1	≈ 9.6 dB

2.3.5 Coding for narrow band noise Scheme A

We use Scheme A to show the effect of coding in the QPSK-OFDM transmission in the presence of frequency disturbances. As done in one of the PLC standards, PLC G3 (see [11]), we employ concatenated coding of a shortened $(n,\ k)$ RS code and a simple permutation code (instead of a convolutional code). The $(n,\ k)$ RS code has symbols of $m = 8$ bits, and the permutation code is of length $M = 4$ and minimum Hamming distance ($d_{\min}$) of two or three. The performance results and discussion of the results of this coding are presented in Section 2.5, for the case where the receiver has information about the position of the frequency disturbers and the case where the receiver has no information, informed and uninformed receiver, respectively.

Frame error rate (FER) is used to compare the performance of coding on QPSK-OFDM. When only the $(n,\ k)$ RS code is used, the FER due to frequency disturbances can be approximated by the first term in $\sum_{i=t+1}^{n} \binom{n}{i} P^i (1-P)^{n-i}$, where $t = (n-k)/2$ is the maximum number of correctable symbol errors for the RS code and P is the probability of the presence of frequency disturbers in the OFDM system. When a concatenation of the $(n,\ k)$ RS code and the permutation code is employed, the FER due to frequency disturbances can be approximated by the first term in $\sum_{i=t+1}^{n} \binom{n}{i} (P')^i (1-P')^{n-i}$, where $P' = \sum_{j=e+1}^{M} \binom{M}{j} (P)^j (1-P)^{M-j}$, and e is the maximum number of correctable symbol errors for the permutation code. For the $d_{\min} = 2$ permutation code, e is approximated to a 1 due to soft decision decoding. For the $d_{\min} = 3$ permutation code, in the uninformed receiver case, $e = 1$ and in the informed receiver case, $e = 2$ because it can correct two erasures. These FER estimates are for high SNR.

2.4 Types of noise

Some of the noise in the PLC channel include, AWGN, frequency selective fading, impulsive noise and frequency disturbances. Our main interest is on frequency disturbances, and their models. Next we discuss impulsive noise and narrow band interference model.

2.4.1 Impulsive noise

Power spectral density (PSD) of the impulsive noise is considered to be flat and covering all frequencies with variance σ_I^2, which is related to the AWGN variance as $T = \sigma_g^2/\sigma_I^2$, where $T < 1$ [14]. Since an impulse can affect more than one transmitted symbol, for simplicity, in this chapter we use a Gilbert-Elliot model with the parameters defined as follows: G is good state, B is bad state, P_{gb} is the probability of moving from a good state to a bad state, P_{bg} is the probability of moving from a bad state to a good state, $1-k$ is the probability of being hit by impulses in a good state and $1-h$ is the probability of being hit by impulses in a bad state, where $0 \leq h < 1$. We assume that a good state is impulse-free, therefore $1-k=0$.

2.4.2 Narrow band interference model

Another one of the most devastating type of noise found in the PLC channel is narrow band noise which appears as frequency disturbances. Narrow band noise is produced by interfering signals from systems sharing the same frequency spectrum as the PLC network in which the transmitter of information is connected. Some possible sources of this kind of noise are, TV vertical scanning frequency and its harmonics, radio amateurs and AM transmission [14]. We shall be referring to the interfering signals causing frequency disturbances as frequency disturbers. The problem of modeling frequency disturbances caused by these sources of narrow band noise is still an open one. In this subsection we propose a simple narrow band noise model for OFDM transmission schemes, taking a slightly different approach to the interference model presented in [15]. Since OFDM is a multi-carrier (or multiple-tones) transmission scheme, the effect of narrow band disturbances can be seen as representing a case of *multiple-tone jamming*. Since the analysis of tone jamming is more complicated than that of simple noise jamming, without multiple

tones, [17], we reduce the problem to a case of *partial-band noise jamming*. To reduce the problem to a case of partial-band jamming, we consider the power spectral density (PSD) of each frequency disturber to be as shown in Fig. 2.2. W is the bandwidth of the frequency disturber, and P_0 is the strength of the frequency disturber, which is considered to be flat for the entire band W. The average normalized power, P_A, is the area under the graph ($P_A = WP_0$), which is kept constant.

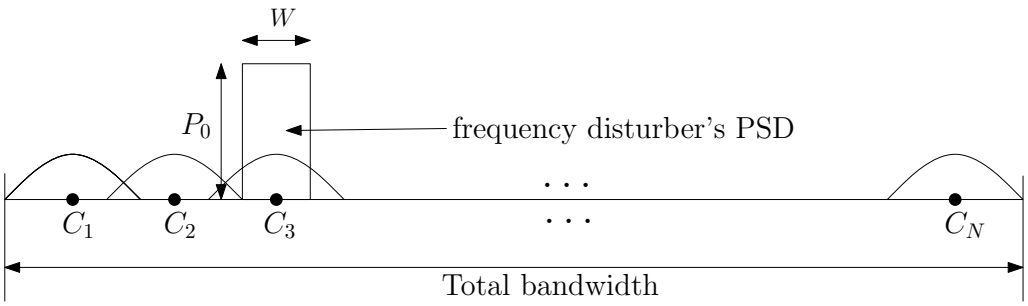

Figure 2.2: Power spectral density of a frequency disturber with strength P_0 and width W, on sub-carrier C_3 of the N-sub-carrier OFDM spectrum.

The frequency disturber of bandwidth W and strength P_0 can be found anywhere along the OFDM bandwidth N. To make the analysis easier, we restrict each frequency disturber to a single OFDM sub-carrier that is, it cannot affect more than one sub-carrier at a time. We now define the probability of frequency disturbances in the OFDM system, due to frequency disturbers, P_h as $P_h = AP$. P is the probability of the presence of frequency disturbers in the OFDM system, where the frequency disturber can be in any of the N sub-carriers. A is the probability that a sub-carrier is hit by a frequency disturber, which is a function of the frequency disturber's bandwidth W, such that increasing W results in an increased A. For the impulsive noise model, the PSD, σ_I^2 is linked to the AWGN PSD, σ_g^2, by a factor T ($\sigma_I^2 = \sigma_g^2/T$) [14]. In the case of narrow band noise there is no link found between its PSD and that of AWGN, hence for each given A and T we take the PSD strength of the frequency disturber as $P_0 = 1/AT$, where $T < 1$ determines the level of the strength of the frequency disturber.

2.5 Simulation Results

Schemes A, B and C are compared in the following types of noise, AWGN, impulsive noise, frequency disturbances and frequency selective fading. For all simulations, background

noise, modeled as AWGN, is considered present with each of the other types of noise, hence we shall only mention the other types of noise when they are present with AWGN.

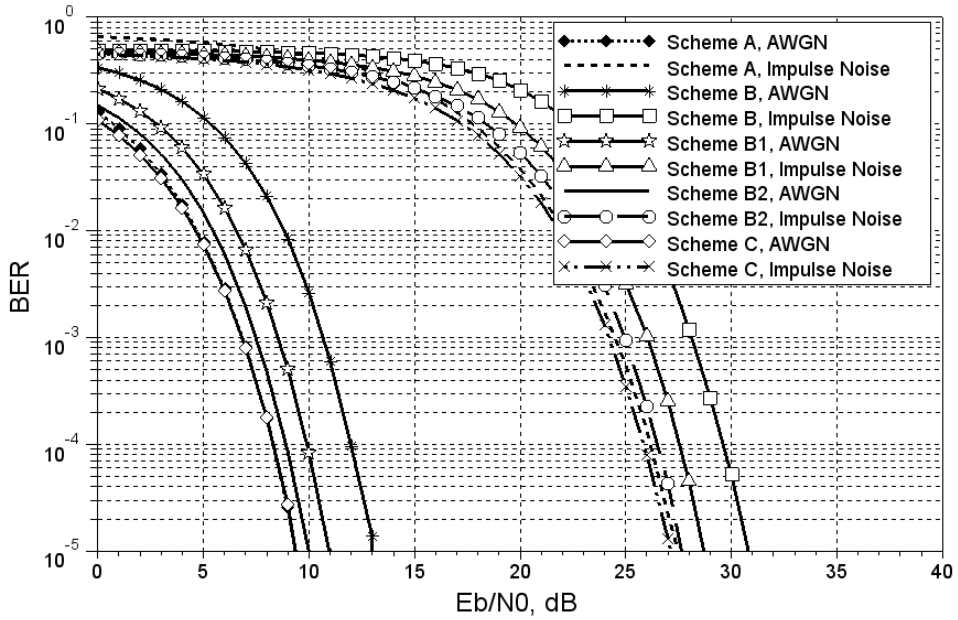

Figure 2.3: Comparison betweem Schemes A, B, B1, B2 and C in the presence of AWGN only, and impulsive noise with $P_{gb} = 0.1$, $P_{bg} = 0.9$, $T = 10^{-2}$, $k = 1$, $h = 0.5$.

In Fig. 2.3, the results for the schemes in AWGN only closely match our SNR estimates in Table 2.1. It can be seen that Scheme A and C have similar performances for both AWGN only and impulsive noise, while Scheme B has the worst performance in both types of noise. Both Schemes B1 and B2 are better than the original Scheme B, in both AWGN only and impulsive noise, and the performance of Scheme B2 is very close to Scheme A and C.

Taking Scheme A as an example, our narrow band noise model parameters are tested to observe their effect on the performance of OFDM transmission as shown in Fig. 2.4. It can be seen in Fig. 2.4 that a larger A which corresponds to larger frequency disturber's bandwidth, has more impact on the transmission than a smaller A, even though the frequency disturber with smaller A may have a larger strength, P_0. This is due to the fact that even though a frequency disturber of high P_0 can be more devastating to the sub-carrier if hit, its probability of hitting a sub-carrier is reduced with reduction in A. Increasing P, while keeping A and T fixed, results in a more devastating effect on the transmitted signal.

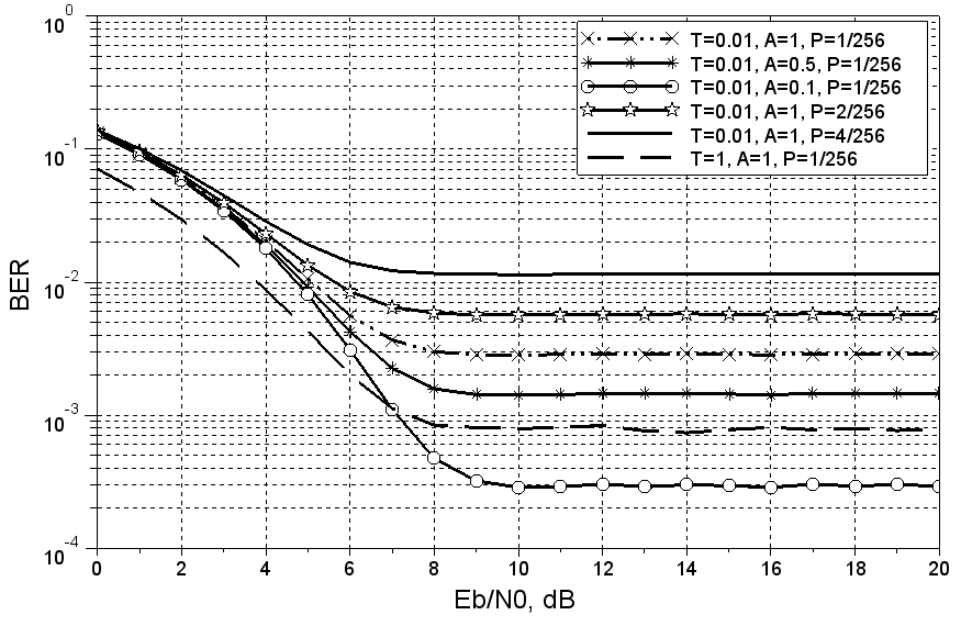

Figure 2.4: Demonstration of the effect of the various parameters of the narrow band noise model (T, A, and P) on transmission, using Scheme A as an example.

In Fig. 2.5, our scheme (Scheme C) has the best performance against all the schemes in the presence of frequency disturbances. Scheme A and B, B1 tend to have the same performance in the presence of frequency disturbances at high SNR and outperform Scheme B2. The best performance of Scheme C over Scheme A is attributed to its better Euclidean distance, and at SNR values lower than 7.5 dB, Scheme A performs better than Scheme C because of its better data rate.

In Fig. 2.6, Scheme C outperforms both Schemes A and B when there is deep fading in some of the sub-carriers. The deep fading effect was simulated by randomly selecting the number of sub-carriers where fading is to occur, and on these sub-carriers the power was set to zero to represent a deep fade such that any information transmitted in the faded sub-carriers is lost. It is interesting to note that Scheme B outperforms Scheme A in the presence of frequency selective fading. This is due to the fact that in Scheme B some of the sub-carriers in a group are already set to zero and as a result when fading occurs in those sub-carriers the system can still correctly demodulate its transmitted symbols. The BER performance of Scheme B is four times better than that of Scheme A.

Fig. 2.7 shows the performance coded Scheme A, in terms of frame error rate (FER), for an informed and uninformed receiver about the position of the frequency disturbers.

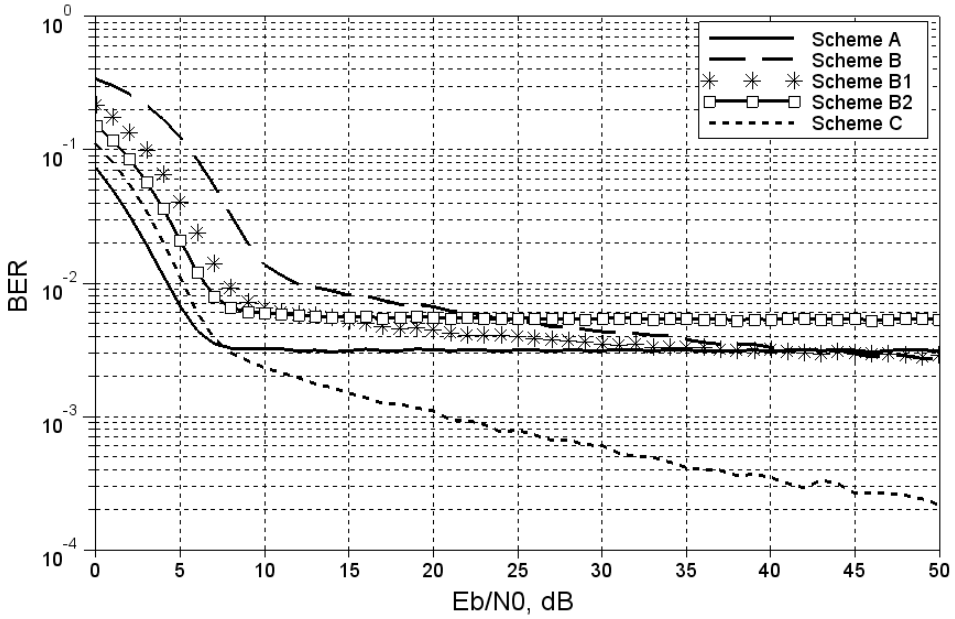

Figure 2.5: Comparison of Scheme A, B, B1, B2 and C in the presence of frequency disturbances with $P = 4/256$, $A = 1$ and $T = 1$.

For the uninformed receiver case, the (64, 48) RS code alone performs poorly compared to the concatenated (32, 24) RS code and ($M = 4$, $d_{\min} = 2$) permutation code (*RS + PC, uninformed*). This is consistent with our approximations in Section 2.3.5. It should be noted that the (64, 48) RS code can correct eight RS symbol errors, while the (32, 24) RS code can only correct four RS symbol errors. For the concatenated (32, 24) RS code and permutation code, we further show that the performance of the coded scheme is slightly improved when the receiver is informed about the position of the frequency disturbances (denoted, *RS + PC, informed* in the figure).

Since G3-PLC uses a convolutional encoder in concatenation with a RS code (see [11]), in Fig. 2.8, we showed the performance comparison of the following codes in the presence of frequency disturbances: concatenation of, (a) a (32, 24) RS code and a ($R = 1/2, K = 7, d_{\text{free}} = 10$) convolutional code, (b) a (32, 24) RS code and a ($M = 4$, $d_{\min} = 2$) permutation code, and (c) a (32, 24) RS code and a ($M = 4$, $d_{\min} = 3$) permutation code [1]. R, K and d_{free} are the rate, constraint length and free distance of the convolutional code, respectively. The parameters of the convolutional code used here are the same as

[1]The ($M = 4$, $d_{\min} = 3$) permutation code is denoted PC^+, in the figure, because extra sequences of length 4 that are not permutations, are added to the permutation code to increase the cardinality while keeping $d_{\min} = 3$.

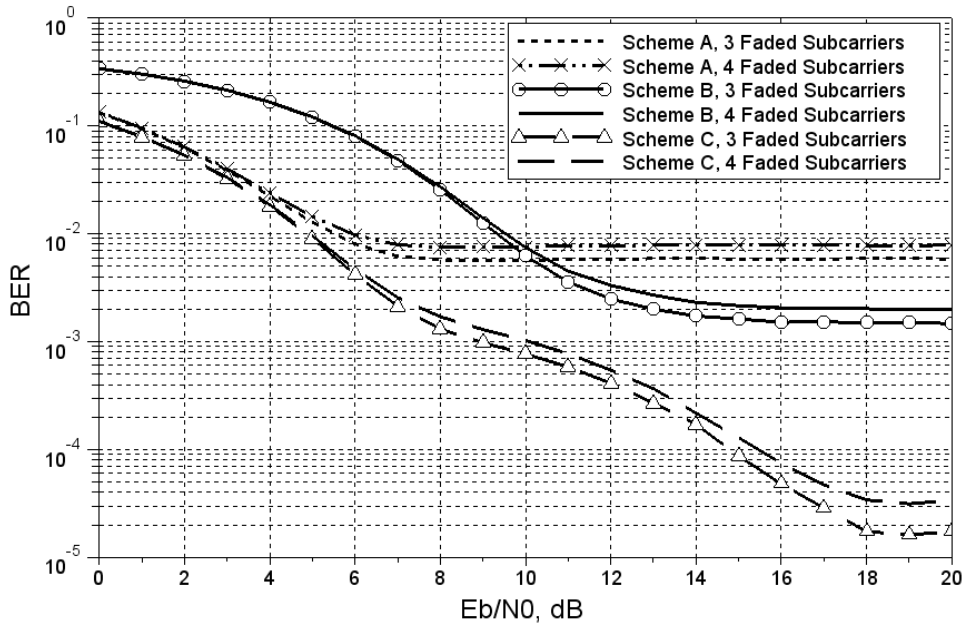

Figure 2.6: Comparison of Scheme A, B and C in the presence of frequency selective fading where deep fading occurs on three or four sub-carriers.

the ones used in G3-PLC. It is important to observe that even though the convolutional code in (a) is more complex than the permutation codes in (b) and (c), its performance is similar to the code in (c) for the informed case.

2.6 Conclusion

We proposed a QPSK-OFDM transmission scheme where real and imaginary components of a QPSK symbol are transmitted in OFDM sub-carriers independently. This is presented in Scheme C. The scheme performed better than other QPSK-OFDM schemes in the presence of frequency disturbances and frequency selective fading. Two more variations of Scheme B were proposed which improved on the performance of the original Scheme B in AWGN only and impulsive noise, and displayed performance that approaches that of Scheme A. A simple narrow band noise model, which we implemented with all schemes in the presence of frequency disturbances, was proposed. We also showed that a concatenation of a shorter (32, 24) RS code with a simple permutation code is effective in dealing with frequency disturbances in OFDM transmission over PLC, for both informed and uniformed receiver cases.

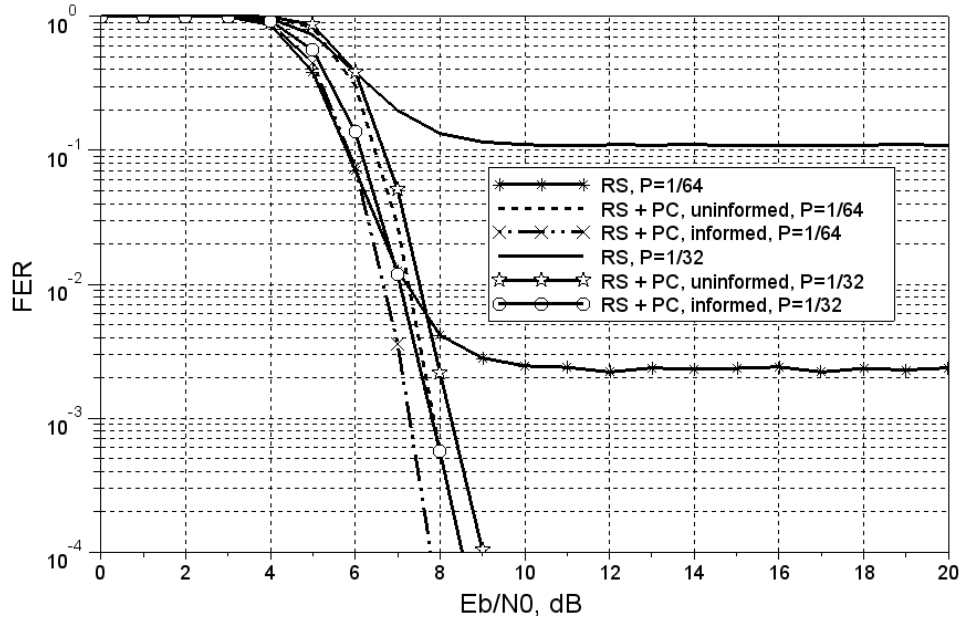

Figure 2.7: Coded Scheme A, in the presence of frequency disturbances with $T = 0.01$ and $A = 1$, for an informed and uninformed receiver. A (64, 48) RS only, and a concatenated (32, 24) RS code and permutation code are compared for frame error rate.

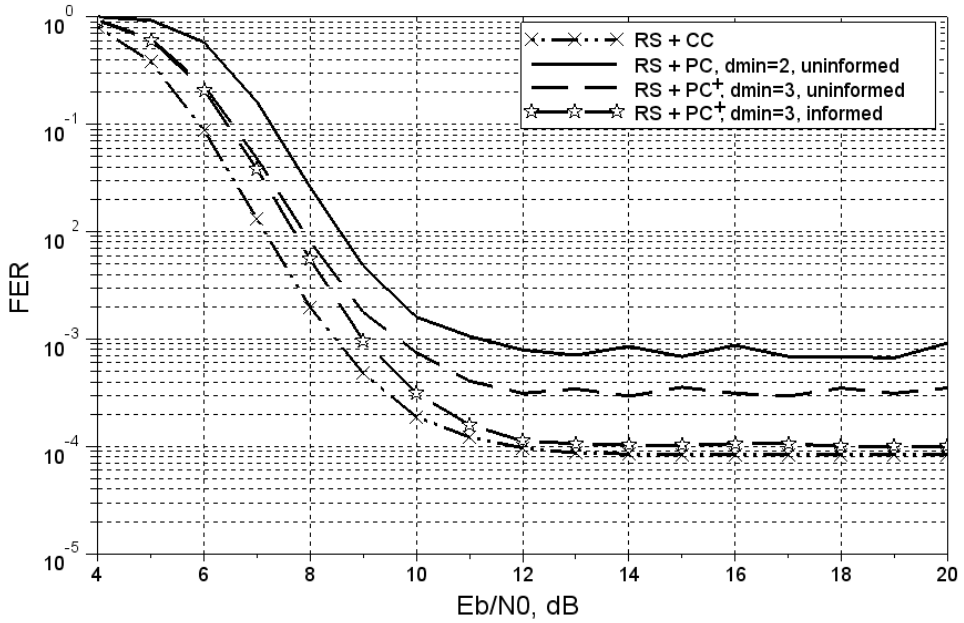

Figure 2.8: A concatenation of: (32, 24) RS code and ($M = 4$, $d_{\min} = 2$) permutation code, (32, 24) RS code and ($M = 4$, $d_{\min} = 3$) permutation code, and (32, 24) RS code and ($R = 1/2, K = 7, d_{\text{free}} = 10$) convolutional code are compared on Scheme A in the presence of frequency disturbances, for $P = 1/16$, $T = 0.01$ and $A = 1$.

3 Narrow-band Interference Model for OFDM Systems for Power line Communications

A narrow-band interference (NBI) model for the power line communications channel is presented. We give frequency domain details and analysis of the NBI model specifically for OFDM systems; it can easily be adapted to model NBI for other communications systems. We also show that by making the same assumptions as in the Middleton class A model, our NBI model becomes the Middleton Class A noise model.

3.1 Introduction

It is widely accepted that power line communications channel is characterized by three main noise types namely, coloured background, impulse and narrow-band interference (NBI). Of these three noise types, the narrow-band interference has not been given much attention and as a result it lacks a well defined model. We find some good efforts in describing or modelling narrow-band interference in [2], [15], [18]–[20]. Galda and Rohling [18] gave a brief NBI model description, where the bandwidth of the interfering signal was considered to be small compared to the OFDM sub-carrier spacing, hence the interfering signal could be modelled as a single-tone. The frequency and phase of the single-tone interfering signal were assumed to be stochastic with a uniform distribution. The power of the interfering signal was a fixed parameter. In [19], the interfering signal was considered to be a stochastic process in the time domain. Authors in [15] and [20] gave descriptions of interference models together with expressions for the interfering signal. With the aid of the expressions, they explained the conditions under which an interfering signal affects only one sub-carrier or several adjacent sub-carriers. The work in [15], [18]–[20] mostly described the signal processing of the NBI which was sufficient for the purposes of that

work. Unfortunately, not much statistical detail of the models was given. The contribution of this chapter is therefore to give a detailed and well-defined narrow-band interference model applicable to an OFDM system, which is an extension of our previous NBI model in [2]. We will focus on OFDM system when used in power line communications (PLC) channel.

Any communications system, with a given finite bandwidth, is susceptible to frequency interference. Frequency interference can originate from several sources and appear on the frequency spectrum of the system as interfering signals. We will call an interfering signal, an *interferer*. In the power line communications, the sources of frequency interference can be classified into two main classes:

1. interference due to electrical devices connected in the same PLC network as the transmitter of the desired signal, and
2. interference due to radio broadcasters.

The devices connected to the PLC network cause interference at their switching frequency and they usually affect PLC transmission taking place in frequencies up hundreds of kilohertz. Radio broadcasters commonly operate in the megahertz region of the frequency spectrum and will interfere with PLC transmission occurring in the megahertz region. In this work, we shall focus on interferers with narrow bandwidth and occurring from independent sources. This view is somewhat generic to two classes of sources of frequency interference in PLC already mentioned.

Now, we assume that interferers originate from different independent sources, and we also assume that a very large number of interferers rarely occurs within a given frequency band. We therefore model the probability of a certain number k of interferers on the system's spectrum as a Poisson distribution,

$$P_k = \frac{\eta^k e^{-\eta}}{k!}, \tag{3.1}$$

where $k = 0, 1, \ldots \infty$.

In general, η in (3.1) is a quantity indicating the average number of occurrences of certain events, defined over a specified observation period. In the Middleton class A noise model [21], η in (3.1) was called "impulsive index". In our model, we define the average

fraction of bandwidth occupied by NBI in a system bandwidth W as $\lambda = \frac{\eta\bar{\Omega}}{W}$, where η the average number of interferers with average bandwidth $\bar{\Omega}$. P_k then is the probability that there are k such interferers on the frequency band W. The next task is then to find the power of the interferer(s) that affects the system as NBI, and to also approximate the probability distribution of the power of this interference (noise) in the system.

We specify our system of interest in this chapter as the OFDM system, and we shall present our NBI model for this system.

Our NBI model defines the interferers in the frequency domain, with the assumption that they correspond to real signals in the time domain. The effect of the interferers on the system is also completely described in the frequency domain.

OFDM Signal Generation Overview

OFDM is a multi-carrier transmission scheme, where data is carried on several sub-carriers which are orthogonal to each other to avoid mutual interference. In the OFDM system of interest, an IDFT (inverse discrete Fourier transform) takes in as input, data symbols carried in vector D_s, from a phase-shift-keying (PSK) modulation scheme and produces a discrete sequence in the time domain, d_n. The relationship between D_s and d_n is represented by

$$d_n = \frac{1}{\sqrt{N}} \sum_{s=0}^{N-1} D_s e^{j2\pi ns/N}, \tag{3.2}$$

where N is the number of sub-carriers used to carry data. d_n is the complex baseband transmit signal from the output of the IDFT normalized by the factor $\frac{1}{\sqrt{N}}$.

3.2 NBI Power Spectral Density

Let us define an arbitrary interferer $x(n)$, of bandwidth Ω, as a discrete-time signal which is a sum of arbitrary single-tone signals as

$$x(n) = \sum_{i=0}^{\Omega} A_i e^{j(2\pi f_i n + \phi_i)}, \tag{3.3}$$

where A_i, f_i and ϕ_i are the corresponding amplitudes, frequencies and phases of the different arbitrary signals, respectively. At the receiver the interferer goes through the N-point DFT and appears on the OFDM spectrum. The result of this operation is described by

$$X(\omega) = \sum_{n=0}^{N-1} x(n) e^{-j\omega n}, \tag{3.4}$$

where $X(\omega)$ is the amplitude spectrum of $x(n)$ after the DFT. We represent the continuous amplitude spectrum of $X(\omega)$, in frequency f, as $X(f)$.

If the interferer is a single-tone then it can be described by the i^{th} signal as

$$x_i(n) = A_i e^{j(2\pi f_i n + \phi_i)} \tag{3.5}$$

and its amplitude spectrum, after applying a rectangular window and DFT, is given by

$$X_i(f) = A_i e^{j\phi_i} e^{j(N-1)(\pi f_i - \pi f)} \frac{\sin N(\pi f_i - \pi f)}{\sin (\pi f_i - \pi f)} \quad [1]. \tag{3.6}$$

From here onwards, we simply will refer to the power or amplitude spectrum of a time domain signal (or interferer) after windowing and DFT, as power or amplitude spectrum of the signal (interferer).

Now, returning to the amplitude spectrum in (3.4) which has a bandwidth Ω. We are interested in the effect of the power spectral density (PSD) of the interferer $x(n)$ on the OFDM spectrum and hence, how the interferer affects the OFDM signal as noise in the

[1] The derivation of the equation can be found in the Appendix

frequency domain.

In Fig. 3.1 we show an arbitrary power spectrum of the interferer $x(n)$ denoted by $|X(f)|^2$; together with that of two consecutive sub-carriers SC_m and $\mathrm{SC}m+1$, centred at f_m and f_{m+1}, respectively.

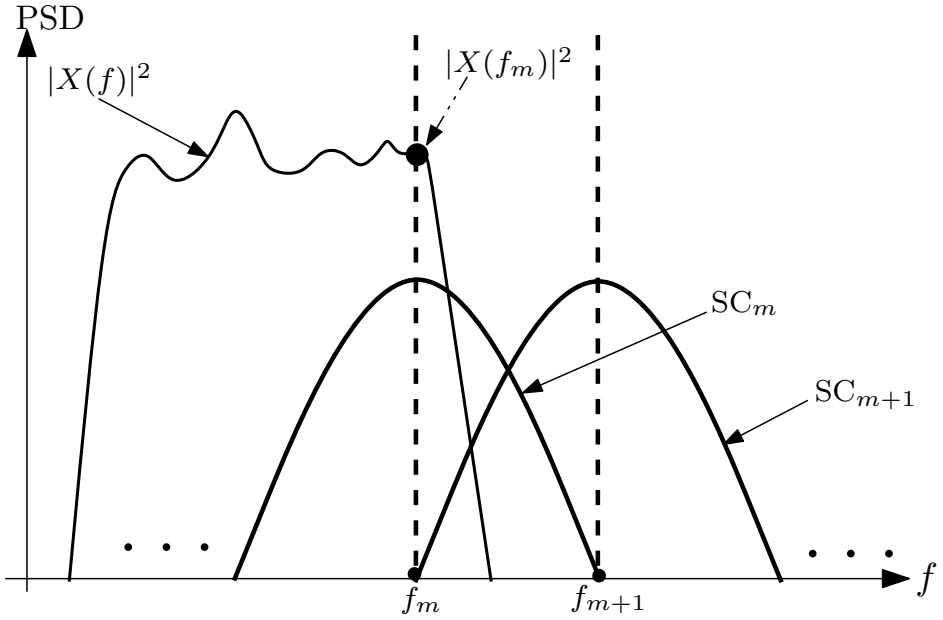

Figure 3.1: The effect of the power spectrum $|X(f)|^2$ of an arbitrary interferer $x(n)$, on the OFDM spectrum showing two neighbouring sub-carriers SC_m and SC_{m+1}. The Center frequencies of SC_m and $\mathrm{SC}m+1$ are f_m and f_{m+1}, respectively. $|X(f_m)|^2$ is the power contribution of the spectrum $|X(f)|^2$, of the interferer, on SC_m.

In Fig. 3.1 we also show some *power contribution* of the interferer on sub-carrier SC_m as $|X(f_m)|^2$. This power contribution on a sub-carrier(s) is the interferer's power that affects the sub-carrier as noise or effective noise power. The power contribution $|X(f_m)|^2$ of the interferer on a sub-carrier(s) can vary depending on the position of the interferer's PSD on the OFDM spectrum. We will shortly explain this power contribution in relation to the position of a given interferer on a sub-carrier.

Focusing on one sub-carrier SC_m, we are interested in finding the power contribution of the interferer $x(n)$ on the sub-carrier, in the frequency domain. The DFT (of the OFDM receiver) samples the received signal at the center frequency of each sub-carrier to get the transmitted data. Therefore, the interferer contributes its power to the sub-carrier centred at f_m when its power spectrum is evaluated at f_m. This evaluation of the

interferer's PSD at f_m results in the power contributed being $|X(f_m)|^2$, as already stated.

It is sufficient to show the power contribution of the interferer(s) on one sub-carrier, because the analysis of the power contribution on every other sub-carrier follows the same manner. As such, the analysis of the power contribution on one sub-carrier can be applied to all sub-carrier.

It should be noted that when the bandwidth of the interferer, Ω is larger than the sub-carrier spacing, the interferer may contribute power to several adjacent sub-carriers. The contribution of the interferer's power to one sub-carrier can be analysed without affecting the contribution to another sub-carrier. This is in agreement with our argument that analysing the interferer's power contribution on one sub-carrier is enough to give us an understanding of the frequency interference on every sub-carrier.

Now, let us have an interferer of fixed average amplitude A and bandwidth Ω ($0 < \Omega < W$). This interferer can be located anywhere along the OFDM frequency spectrum W, its position is therefore unknown (variable y). We are interested in finding the noise power contribution of this interferer on a particular sub-carrier with a center frequency f_m. The power contributions of the interferer at f_m are the instantaneous points on the interferer's PSD when evaluated at f_m. Let the position of the interferer, around the sub-carrier, have a uniform probability distribution. Since the interferer has bandwidth Ω, then the probability distribution of its power contributions on the sub-carrier at f_m, is $P = 2\Omega/W$. The factor of 2 is due to the fact that the interferer's PSD can be on either side of f_m, in position, and still contribute power at f_m. So, each power contribution of the interferer on a sub-carrier has equal probability P, where each power contribution corresponds to the instantaneous location/position of the interferer. This enables us to calculate the average power contribution of the interferer in question on a sub-carrier, which will be the sum of all the possible power contributions weighted by the their probabilities P. We denote this average power contribution of a single interferer on sub-carrier centred at f_m by $\bar{\chi}$, and is defined as

$$\begin{aligned} \bar{\chi} &= \int_0^{\Omega} P|X_y(f_m)|^2 dy \\ &= \frac{2\Omega}{W} \int_0^{\Omega} |X_y(f_m)|^2 dy, \end{aligned} \tag{3.7}$$

where y are the different frequency values (positions on the spectrum) the interferer can assume, which is a variable over the bandwidth of the interferer. The term $\int_0^{\Omega} |X_y(f_m)|^2 dy$

in (3.7) gives the total power of the interferer, and $\bar{\chi}$ gives the average effective power, which is the power contributed by the interferer on the sub-carrier.

To make the analysis simpler for any given number of interferers k, we assume they have an average bandwidth $\Omega = \bar{\Omega}$ and the same A, and hence the same average effective power $\bar{\chi}$ as calculated in (3.7). Therefore the power contribution, due to the k interferers, is the sum of the average effective power of the individual interferers,

$$\sigma_k^2 = k\bar{\chi}. \tag{3.8}$$

We call σ_k^2 the effective narrow-band interference (NBI) power, given k interferers. The total average effective NBI power in the system is

$$\begin{aligned} \sigma^2 &= \sum_{k=1}^{\infty} \sigma_k^2 P_k \\ &= \bar{\chi} \sum_{k=1}^{\infty} k P_k \\ &= \bar{\chi}\eta, \end{aligned} \tag{3.9}$$

where P_k is as defined in (3.1) and $\bar{\chi}$ as defined in (3.7).

Note: If the positions of the interferers are mostly static on the frequency band of interest, as might be the case with the PLC channel, the model will still apply, but with the following changes on the average effective power $\bar{\chi}$ in (3.7). The position of an interferer will no longer have a probability distribution because it is fixed, and its power that affects a sub-carrier centred at f_m will be one of the $|X_y(f_m)|^2$, for $y = 0 \ldots \Omega$. We can define the average effective power, $\bar{\chi}$, as the average of all the values $|X_y(f_m)|^2$, for $y = 0 \ldots \Omega$.

$$\bar{\chi} = E\left\{|X_y(f_m)|^2\right\}, \tag{3.10}$$

where $E\{.\}$ means the expectation. It should be noted that whether the positions of the interferers are static or changing, that has no bearing on the probability of having interferers in the system, P_k.

A second issue to be noted is that when the average bandwidth of the interferers $\bar{\Omega}$

gets larger, there is likely going to be more adjacent sub-carriers affected by an interferer as NBI. Remembering from Section 3.1 that $\lambda \propto \bar{\Omega}$, then as $\bar{\Omega}$ gets larger so does λ. This means that the probability of having NBI in the system increases in proportion to an increased $\bar{\Omega}$. As stated, interferers with larger bandwidth may affect adjacent sub-carriers and this will likely result in a burst of errors. Whether adjacent or random sub-carriers are affected, the average number of errors that will occur in the system does not change. This burst error phenomenon can easily be taken into account by using models that consider channels with memory for example, a Gilbert-Elliot model.

Similarities to Middleton's Class A Noise Model

Just as in the Class A noise model by Middleton [21], the NBI model, in the frequency domain, can be seen as an infinite number of parallel channels each with effective NBI power σ_k^2 ($k = 0 \ldots \infty$) and additive white Gaussian noise of variance σ_g^2, where each channel is selected with probability P_k prior to transmission. This channel model is shown in Fig. 3.2, where a symbol D is affected by AWGN of variance σ_g^2 and NBI of variance σ_k^2.

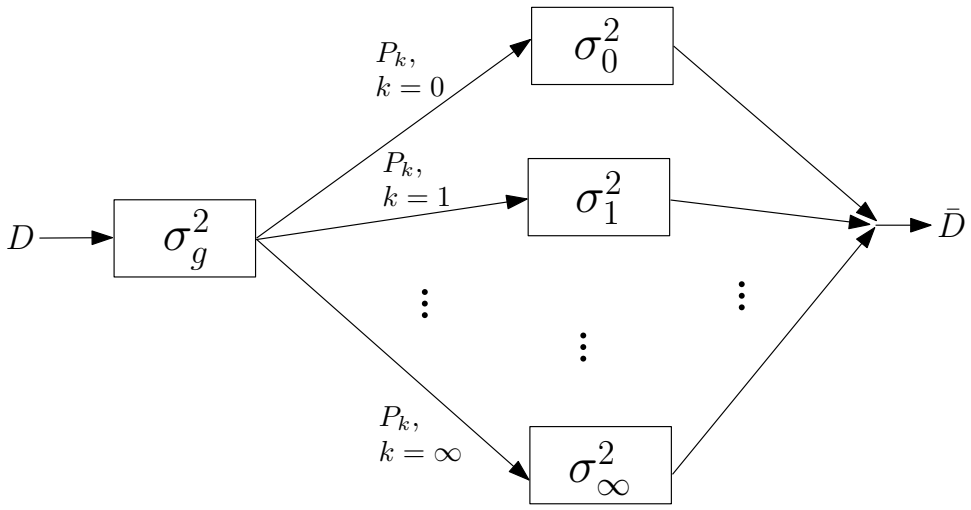

Figure 3.2: Narrow-band interference model including additive white Gaussian noise (AWGN). A symbol D affected by AWGN of variance σ_g^2. Then it enters one of infinite parallel channels with probability P_k, and in that channel the symbol is affected by NBI of power σ_k^2 such that the output data symbol $\bar{D}$ is the original D plus noise of variance $\sigma_g^2 + \sigma_k^2$.

Now, let us make the assumption that the NBI amplitude due to k interferers is a Gaussian random variable, and can take any value z, with mean μ and variance σ_k^2. Then

this interference (noise) due to k interferers has a Gaussian distribution with a PDF (probability density function) defined as $\mathcal{P}(z|k) = \mathcal{N}(z; \mu, \sigma_k^2)$.

$$\mathcal{P}(z|k) = \frac{1}{\sqrt{2\pi\sigma_k^2}} \exp \frac{-(z-\mu)^2}{2\sigma_k^2}. \tag{3.11}$$

Then the probability distribution of the NBI z is

$$\mathcal{P}(z) = \sum_{k=1}^{\infty} \mathcal{P}(z|k) P_k. \tag{3.12}$$

With the results in (3.11) and (3.12), we have arrived at the same result of Middleton Class A noise model [21], where it was assumed that the noise has a Gaussian distribution.

3.3 How the NBI Model is Applied

To demonstrate the application of our NBI model, we shall use an example. Firstly, we modify the infinite-parallel-channel model in Fig. 3.2 into an easy to use two-parallel-channel model as shown in Fig. 3.3.

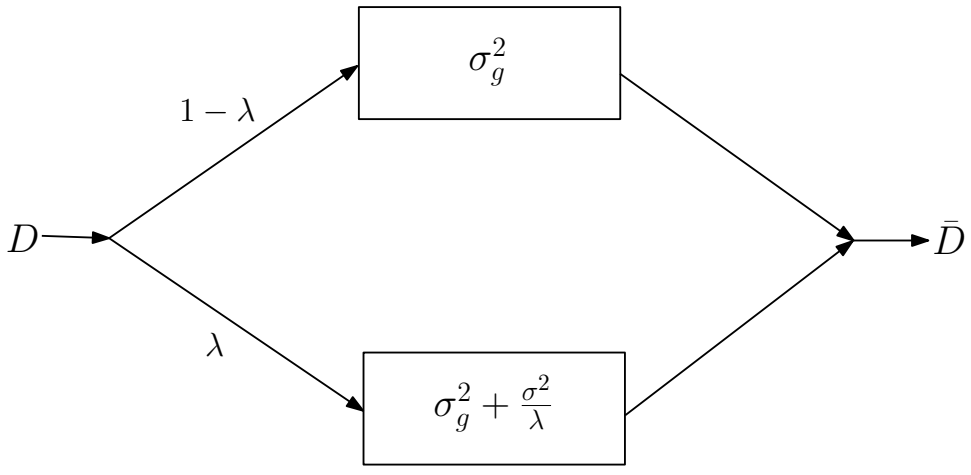

Figure 3.3: Narrow-band interference model including additive white Gaussian noise (AWGN). A symbol D either enters a channel with AWGN (variance σ_g^2), with probability $1-\lambda$, or enters a channel with noise $\sigma_g^2 + \sigma^2/\lambda$, with probability λ. σ^2 is the total average effective NBI power in the system as defined in (3.9).

A transmitted symbol from any modulation is affected by AWGN of variance σ_g^2, with probability $1-\lambda$. The symbol is affected by AWGN and NBI of average power $\sigma_g^2+\sigma^2/\lambda$, with probability λ. That is, a symbol "chooses" one of the channels in Fig. 3.3 according to the entrance probabilities λ or $1-\lambda$. σ^2 is the total average effective NBI power in the system as defined in (3.9).

Now, let $\lambda = 10^{-2}$ and $\sigma^2/\lambda = \bar{\chi} = 10$. For AWGN, $\sigma_g^2 = 1$. Having specified the variances of the AWGN and the NBI, we now want to specify the noise samples of the AWGN and that of the NBI, which we call n_g and n_N, respectively. We focus on n_N because n_g is known, it is AWGN.

Let us look at two distributions for the NBI sample n_N, which are the *uniform distribution* and *Gaussian distribution*.

Case A: NBI has a uniform distribution.
For a uniform distribution with limits a and b:

- $n_N = a + (b-a)R_u$.
- R_u, a function that generates a random number from a standard uniform distribution on the open interval $(0, 1)$.
- the variance $\sigma^2/\lambda = \bar{\chi}$ is given by $(b-a)^2/12$.
- since we know the variance we need to specify a and b, let $a = -b$, then we have $b = \sqrt{\bar{\chi}}\sqrt{3} = \sqrt{10}\sqrt{3}$.
- $n_N = -\sqrt{10}\sqrt{3} + 2\sqrt{10}\sqrt{3}R_u$.

Case B: NBI has a Gaussian distribution with mean $\mu = 0$.

- $n_N = \sqrt{\mu} + \sqrt{\bar{\chi}}R_g$.
- R_g, a function that generates a random number from a standard normal distribution.
- $n_N = \sqrt{10}R_g$.

The symbol is affected by noise as follows:

- with probability λ: $\bar{D} = n_g + n_N + D$
- with probability $1 - \lambda$: $\bar{D} = n_g + D$,

where $n_g = R_g$ because $\sigma_g^2 = 1$.

If D is complex valued, then n_N and n_g have to be complex too. For example, in [2] we generated each NBI sample n_N as a complex random value using the function R_g, such that the sample was $\sqrt{\frac{\sigma^2}{\lambda}}R_g + j\sqrt{\frac{\sigma^2}{\lambda}}R_g$. As such, NBI generated in [2] can be viewed as a random phasor that can rotate in any direction, with the real and imaginary components each having a magnitude determined by R_g and $\sqrt{\frac{\sigma^2}{\lambda}}$.

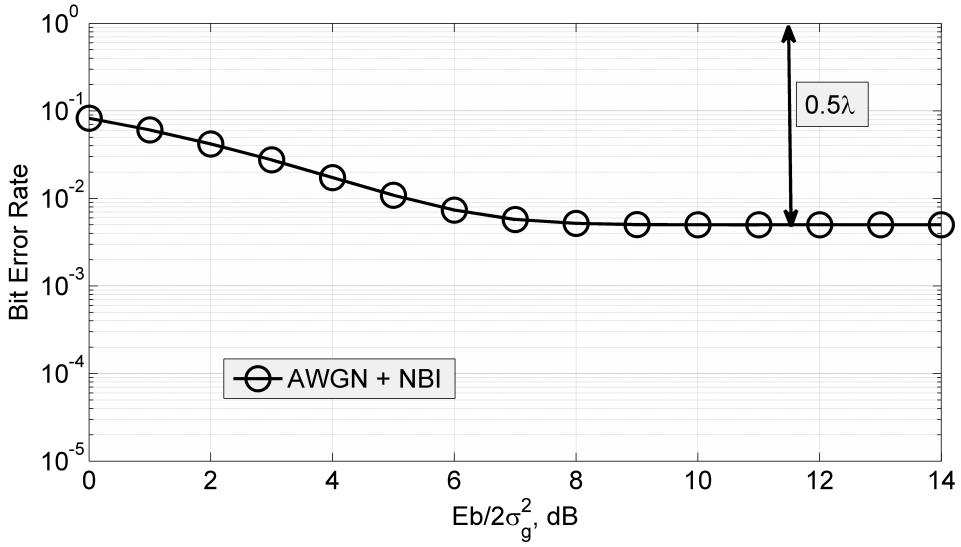

Figure 3.4: BPSK–256OFDM modulation bit error rate performance in the presence of NBI with $\sigma^2/\lambda = 10$ and $\lambda = 10^{-2}$, and AWGN with $\sigma_g^2 = 1$.

In Figures 3.4 and 3.5 we give the simulation results of **Case B**, where the system is OFDM with $N = 256$ sub-carriers, and BPSK is used as the modulation. In Fig. 3.4, we set $\lambda = 10^{-2}$ and $\sigma^2/\lambda = 10$. The probability of error caused by NBI for a BPSK modulation will be $0.5 \times \lambda = 0.5 \times 10^{-2}$. The error floor in Fig. 3.4 confirms this estimate of the probability of error. The Signal to Noise Ratio (SNR) is $Eb/2\sigma_g^2$ in Fig. 3.4, hence the persistent error floor. The role of Fig. 3.4 is to indicate the probability of error caused

by NBI without paying special attention to the power of the NBI. We addressed the issue of the effect of the NBI power in the SNR in Fig. 3.5.

Fig. 3.5 shows the simulation result with similar parameters to those in Fig. 3.4, except that now the SNR which includes the NBI power and is $Eb/2(\sigma_g^2 + \sigma^2/\lambda)$. Also in Fig. 3.5, we have set $\lambda = 10^{-2}$ and $\sigma^2/\lambda = 100$. The SNR gap between the graph of AWGN only and that of AWGN + NBI confirms the NBI power, $\sigma^2/\lambda = 100$.

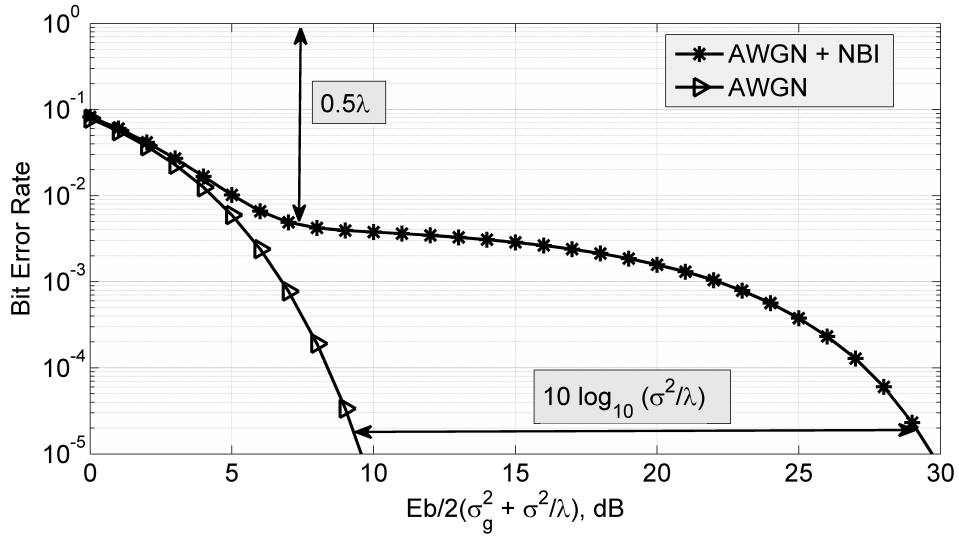

Figure 3.5: BPSK–256OFDM modulation bit error rate performance in the presence of NBI with $\sigma^2/\lambda = 100$ and $\lambda = 10^{-2}$, and AWGN with $\sigma_g^2 = 1$.

3.4 Conclusion

We have designed a narrow-band interference model which is applicable to PLC channel when an OFDM system is used. In the given model, the probability with which this NBI power affects data has to be provided. We also showed how to calculate the average effective power of the narrow-band interference, from a number of interferers, that affects the OFDM system. The average effective NBI power can be modelled with an appropriate distribution; in this chapter we demonstrated the use of two distributions which were the uniform and Gaussian distribution, and gave numerical results for the Gaussian distribution case.

Appendix

Let $x_i(n)$ denote a discrete time signal,

$$x_i(n) = A_i e^{j(\omega_i n + \phi_i)}, \tag{3.13}$$

where $\omega_i = 2\pi f_i$, A_i is the amplitude and ϕ_i phase of the signal. To simplify the expression we set $A_i = 1$ since it is a constant that does not play any role in the finding of the Fourier transform of $x_i(n)$.

The Fourier transform of $x_i(n)$, $X_i(\omega)$ from an N-point DFT, is

$$\begin{aligned}
X_i(\omega) &= \sum_{n=0}^{N-1} e^{j(\omega_i n+\phi_i)} e^{-j\omega n} \\
&= e^{j\phi_i} \sum_{n=0}^{N-1} e^{jn(\omega_i-\omega)} \\
&= e^{j\phi_i} \frac{1 - e^{jN(\omega_i-\omega)}}{1 - e^{j(\omega_i-\omega)}} \\
&= e^{j((\frac{N-1}{2})\omega_i+\phi_i)} e^{-j(\frac{N-1}{2})\omega} \frac{\sin\frac{N}{2}(\omega_i-\omega)}{\sin\frac{1}{2}(\omega_i-\omega)} \\
&= e^{j\phi_i} e^{j\frac{N-1}{2}(\omega_i-\omega)} \frac{\sin\frac{N}{2}(\omega_i-\omega)}{\sin\frac{1}{2}(\omega_i-\omega)},
\end{aligned}$$

where $\omega = r\frac{2\pi}{N}$, for $r = 0 \ldots N$.

4 A New Joint Impulsive Noise Mitigation Scheme for OFDM System

Impulsive noise mitigation for OFDM can be done with a clipping-nulling scheme using two thresholds. We introduce a new joint impulsive noise mitigation scheme, called *clipping-replacement-nulling* scheme, in which there are three considered thresholds: the clipping threshold T_{clip}, the replacement threshold T_{rep}, and the nulling threshold T_{null}. When the magnitude of a received OFDM sample is above T_{rep} and below T_{null} we set it to the average magnitude $|\bar{x}|$ of the noiseless OFDM samples. The simulation results show that an additional action, *the replacement action*, with a good choice of T_{rep} brings a reduction in the bit error rate.

4.1 Introduction

Using OFDM system in the presence of impulsive noise can bring benefits over single carrier systems because of the spreading effect of the impulsive noise (IN) power over the sub-carriers [4]. However, for large IN power many symbols can be corrupted leading to enormous loss in performance [22].

There are some good solutions for limiting the spreading effect such as clipping, nulling, and also the combined clipping-nulling [4], [8], [10]. Basically, these solutions consider two actions to be applied to the OFDM samples that are corrupted by impulsive noise.

The first action is to limit the maximum magnitude of received samples by using a threshold T_{clip}. This action can be considered as an effort to mitigate the effect of impulsive noise. If we put T_{clip} too low then it might corrupt the transmitted signal but if we put T_{clip} too high then we allow more samples to be corrupted by impulsive noise.

Zhidkov [8] suggested the usage of numerical software tools to find the optimal threshold T_{clip} value(s), whereas Mengi [10] showed the steps to find a threshold that gives the minimum bit error rate (BER). In [23], T_{clip} relies on the probability of occurrence of IN.

The second action is to null the corrupted received samples using a threshold T_{null}. Considering its severe effect [4], it is clear that we should put the nulling threshold T_{null} as high as possible such that with high probability only magnitudes of samples corrupted by impulsive noise will exceed T_{null}.

We investigate the question whether an additional threshold can improve the overall performance. Two problems arise:

1. the position of an additional threshold, and
2. the action applied when the magnitude of received samples is above the additional threshold.

We propose a new action in the mitigation process called *replacement*, where a threshold T_{rep} is located in between T_{clip} and T_{null}. When the magnitude of a received sample is above T_{rep} and below T_{null} we set it to the average magnitude $|\bar{x}|$ of the noiseless OFDM samples.

As an impulsive noise model, we use a two state IN model which will be explained in Section 4.4, and consider two threshold setting scenarios in which we compare the performance, in terms of BER, between the joint clipping-nulling scheme and the proposed joint clipping-replacement-nulling scheme.

In the first scenario, where T_{clip}, T_{rep} and T_{null} are based on the predetermined probability of a received sample magnitude crossing the thresholds, the proposed mitigation scheme brings a reduction in the BER.

In the second scenario, we follow the suggestion of threshold setting as given in the references [8], [10]. They keep the relation between T_{clip} and T_{null} fixed and T_{clip} is optimized for a specific channel situation with respect to BER. We will show that the proposed scheme can always achieve a good performance.

This chapter is organized as follows. In Section 4.2, we describe briefly the OFDM system model and its relation to the Rayleigh distribution, because the new proposed IN

mitigation is based on this distribution. IN mitigation schemes and their thresholds are explained in Section 4.3. Simulation settings and results are described in Sections 4.4 and 4.5, respectively. Finally, Section 4.6 shows the conclusion of this chapter.

4.2 OFDM system and Rayleigh distribution

OFDM is a multi-carrier transmission scheme, where data is carried in several sub-carriers which are orthogonal to each other. In the OFDM system of interest, an IDFT (inverse discrete Fourier transform) takes in as input, N data symbols carried in vector X_k, from a phase-shift-keying (PSK) modulation scheme and produces OFDM samples in the time domain, x_n. The relationship between X_k and x_n is described as follows:

$$x_n = \frac{1}{\sqrt{N}} \sum_{k=0}^{N-1} X_k e^{j2\pi nk/N}, \tag{4.1}$$

where N is the number of sub-carriers used to carry data, and X_k is of the same length as x_n. The complex baseband transmit signal x_n from the output of the IDFT is normalized by the factor $\frac{1}{\sqrt{N}}$.

Under the assumption that OFDM *samples* are Gaussian distributed random variables with zero mean and variance σ_S^2, the *magnitude* of OFDM samples are Rayleigh distributed [10], [24]. In the following subsections we present the theoretical values of two important parameters of the Rayleigh distribution, its variance $\sigma_{|x|}^2$ and average $|\bar{x}|$, and also their measurement values. As will be shown, the theoretical and measurement values are comparable and therefore, in the simulations we use the theoretical values of $\sigma_{|x|}^2$ and $|\bar{x}|$.

4.2.1 Theoretical values of $\sigma^2_{|x|}$ and $|\bar{x}|$

Under the previous assumption, the variance $\sigma^2_{|x|}$ of the magnitude of noiseless OFDM samples is

$$\sigma^2_{|x|} = \frac{4-\pi}{4} Es, \tag{4.2}$$

where Es is the energy per symbol. The average magnitude $|\bar{x}|$ of noiseless OFDM samples is

$$|\bar{x}| = \sqrt{\frac{\pi Es}{4}}. \tag{4.3}$$

For $Es = 1$, $|\bar{x}| = 0.886$ and $\sigma^2_{|x|} = 0.215$.

4.2.2 Measurement values of $\sigma^2_{|x|}$ and $|\bar{x}|$

Tables 4.1 and 4.2 show the measurement/empirical results of $|\bar{x}|$ and $\sigma^2_{|x|}$ when $Es = 1$. BPSK-OFDM and QPSK-OFDM systems with a different number of sub-carriers N are considered.

Table 4.1: The empirical result of $|\bar{x}|$ and $\sigma^2_{|x|}$ for BPSK-OFDM system

N	$\lvert\bar{x}\rvert$	$\sigma^2_{\lvert x\rvert}$
64	0.8850	0.2195
128	0.8857	0.2169
256	0.8861	0.2156
512	0.8862	0.2151

Table 4.2: The empirical result of $|\bar{x}|$ and $\sigma^2_{|x|}$ for QPSK-OFDM system

N	$\lvert\bar{x}\rvert$	$\sigma^2_{\lvert x\rvert}$
64	0.8871	0.2161
128	0.8866	0.2153
256	0.8864	0.2149
512	0.8863	0.2148

4.3 Mitigation schemes and thresholds

Impulsive noise mitigation schemes considered in this chapter are threshold based schemes. We consider *clipping* [4], *nulling* [5], [6], and *clipping-nulling* [8] schemes and introduce two additional schemes, *replacement* and combined *clipping-replacement-nulling*.

Let r_n be a received sample and $\widetilde{r_n}$ be the sample that is obtained after the mitigation process. The schemes are described by the following equations.

Clipping

$$\widetilde{r_n} = \begin{cases} r_n, & for \quad |r_n| \leq T_{clip} \\ T_{clip}e^{jargr_n}, & for \quad |r_n| > T_{clip}, \end{cases} \tag{4.4}$$

Nulling

$$\widetilde{r_n} = \begin{cases} r_n, & for \quad |r_n| \leq T_{null} \\ 0, & for \quad |r_n| > T_{null}, \end{cases} \tag{4.5}$$

Clipping-Nulling

$$\widetilde{r_n} = \begin{cases} r_n, & for & |r_n| \leq T_{clip} \\ T_{clip}e^{jargr_n}, & for & T_{clip} < |r_n| \leq T_{null} \\ 0, & for & |r_n| > T_{null} \end{cases}, \tag{4.6}$$

Proposed scheme 1: Replacement

$$\widetilde{r_n} = \begin{cases} r_n, & for \quad |r_n| \leq T_{rep} \\ \bar{|x|}e^{jargr_n}, & for \quad |r_n| > T_{rep}, \end{cases} \tag{4.7}$$

Proposed scheme 2: Clipping-Replacement-Nulling

$$\widetilde{r_n} = \begin{cases} r_n, & for \quad |r_n| \leq T_{clip} \\ T_{clip}e^{jargr_n}, & for \quad T_{clip} < |r_n| \leq T_{rep} \\ |\bar{x}|e^{jargr_n}, & for \quad T_{rep} < |r_n| \leq T_{null} \\ 0, & for \quad |r_n| > T_{null} \end{cases} . \tag{4.8}$$

In this chapter, the value of a threshold is calculated from the complementary cumulative distribution function (CCDF) of a Rayleigh distribution. Two distributions are considered: first, the distribution of the noiseless OFDM samples as shown in (4.9),

$$CCDF(T) = Pr(|x_n| > T) = e^{\frac{-T^2}{2\sigma^2_{|x|}}}, \tag{4.9}$$

where $Pr(|x_n| > T)$ is the probability of a noiseless OFDM sample exceeding T. Second, the distribution of the OFDM samples corrupted by IN as shown in (4.10),

$$CCDF(T|bad) = Pr(|r_n| > T|bad) = e^{\frac{-T^2}{2\sigma^2}}, \tag{4.10}$$

where $Pr(|r_n| > T|bad)$ is the probability of a received OFDM sample exceeding T in the *bad* state and $\sigma^2 = \frac{4-\pi}{4}(\sigma_S^2 + \sigma_G^2 + \sigma_I^2/A)$ is the average variance of received samples in the *bad* state – the state which happens with probability A. The variance of the signal is indicated by σ_S^2, whereas σ_G^2 indicates the variance of background noise, and σ_I^2 is the *average* variance of IN noise. In the calculation of T, the contribution of background noise is assumed neglectable. We call $Pr(|x_n| > T)$ and $Pr(|r_n| > T|bad)$ *crossing probability* and T can be the value of T_{clip}, T_{rep}, and/or T_{null}.

In Tables 4.3 and 4.4, we showed examples of values of generated thresholds T and their corresponding crossing probabilities. Without loosing our essential observation, the benefit of an additional threshold, we consider the difference between the crossing probabilities to be a factor of 10.

TABLE 4.3: THE LIST OF SOME THRESHOLDS T AND $Prob(|x_n| > T)$ FOR $Es = 1$. EQUATION (4.9) IS USED.

T	$Prob(\|x_n\| > T)$
1.99	10^{-4}
2.23	10^{-5}
2.44	10^{-6}
2.63	10^{-7}
2.81	10^{-8}
2.99	10^{-9}
3.14	10^{-10}

TABLE 4.4: THE LIST OF SOME THRESHOLDS T AND $Prob(|r_n| > T|bad)$ FOR $Es = 1$, $A = 0.1$ AND $\sigma_S^2/\sigma_I^2 = 1$. EQUATION (4.10) IS USED.

T	$Prob(\|r_n\| > T\|bad)$
3.30	10^{-1}
4.67	10^{-2}
5.72	10^{-3}

TABLE 4.5: THE LIST OF SOME THRESHOLDS T AND $Prob(|r_n| > T|bad)$ FOR $Es = 1$, $A = 0.01$ AND $\sigma_S^2/\sigma_I^2 = 1$. EQUATION (4.10) IS USED.

T	$Prob(\|r_n\| > T\|bad)$
10.00	10^{-1}
14.14	10^{-2}
17.32	10^{-3}

4.4 Simulation and threshold setting

4.4.1 General setting

In our simulation, we consider uncoded transmissions using QPSK-OFDM where the number of sub-carriers is 64. We use a two state IN model for which the noise variance or Power Spectral Density (PSD) is $\sigma_I^2/A + \sigma_G^2$ with probability A, and with probability $1-A$, the noise PSD is σ_G^2. Furthermore, two models of setting IN PSD σ_I^2 are considered, $\sigma_I^2 = \sigma_G^2/\Gamma$ and $\sigma_I^2 = \sigma_S^2/\Delta$, where σ_G^2 and σ_S^2 indicate the background noise PSD and the transmitted signal PSD, respectively. Fig. 4.1 shows our simulation block diagram.

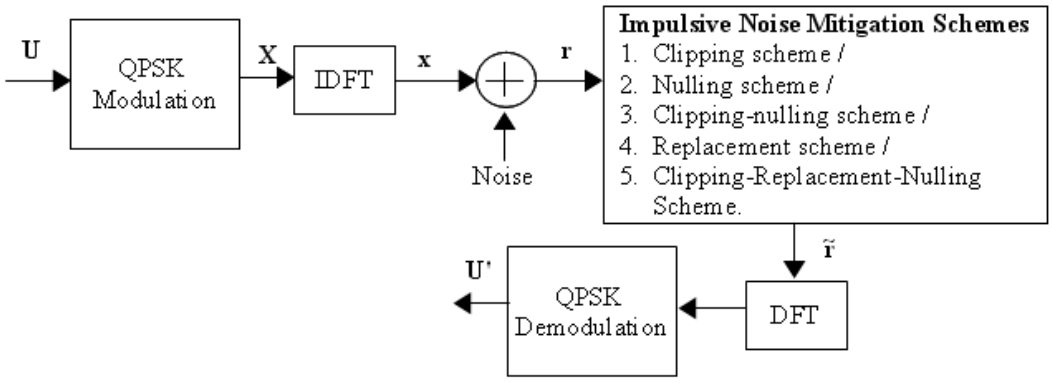

Figure 4.1: Simulation block diagram.

4.4.2 Specific setting for probability based thresholds

We first choose the reference probabilities of a received signal corrupted by background noise crossing T_{clip}, T_{rep} and T_{null}. The constraint applied is that IN mitigation schemes which employ their corresponding threshold values should bring a neglectable degradation in the BER performance of the transmitted signal. To achieve that, the PSD of the background noise added to the transmitted signal is assumed to be small enough such that the chosen reference probabilities are good enough to reduce the possibility of IN noise mitigation schemes to be applied on the transmitted signal. We consider transmissions in AWGN channel when $SNR = 13dB$ and choose 10^{-5} as the level of the neglectable degradation on the BER performance. This considered level of degradation is achieved if the crossing probabilities of T_{clip}, T_{rep} and T_{null} are, for instance, 10^{-5}, 10^{-7} and 10^{-10}, respectively (Fig. 4.2). Their corresponding threshold values (see Table 4.3), $T_{clip} = 2.23$, $T_{repref} = 2.63$ and $T_{nullref} = 3.14$, calculated using (4.9) are the lower bound values for T_{clip}, T_{rep}, and T_{null}, since we have a constraint on the level of the neglectable degradation on the BER performance, and reducing these values makes the constraint no longer valid. For all channel situations we fix T_{clip} because its value is a good value, based on our constraint, whereas T_{null} is allowed to change based on the IN parameters. To calculate the new value of T_{null} using (4.10) when IN parameters change, we need to determine $Prob(|r_n| > T|bad)$. We choose $Prob(|r_n| > T|bad) = 10^{-1}$ because we consider the average variance of the received samples in the *bad* state for calculating T and we want to combat as much IN as possible. To put T_{rep} in between T_{clip} and T_{null}, and also to make sure that the constraint on the level of degradation on the transmitted signal still holds, we apply the following algorithm:

1) if $T_{repref} \leq T_{null} < T_{nullref}$ then $T_{rep} = T_{null}$ and $T_{null} = T_{nullref}$;

2) if $T_{null} = T_{nullref}$ or $T_{null} < T_{repref}$ then $T_{rep} = T_{repref}$ and $T_{null} = T_{nullref}$;

3) if $T_{null} > T_{nullref}$ then $T_{rep} = T_{nullref}$.

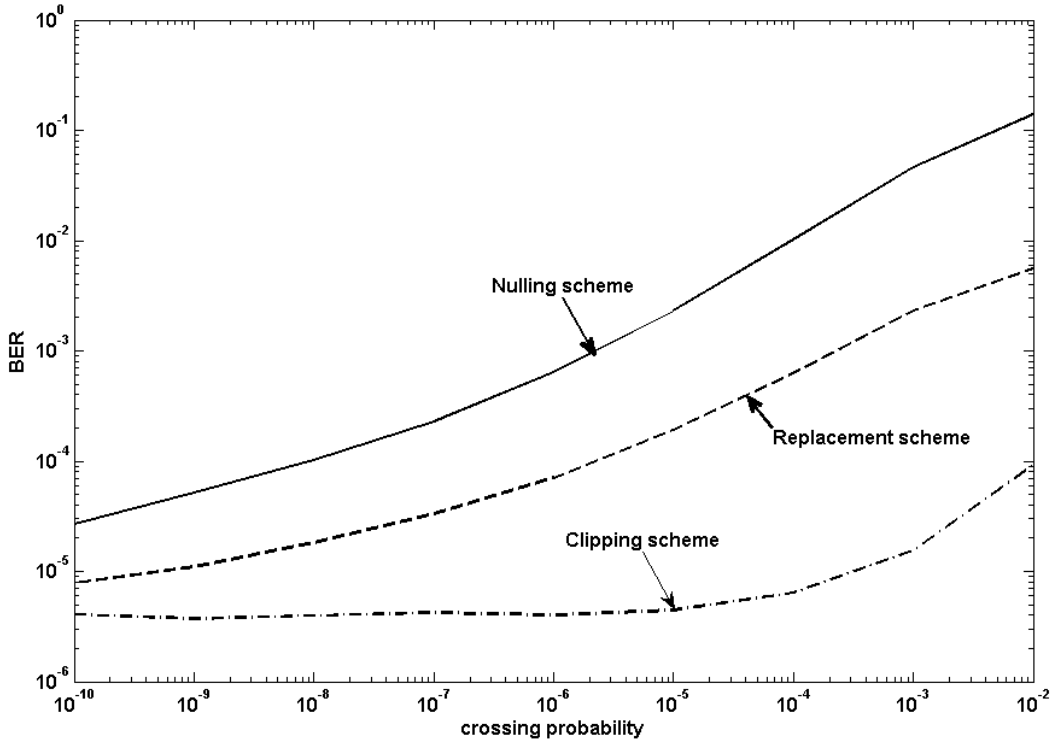

Figure 4.2: The BER performance of IN mitigations with different threshold values calculated using (4.9) in an AWGN channel when $SNR = 13dB$. The BER performance without any IN mitigation scheme is at 10^{-5}.

4.4.3 Specific setting for fixed thresholds

We fix T_{clip} and T_{null} for all channel situations and optimize T_{rep}. The T_{clip} used is defined as $c\sigma^2_{|x|}$, where c is a constant factor which needs to be optimized for a specific channel situation with respect to BER, and $T_{null} = 1.4T_{clip}$ [8], [10]. In the optimization process of T_{rep}, we choose a T_{rep} from Table 4.3 for which $Pr(|x_n| > T_{rep})$ is in between $Pr(|x_n| > T_{clip})$ and $Pr(|x_n| > T_{null})$ which gives the lowest BER.

4.5 Simulation results and discussions

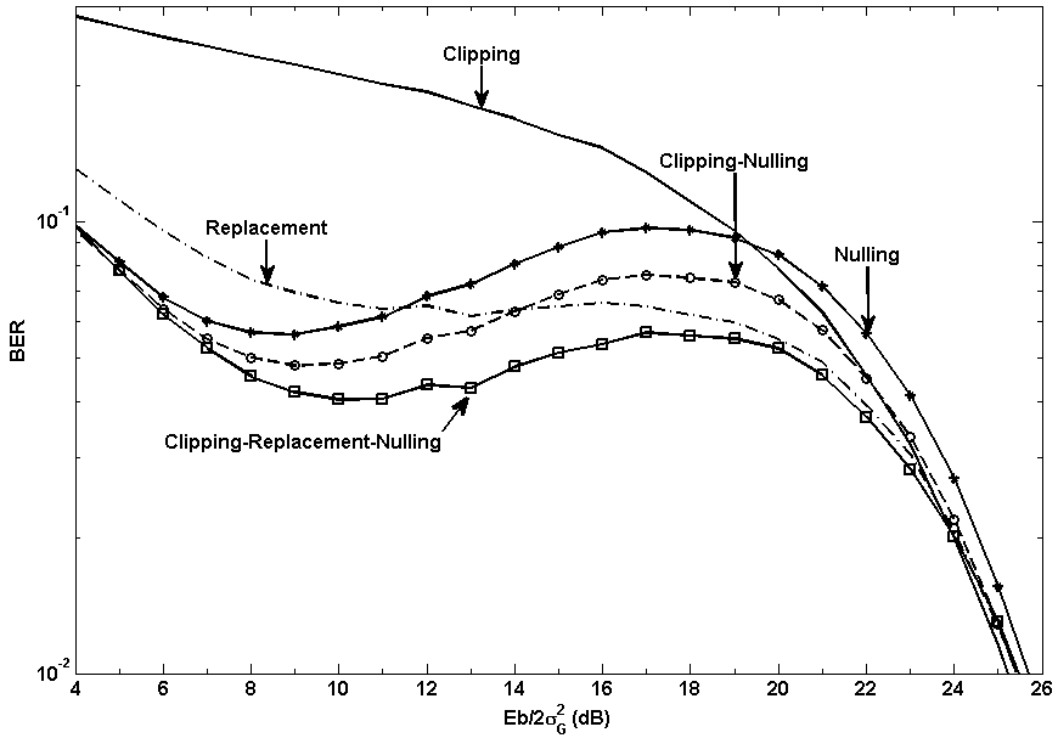

Figure 4.3: The performance of all mitigation schemes when $A = 0.1$ and $\Gamma = 0.01$. All thresholds are optimized with respect to the BER for channel with parameters $A = 0.1$ and $\Delta = 0.01$.

Fig. 4.3 shows the BER performance of all IN mitigation schemes for the channel where the PSD of IN depends on the PSD of the background noise. As can be seen, the proposed replacement (R) scheme brings a comparable result to the clipping-nulling (CN) scheme, while the clipping-replacement-nulling (CRN) scheme brings the best performance. We realize that the performance for this type of channel is strongly influenced by the SNR, since $\sigma_I^2 = \sigma_G^2/\Gamma$. Therefore, in the next simulations we consider the PSD of IN, $\sigma_I^2 = \sigma_S^2/\Delta$, which does not depend on the PSD of the background noise. Fig. 4.4 shows the performance of all non-joint mitigation schemes when the PSD of IN is independent of the background noise PSD. The nulling (N) scheme brings the best performance, whereas R scheme is better than the clipping (C) scheme. This result gives an indication that for a joint IN mitigation scheme, placing T_{rep} in between T_{clip} and T_{null} is a reasonable setting.

The results of the first scenario (see Section 4.4.2 and Figures 4.5 and 4.6) show that the performance of CRN scheme is better than the performance of CN scheme. This is

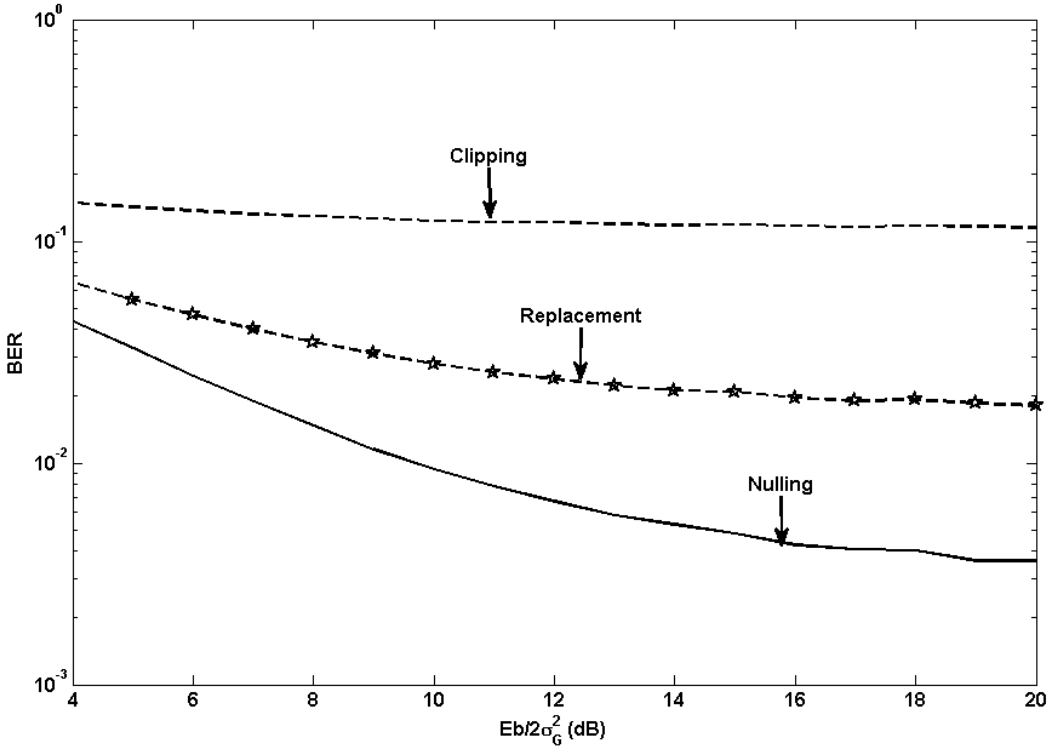

Figure 4.4: The performance of all non-joint IN mitigation schemes when $A = 0.1$ and $\Delta = 0.01$. All thresholds are optimized with respect to the BER.

due to the fact that for low IN PSD, T_{null} becomes closer to T_{clip} and thus more samples are nulled. To improve the performance, lower bound values, $T_{nullref}$ and T_{repref}, are needed. We put $T_{null} \geq T_{nullref}$ and put $T_{rep} \geq T_{repref}$ which is in between T_{clip} and T_{null} according to the algorithm. For high IN PSD, T_{null} becomes high and thus more samples with IN are clipped instead of nulled. We improve this situation by applying R scheme on the samples corrupted by IN which are above T_{rep} and below T_{null}. These results also confirm the correctness of the $Prob(|r_n| > T|bad)$ used, 10^{-1}, for calculating T. As can be seen, the performance produced by considering $Prob(|r_n| > T|bad) = 10^{-1}$ is better than the performance produced by $Prob(|r_n| > T|bad) = 10^{-3}$.

In the average of crossing probability point of view, as shown in (4.11), the performance of the first scenario can be explained as follows. Assuming that a good crossing probability is used then, when A is small, e.g. $A \leq 0.1$, a good T should be based on the first term. Whereas for larger A, a good T should be based on the second term.

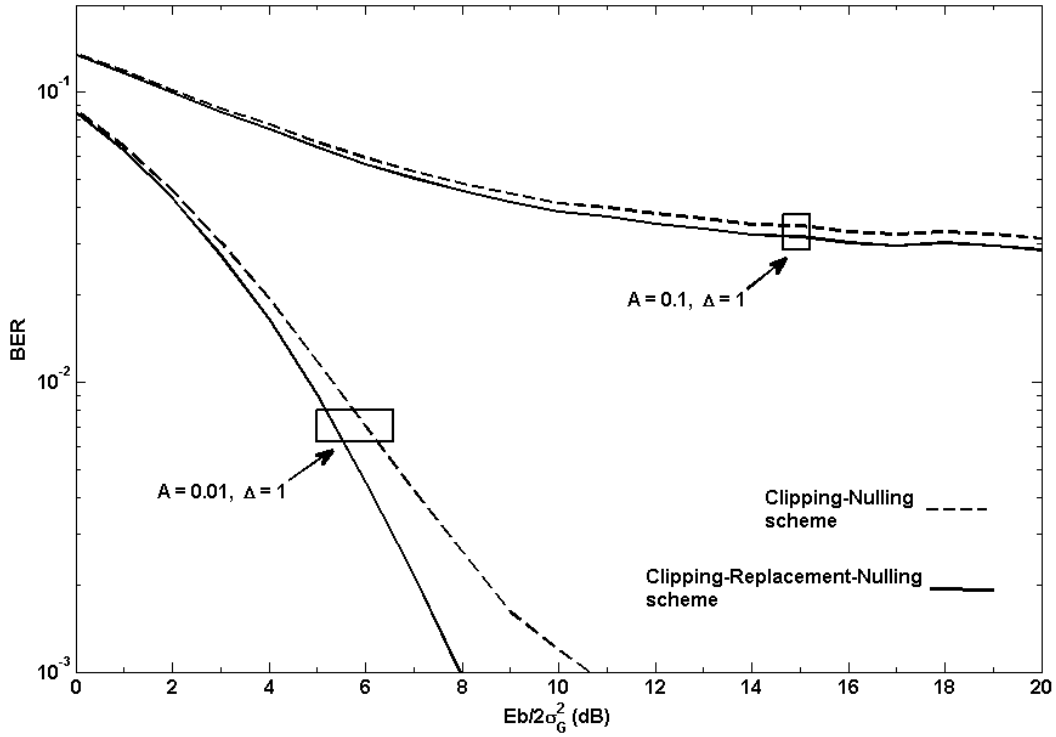

Figure 4.5: The performance of CN vs. CRN scheme in the first scenario when $\Delta = 1$. $Prob(|r_n| > T|bad) = 10^{-1}$ is used to calculate the new value of T_{null} using (4.10).

$$Pr(|r_n| > T) = (1 - A)(4.9) + (A)(4.10). \tag{4.11}$$

The important threshold, T_{null}, used by CN and CRN schemes is only based on the second term, whereas in CRN scheme, we introduce another important threshold, T_{rep}, which is actually based on the first term. As a result, the performance of CRN scheme is better than the performance of CN scheme. Fig. 4.7 shows the performance of CRN scheme in the situation where T_{rep} is based on the second term. It is clear to be observed that in this situation, the performance of CRN scheme is getting worst compared to that when T_{rep} is based on the first term. Fig. 4.8 shows the result in which only the first term is considered to calculate the new values of all thresholds. As can be seen, in *average* the performance of CRN scheme is better than the performance of CN scheme. But, the chosen crossing probability for calculating T_{rep} is not a good choice for all channel situations. Therefore, in a weakly disturbed channel, $A = 0.01$, the performance of CN scheme is better than the performance of CRN scheme.

Then, we also investigated the performance of CN and CRN schemes, in the situation

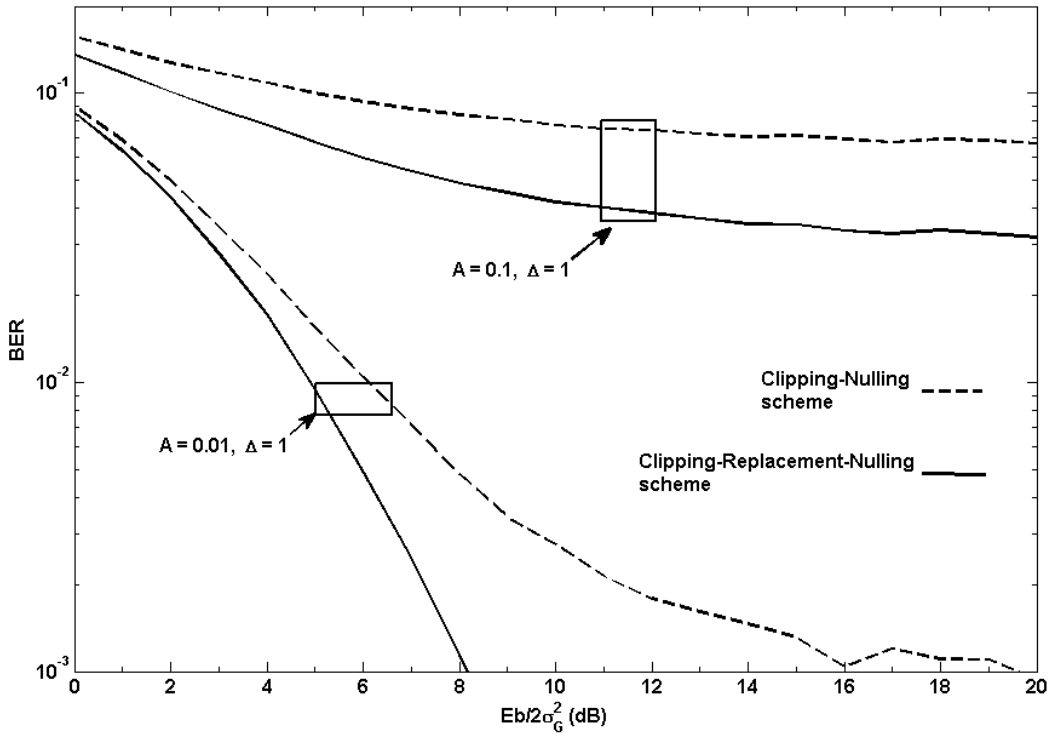

Figure 4.6: The performance of CN vs. CRN scheme in the first scenario when $\Delta = 1$. $Prob(|r_n| > T|bad) = 10^{-3}$ is used to calculate the new value of T_{null} using (4.10).

where T_{clip} is based on (4.10), whereas $T_{null} = 1.4T_{clip}$ [10][8]. For CRN scheme, $T_{rep} = 1.4T_{clip}$ and $T_{null} = 1.4T_{rep}$. We use $Prob(|r_n| > T|bad) = 10^{-1}$ to calculate the new value of T_{clip}. The result (Fig. 4.9) shows that the performance of CN and CRN schemes are comparable. It also shows that the scenario of setting T in which T_{clip} is allowed to move based on the IN parameters is a bad scenario compared to the first scenario (see Section 4.4.2).

In the second scenario (Section 4.4.3), we investigate the benefits of adding T_{rep} when we have a fixed threshold pair T_{clip} and T_{null}. The simulation results show that when T_{clip} and T_{null} are not optimized for the channel considered, the proposed CRN scheme is only beneficial for low PSD of IN (Fig. 4.10), while for high PSD of IN, no improvement can be expected (Fig. 4.11). This result is obvious because for low PSD of IN, with high probability OFDM samples corrupted by IN are below T_{null} and thus they will be detected only by either T_{clip} or T_{rep}. Since R scheme is better than C scheme (Fig. 4.4) then CRN scheme is better than CN scheme. In high PSD of IN, the performance of CN and CRN schemes are comparable because one can expect that OFDM samples corrupted by IN

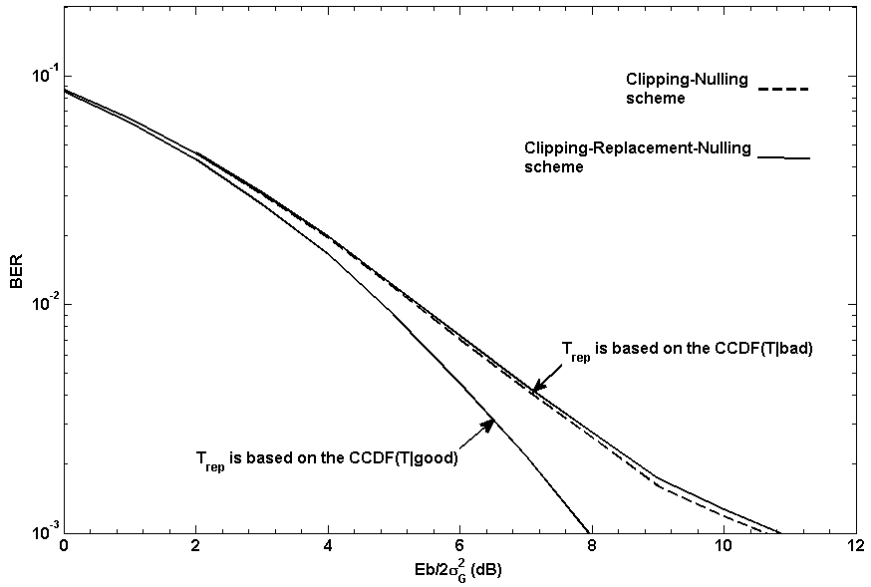

Figure 4.7: The performance of CN vs. CRN scheme when $A = 0.01$ and $\Delta = 1$. $Prob(|r_n| > T|bad) = 10^{-1}$ is used to calculate the new value of T_{rep} using (4.10), whereas $T_{null} = 1.4T_{rep}$.

are always above T_{null}. In the case where all thresholds are optimized, no benefits can be obtained (Fig. 4.12).

4.6 Conclusion

We introduced a new simple IN mitigation scheme called *replacement scheme*. In this scheme, the magnitude of a received OFDM sample which is above T_{rep} is replaced with the average magnitude $|\bar{x}|$ of the noiseless OFDM samples. The simulation result shows that in the channel where the PSD of IN depends on the PSD of the background noise, this scheme produces a comparable performance to the clipping-nulling scheme, whereas when the PSD of IN is independent of the background noise PSD then the replacement scheme is better than the clipping scheme.

Having the replacement scheme, we introduced and investigated the benefits of the joint *clipping-replacement-nulling scheme*. The investigation involves two basic scenarios of setting T_{clip} and T_{null}, i.e. T_{clip} and T_{null} which are based on the CCDF of a Rayleigh distribution, and the classical setting of T_{clip} and T_{null}, as also used in [8], [10]. The results show that the proposed scheme brings a reduction in the BER under the condition that

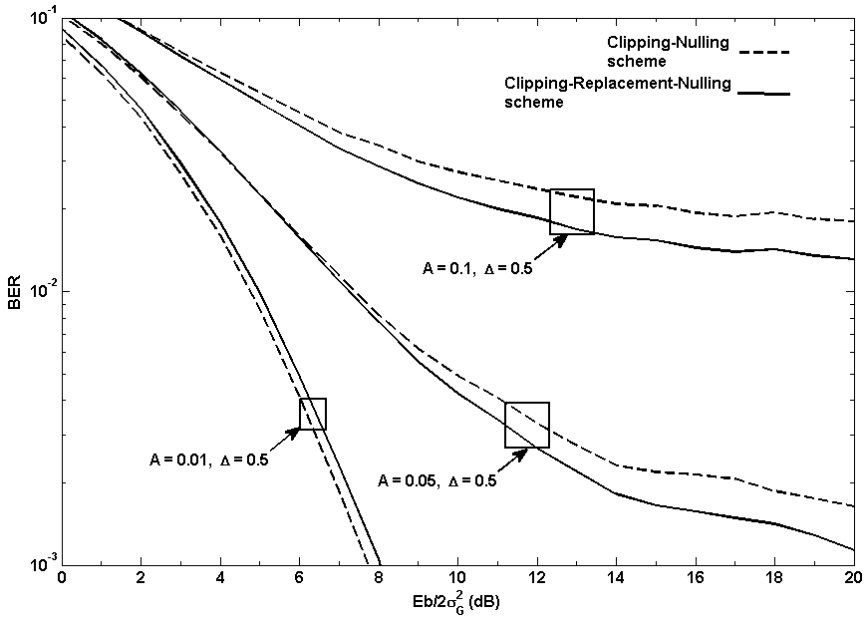

Figure 4.8: The performance of CN vs. CRN scheme when $\Delta = 0.5$. $Prob(|x_n| > T) = 10^{-5}$, $Prob(|x_n| > T) = 10^{-7}$, and $Prob(|x_n| > T) = 10^{-10}$ are used to calculate the new values of T_{clip}, T_{rep} and T_{null} using (4.9).

a good crossing probability for calculating the value of T_{rep} is used.

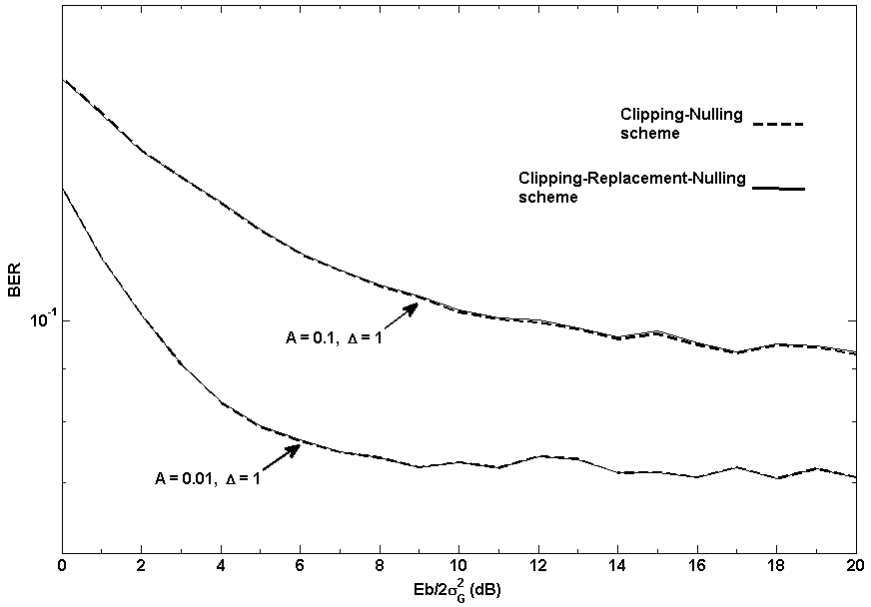

Figure 4.9: The performance of CN vs. CRN scheme when $\Delta = 1$. $Prob(|r_n| > T|bad) = 10^{-1}$ is used to calculate the new value of T_{clip} using (4.10). For the CN scheme, $T_{null} = 1.4T_{clip}$. For the CRN scheme, $T_{rep} = 1.4T_{clip}$ and $T_{null} = 1.4T_{rep}$.

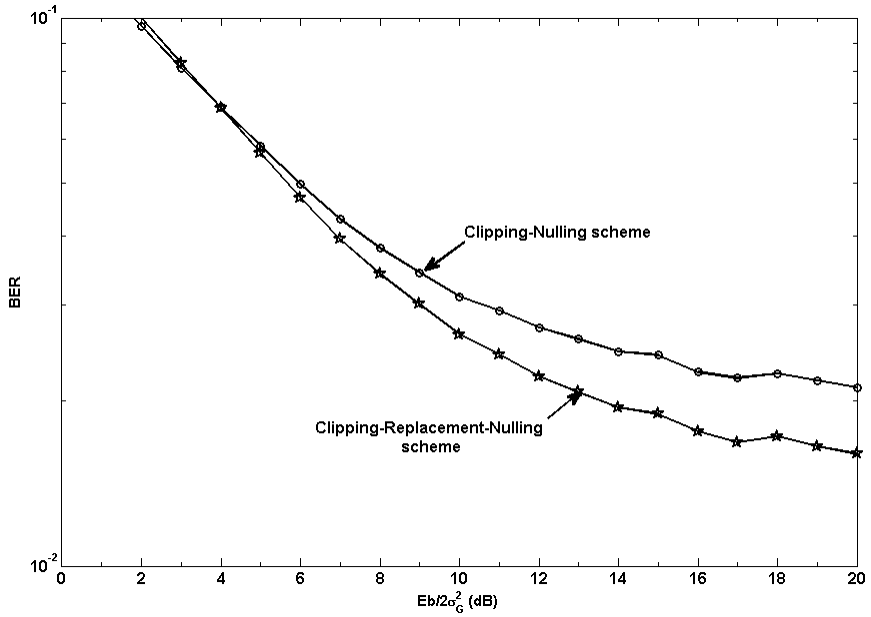

Figure 4.10: The performance of CN vs. CRN scheme in the second scenario when $A = 0.1$ and $\Delta = 1$. T_{clip} and T_{null} are optimized for channel with parameters $A = 0.1$ and $\Delta = 0.1$.

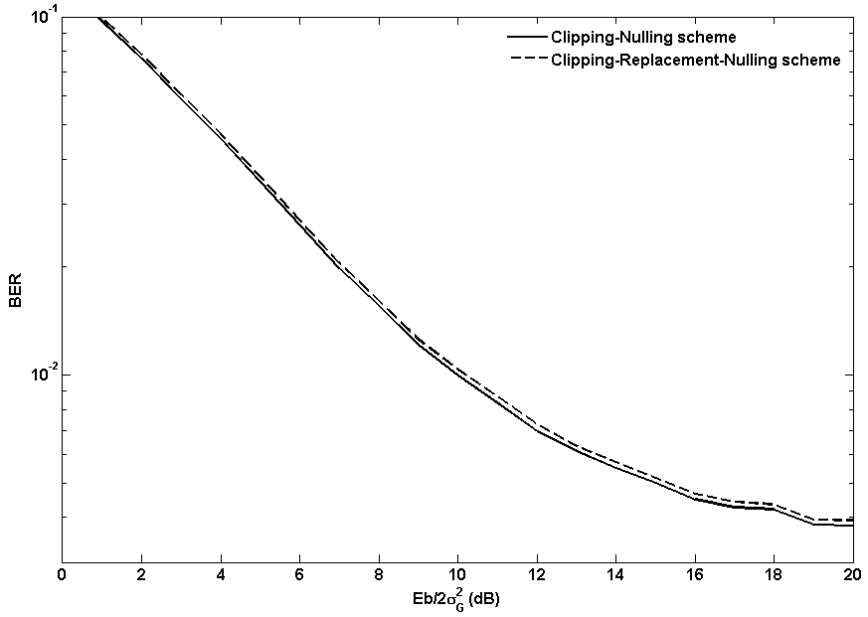

Figure 4.11: The performance of CN vs. CRN scheme in the second scenario when $A = 0.1$ and $\Delta = 0.01$. T_{clip} and T_{null} are optimized for channel with parameters $A = 0.1$ and $\Delta = 0.1$.

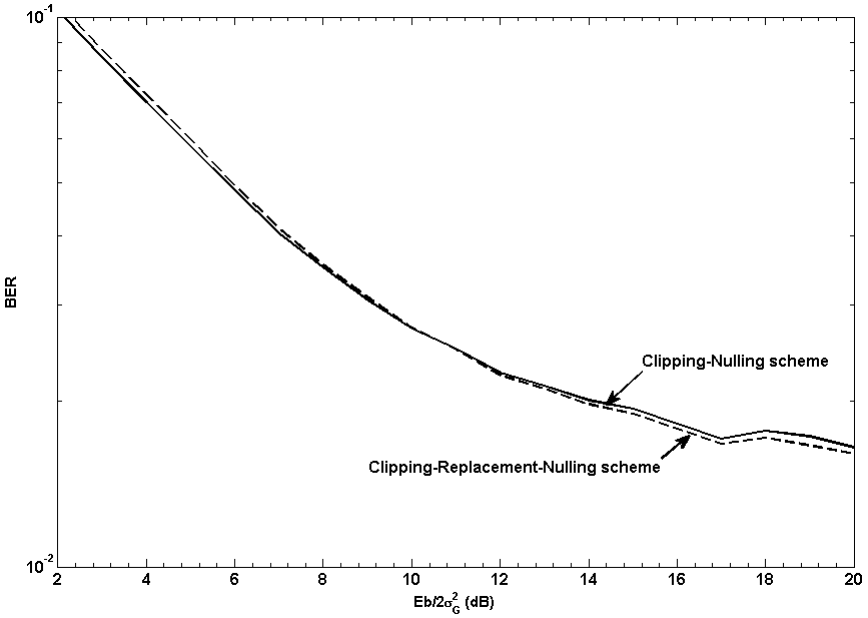

Figure 4.12: The performance of CN vs. CRN scheme in the second scenario when $A = 0.1$ and $\Delta = 1$. All thresholds are optimized for the considered channel.

5 A New Way of Combining Impulsive Noise Mitigation Schemes

A conventional joint impulsive noise (IN) mitigation scheme allows a combination between two or more different IN mitigation schemes with different threshold values. As an example, the clipping-nulling scheme joins the clipping scheme and the nulling scheme, where the clipping threshold is different from the nulling threshold. It is expected that a joint scheme must deliver a good performance compared to the performance of its individual schemes: the clipping-nulling scheme is expected to deliver a better performance than the performance of the clipping and the nulling schemes. However, this expectation can only be fulfilled if and only if the threshold value(s) used matches the channel parameters, i.e. it is well optimized. We proposed a new way of combining IN mitigation schemes such that the performance of a combined scheme is at least the same as the performance of its individual schemes. Furthermore, our proposed scheme offers a higher flexibility in combining any of the known IN mitigation schemes, compared to the conventional joint IN mitigation scheme.

5.1 Introduction

An L-point discrete Fourier transform (DFT) orthogonal frequency division multiplexing (OFDM) system spreads the power of impulsive noise (IN) over L-OFDM sub-carriers. As a result, all transmitted symbols are affected which leads to degradation in performance [22]. To solve this problem, the magnitudes of OFDM samples which are corrupted by the IN must be limited prior to the DFT process. Two examples of ways to do this are: to clip (the clipping scheme) [4] or to null (the nulling scheme) [5], [6] the magnitudes of OFDM corrupted samples.

Zhidkov [8] showed that by joining the clipping (C) and nulling (N) schemes, forming the joint CN scheme (or simply the CN scheme), an additional gain can obtained. In [7], we introduced a replacement (R) scheme and proved that a CRN scheme brings further additional gain. However, a problem remains. A joint scheme brings a lower performance than its individual schemes when the threshold values used do not match the channel parameters.

In this chapter, we reported on a new idea of combining IN mitigation schemes that can deliver the best performance that can be obtained by its individual schemes. This capability is obtained even if the threshold value used is not well optimized. Furthermore, the proposed scheme allows not only the combination between different IN mitigation schemes with different threshold values, as a conventional joint scheme does, but also: the combination between different IN mitigation schemes with the same threshold value; and the combination of an IN mitigation scheme with different threshold values.

Having the properties mentioned and an optimum decision to select the best IN mitigation output as will be explained in the next section, the proposed scheme enables an OFDM system to obtain a good performance even when the signal-to-noise ratio (SNR) is unknown.

5.2 New combined scheme

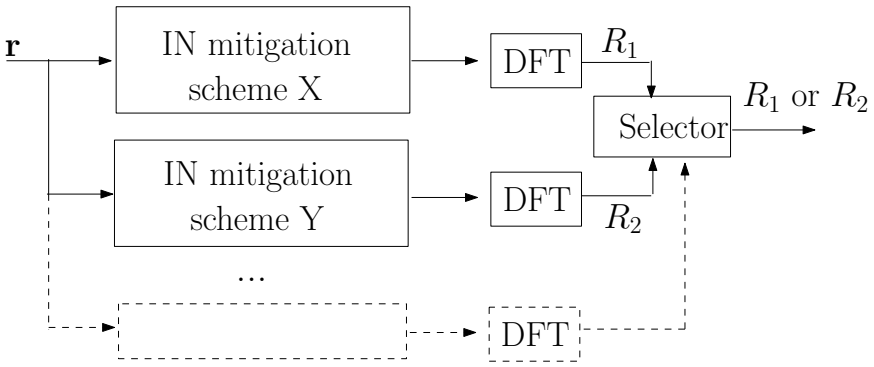

Figure 5.1: New combined scheme.

Fig. 5.1 illustrates the proposed scheme. We apply two different IN mitigation schemes on the received samples **r** in the time domain. In the frequency domain, a selector is used to select the best mitigation output. It is important to notice that: 1) the schemes X and

Y, where X, Y ∈ { C, N, R, CR, CN, RN, CRN }, 2) and the scheme X can also be the scheme Y with a different threshold value.

The selection mechanism is as follows. An element of an output vector, i.e. R_{1i} or R_{2i}, is a complex value $a_i + b_i j$. Each element has its referenced value $a_0 + b_0 j$ in the complex band, which is a baseband symbol with the least Euclidean distance E_i,

$$E_i = \sqrt{(a_i - a_0)^2 + (b_i - b_0)^2}. \tag{5.1}$$

The total Euclidean distance D_r of the output vector R_r is then defined as

$$D_r = \sqrt{\sum_{i=1}^{L} E_i^2}, \tag{5.2}$$

Definition 1 The best output vector is the vector with the least total Euclidean distance. As an example, if $D_1 < D_2$ then R_1 is selected as the best IN mitigation output.

The justification of the proposed selecting algorithm is as follows. The minimum Euclidean distance detection is optimum under the assumption that the noise power after a DFT appears as independent Gaussian noise on every OFDM sub-carrier. We assume that the assumption is true for $L \geq 64$.

5.3 Simulations

We used the simplified model of the Middleton's additive white class A noise (AWCN) model – the two-state additive noise model – as depicted in Fig. 5.2. The transmitted signal is corrupted by the additive white Gaussian noise (AWGN) and the IN with probability A, and is corrupted by only the AWGN with probability $1 - A$. The variances of the AWGN and the IN are σ_G^2 and σ_I^2, respectively. For all simulations, QPSK-64OFDM transmission is used.

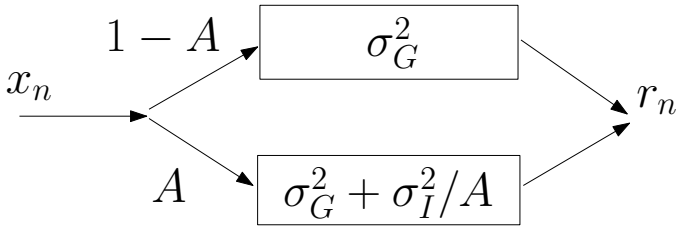

Figure 5.2: Two-state additive noise model.

5.3.1 Simulation 1

We showed that as opposed to the conventional joint scheme, our proposed scheme delivers the best performance that can be obtained by its individual schemes (Figures 5.3 - 5.5). In the simulations, the threshold values for the clipping threshold T_{clip} and the nulling threshold T_{null} are not optimized.

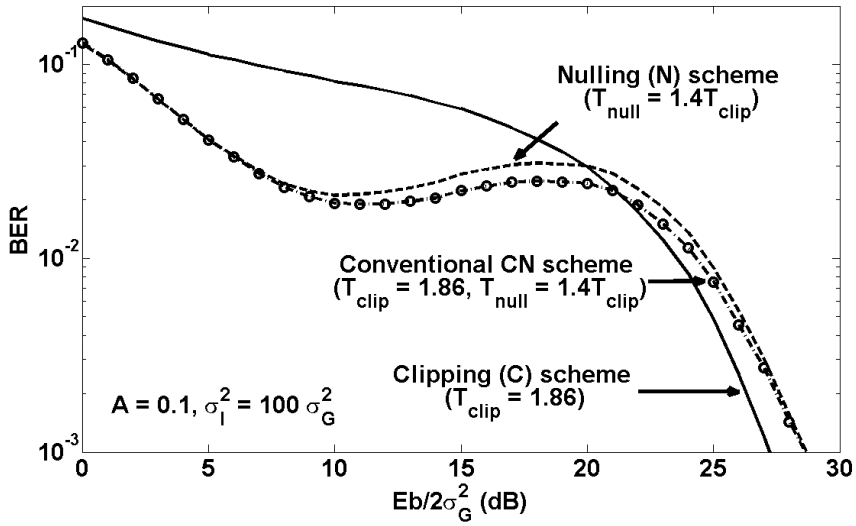

Figure 5.3: The performance of the C, the N, and the conventional CN scheme, when $A = 0.1$ and $\sigma_I^2 = 100\sigma_G^2$.

5.3.2 Simulation 2

This simulation shows the performance of the conventional CN scheme and the proposed combined R-N scheme in a coded system. As the error control code, we use the "permutation code plus" [2], with minimum Hamming distance $d_{min} = 3$ and code efficiency

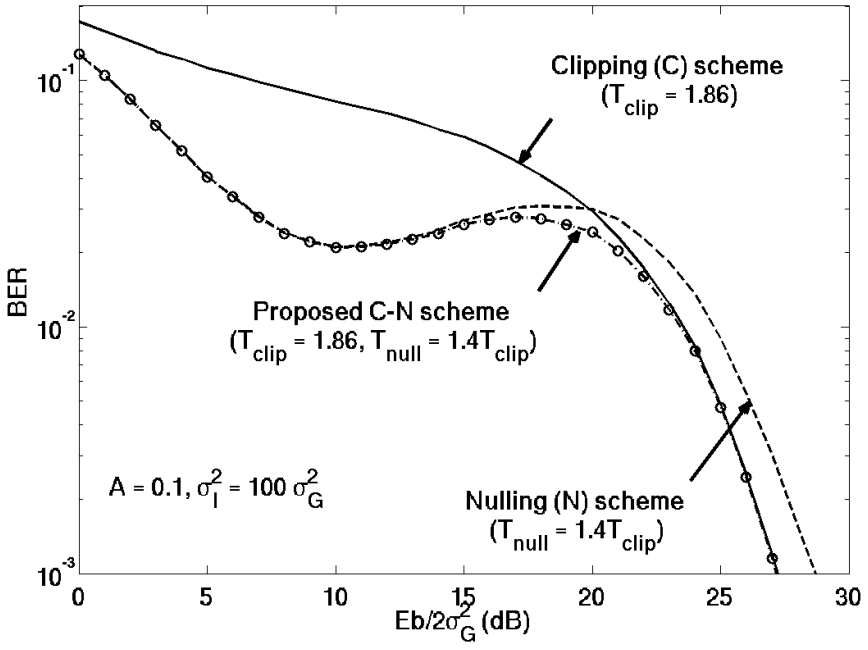

Figure 5.4: The performance of the C, the N, and the proposed combined C-N scheme, when $A = 0.1$ and $\sigma_I^2 = 100\sigma_G^2$.

$R = 1/2$. Hard decision decoding is used. The threshold setting is as follows: T_{clip} is optimized with respect to the bit error rate (BER); the replacement threshold $T_{rep} = T_{clip}$; and $T_{null} = 1.4T_{clip}$ [8]. Fig. 5.6 shows that the coded system performance is worse than that of uncoded system in the higher SNR. This is due to the fact that the net coding gain G_c in dB for hard decision decoding (Eq. 5.3, see [25]) is negative. As it can be seen the proposed scheme delivers additional gain in the BER, and as a result the loss introduced by the G_c is minimized.

$$G_c := 10log_{10}R\frac{d_{min}}{2}\ dB. \tag{5.3}$$

5.4 Conclusion

We have shown a new idea of combining impulsive noise (IN) mitigation schemes. The simulation results confirm that the proposed idea has the following properties:

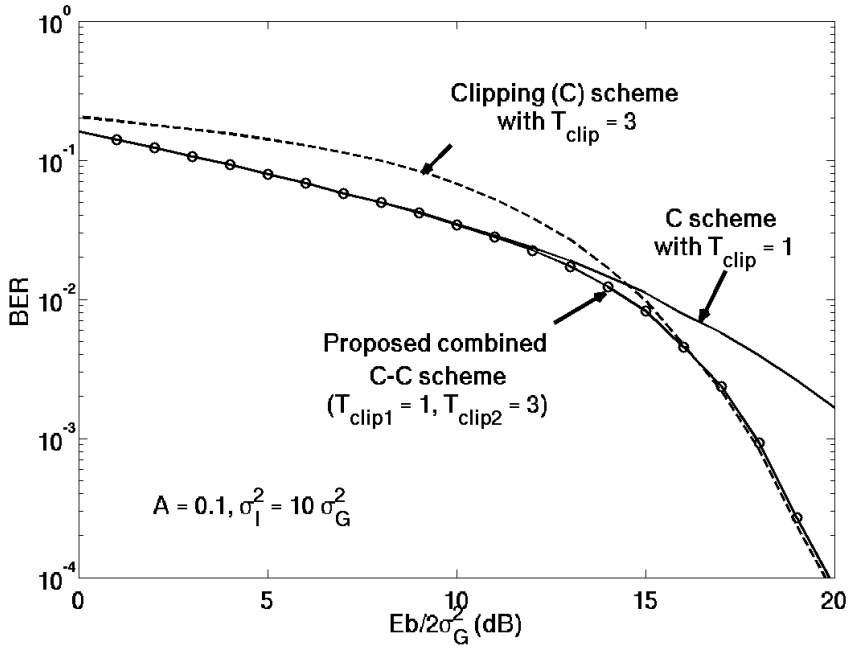

Figure 5.5: The performance of the C scheme with different threshold values and the proposed combined C-C scheme, when $A = 0.1$ and $\sigma_I^2 = 10\sigma_G^2$.

1. it provides a high flexibility in combining any of the known non-iterative IN mitigation schemes considered in this article and

2. it delivers the best performance that can be obtained by its individual schemes.

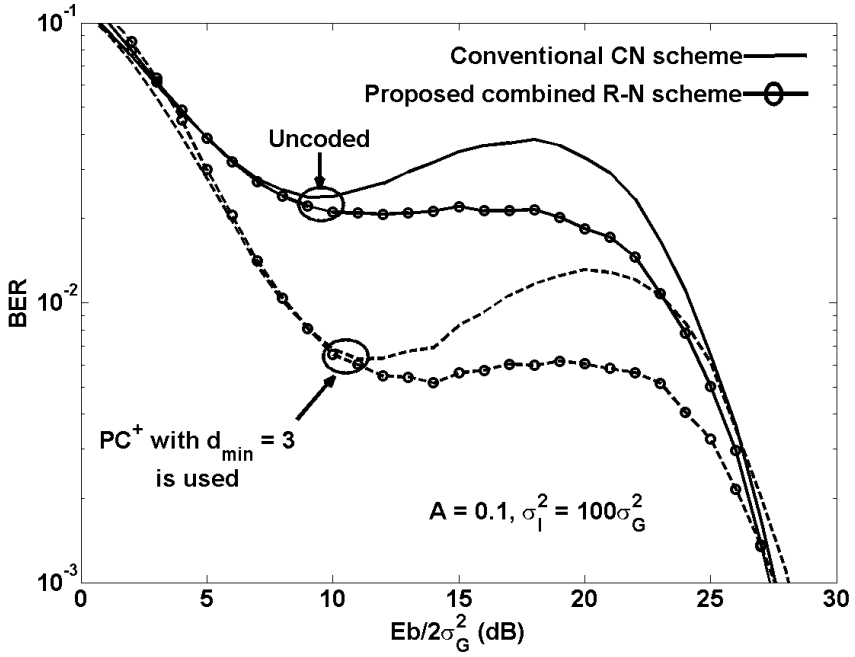

Figure 5.6: The coded system performance of the conventional CN scheme and the proposed combined R-N scheme for $A = 0.1$ and $\sigma_I^2 = 100\sigma_G^2$. "Permutation code plus" with Hamming distance $d_{min} = 3$ is used.

6 Improving performance of the MH-iterative Impulsive Noise Mitigation Scheme

We call Häring (H)-iterative scheme with the clipping-nulling (CN) as the pre-processing impulsive noise (IN), the Mengi-Häring (MH)-iterative scheme. In this chapter, we report two ideas that can significantly improve its performance. The first idea is to use the replacement-nulling (RN) scheme as the pre-processing IN mitigation scheme. The second idea is to use the output vector of the pre-processing IN mitigation scheme in all iterations. To show the performance comparison between the MH-iterative scheme and our proposed scheme, we conduct some simulations in the simplified model of the Middleton's additive white class A noise (AWCN) model and present performance in terms of the bit error rate (BER) as a function of the signal-to-noise ratio (SNR).

6.1 Introduction

The usage of the power line channel (PLC) as a communication medium is an interesting idea. However, the PLC is not a friendly channel for information delivery. It has many problems such as signal attenuation, narrow-band interference and also impulsive noise (IN). We presented a solution for handling degradation in performance of orthogonal frequency-division multiplexing (OFDM) based transmission caused by the presence of IN.

The research direction of the IN mitigation schemes for OFDM is basically divided into two categories: parametric and non-parametric IN mitigation schemes. The parametric scheme requires the knowledge of IN parameters, while the non-parametric does not require any knowledge of the IN parameters. Thus, the benefit of the non-parametric

IN mitigation scheme over the parametric scheme is that it can be used on different IN channel models.

The basic idea of a parametric scheme, which is a threshold based approach, can be divided into two parts: determining the threshold value to be used and determining the action to be taken. Only the first part – the determination of the threshold value to be used – requires the full [10] or partial [23] knowledge of the IN parameters . The second part on the other hand requires no knowledge of the IN parameters. Therefore, when the first part of a parametric scheme is designed to not depend on the IN parameters, the parametric scheme has been turned into a non-parametric scheme. Some recent publications on the non-parametric IN mitigation schemes for OFDM system are in [7], [26], [27].

The two categories of the IN mitigation schemes mentioned before can be further divided into two types: iterative and non-iterative schemes. The difference between these two types is on the usage of a feedback mechanism that allows iterative IN mitigation processes: an output of i^{th} IN mitigation process is used as an input of $(i+1)^{th}$ mitigation process. An iterative scheme uses the feedback mechanism whereas, a non-iterative scheme does not use it.

This chapter focuses on ideas to improve a known iterative IN mitigation scheme for an OFDM system, called Mengi-Häring (MH)-iterative scheme [10]. The MH-iterative scheme is an extension of the Häring (H)-iterative scheme [22] where the clipping-nulling (CN) scheme [8] is added as a pre-processing IN mitigation scheme. The usage of the pre-processing IN mitigation scheme is to increase the reliability of the first noise estimate by reducing the IN power. This simple idea is an interesting idea since it improves the performance of the H-iterative scheme while maintaining low complexity in the receiver design. However, we notice that the structure of the MH-iterative scheme allows the usage of unreduced IN power in the IN iterative mitigation process, which reduces the reliability of the noise estimate in the next iterations.

In this chapter, we show two ideas that can improve the performance of the MH-iterative scheme significantly. First, the modification of the MH-iterative scheme structure, such that the IN power is reduced in all IN iterative mitigation processes, and therefore a good reliability of the noise estimate can be preserved in all iterations. Second, we show that the usage of the replacement-nulling (RN) scheme as the pre-processing IN mitigation scheme, instead of the CN scheme, will bring additional performance improvement.

The rest of the chapter is organized as follows. Section 6.2 explains the system model used. In Section 6.3 the MH-iterative scheme will be explained, whereas in Section 6.4, we present the proposed ideas. Sections 6.5 and 6.6 are to report the simulation results and to conclude our chapter.

6.2 System model

An OFDM system is a pair of Inverse Discrete Fourier Transform (IDFT) and Discrete Fourier Transform (DFT). The IDFT is commonly used at the transmitter side, while the DFT is used at the receiver side.

The IDFT at the transmitter side is used to generate the time-domain OFDM samples x_n, or the complex baseband transmitted signal, from baseband symbols X_k as

$$x_n = \frac{1}{\sqrt{N}} \sum_{k=0}^{N-1} X_k e^{j2\pi nk/N}, \tag{6.1}$$

where N is the number of OFDM sub-carriers, X_k is a baseband symbol, and x_n is of the same length as X_k.

At the receiver side, the DFT is then used to transform the received time-domain OFDM samples r_n to its frequency-domain representation. It is obvious that if the received time-domain OFDM samples are noiseless, i.e. $r_n = x_n + n_n$, where n_n is the additive noise sample and $n_n = 0$, then the output of the DFT is basically the transmitted baseband symbols X_k,

$$X_k = \sum_{n=0}^{N-1} r_n e^{-j2\pi nk/N}. \tag{6.2}$$

If r_n is noisy, i.e. $n_n \neq 0$, then an additional step such as e.g. Maximum-likelihood (ML) estimation is needed to get the approximation U_k of the transmitted baseband symbols X_k.

The MH-iterative scheme, and thus our proposed scheme, uses the combination between IDFT, DFT and also the Maximum-likelihood (ML) estimation to form the IN

iterative mitigation process at the receiver side as will be discussed in Sections 6.3 and 6.4.

To simplify simulations and analysis, we use the simplified model of the Middleton's additive white class A noise (AWCN) model to describe the presence of the noise (Fig. 6.1). In this model, which is also called *two-state IN channel model* and can be seen as a simplified PLC channel model (see also [28]), the transmitted signal is corrupted by the AWGN and the IN with probability A, and is corrupted by only the AWGN with probability $1 - A$. The variances of the AWGN and the IN are σ_G^2 and σ_I^2, respectively. The AWCN model was also used in [10] and [22], and therefore it is sufficient to be used to show a fair comparison between the MH-iterative scheme and the proposed scheme.

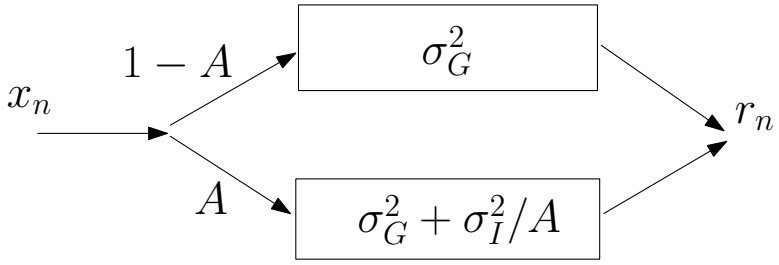

Figure 6.1: The simplified model of the Middleton's additive white class A noise (AWCN) model.

6.3 MH-iterative scheme

Fig. 6.2 [10] shows the blocks diagram of the MH-iterative scheme, which works as follows.

In the zeroth iteration, $l = 0$, the CN scheme is used to do preliminary IN mitigation. Its result, vector $\widetilde{r}$, is then used as an input to the DFT. In the next iterations, $l > 0$, where the vector $\widetilde{r}$ is not used anymore, the following steps are applied.

In every iteration $l > 0$, the better approximation of the transmitted time-domain OFDM samples vector $r^{(l+1)}$ are transformed to the frequency-domain representation with the help of the DFT. After that, the Maximum-likelihood (ML) estimation is used to approximate transmitted baseband symbols $U^{(l)}$. The noise vector $n^{(l)}$ in the received samples vector r (or $r^{(0)}$) is defined as $n^{(l)} = r^{(0)} - c^{(l)}$, where $c^{(l)}$ is the representation of $U^{(l)}$ in the time-domain. The detection of the components in $n^{(l)}$ which are the IN, $\widetilde{n}^{(l)}$,

is done in the time-domain with the help of a threshold Thr as follows:

$$\widetilde{n}_i^{(l)} = \begin{cases} 0, & for \quad |n_i|^{(l)} \leq Thr \\ n_i^{(l)}, & for \quad |n_i|^{(l)} > Thr \end{cases} . \tag{6.3}$$

The input vector for the next iteration is defined as $r^{(l+1)} = r^{(0)} - \widetilde{n}^{(l)}$.

Having the mechanism explained, the scheme is expected to improve $U^{(l)}$ (or $c^{(l)}$) in every iteration, such that the approximation of the noise $n^{(l)}$ becomes more accurate.

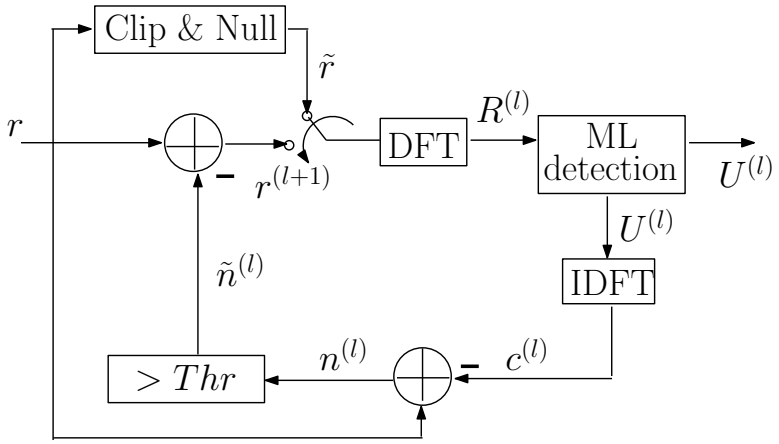

Figure 6.2: MH-iterative scheme.

As can be noticed, the structure of the MH-iterative scheme allows the usage of unreduced IN power in the IN iterative mitigation process. This leads to a reduction in the reliability of the noise estimate in the next iterations, since the IN variance influences strongly the calculation of the threshold Thr. The detailed discussion on this topic is covered in Section 6.5.2. Therefore in the next section, we propose a modification on the MH-iterative scheme structure as a solution to this problem. We also explain the motivation of replacing the CN scheme with the RN scheme as the pre-processing IN mitigation scheme.

6.4 Proposed modifications

The proposed modifications for the MH-iterative scheme are described using Fig. 6.3.

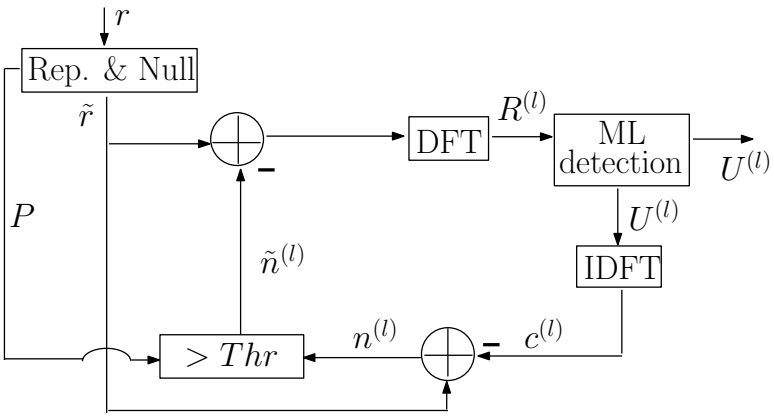

Figure 6.3: Proposed modifications for the MH-iterative scheme.

6.4.1 First modification: we use the RN scheme as the pre-processing IN mitigation scheme

In [7] we introduced the replacement (R) scheme and showed that it delivers a better performance than the C scheme. Therefore our first proposed modification is to use the combination between the R scheme and the N scheme, forming the replacement-nulling (RN) scheme, instead of the combination between the C scheme and the N scheme, as the pre-processing IN mitigation scheme. The decision of the RN scheme is as follows,

$$\widetilde{r_n} = \begin{cases} r_n, & for \quad |r_n| \leq T_{rep} \\ |\bar{x}|e^{jargr_n}, & for \quad T_{rep} < |r_n| \leq T_{null} \\ 0, & for \quad |r_n| > T_{null} \end{cases}, \tag{6.4}$$

where $\widetilde{r_n}$ is the sample that is obtained after the mitigation process, $|\bar{x}|$ is the average magnitude of the OFDM noiseless samples,

$$|\bar{x}| = \sqrt{\frac{\pi\sigma_S^2}{4}}, \tag{6.5}$$

where σ_S^2 is the variance of the transmitted signal. The replacement threshold and the nulling threshold are defined as T_{rep} and T_{null}, respectively.

6.4.2 Second modification: we use $\widetilde{r}$ in all iterations

The second modification is to use the vector $\widetilde{r}$ in all iterations instead of only in the zeroth iteration as the MH-iterative scheme does. In this way, we limit the power spectral density (PSD) of the IN, σ_I^2, in the received samples vector r that will be used in all iterations.

Now, we discuss the basic reason of using a pre-processing IN mitigation scheme in the zeroth iteration, $l = 0$, and its relation to the next iterations $l > 0$. When a sample r_i is detected as being corrupted by the IN, then the pre-processing IN mitigation scheme changes the magnitude of the corrupted samples to a "better" magnitude based on its rule: for the R scheme, the "better" magnitude is $|\bar{x}|$ whereas for the N scheme it is zero. The "better" magnitude can be further improved by replacing it with the output of the IDFT on every iteration, $c_i^{(l)}$. We assume that $c^{(l)}$, which is the approximation of the transmitted OFDM noiseless samples in iteration l, gets better from iteration to iteration. Therefore, in the set of positions P where the pre-processing IN mitigation scheme has been applied, we set $Thr = 0$. As a result, $\widetilde{r}_i^{(l+1)} = \widetilde{r}_i^{(0)} - \widetilde{n}_i^{(l)} = c_i^{(l)}$, where $i \in P$. For other positions $k \notin P$ in which the pre-processing IN mitigation scheme has not been applied, the following situations occur:

6.4.2.1 $c_k^{(l)}$ is the correct estimate of the transmitted sample

let x_k be the correct transmitted sample and $\widetilde{r}_k^{(0)} = x_k + n_k$, where n_k is a noise component. Thus, in this case the $n_k^{(l)} = \widetilde{r}_k^{(0)} - c_k^{(l)}$ contains only the underlying background noise or the IN. The input vector for the next iteration $\widetilde{r}^{(l+1)}$ is then decided as follows,

$$\widetilde{r}_k^{(l+1)} = \begin{cases} \widetilde{r}_k^{(0)}, & for \quad |n_k|^{(l)} \leq Thr \\ c_k^{(l)}, & for \quad |n_k|^{(l)} > Thr \end{cases} . \tag{6.6}$$

It is important to notice, that when $|n_k|^{(l)} \leq Thr$ the basic iterative algorithm takes the corrupted transmitted sample, $\widetilde{r}_k^{(0)}$, instead of taking the correct transmitted sample itself, $c_k^{(l)}$. This means it might degrade the performance at high-SNR.

6.4.2.2 $c_k^{(l)}$ is the incorrect estimate of the transmitted sample

in this case, there is an additional noise $e_k^{(l)} = x_k - c_k^{(l)}$ which is called wrong decision noise. The input vector for the next iteration $\widetilde{r}^{(l+1)}$, on the other hand, remains the same as it is given in (6.6).

6.5 Simulations and discussions

We simulate QPSK-256OFDM uncoded transmission (see Fig. 6.4) with variance of the transmitted signal $\sigma_S^2 = 1$. The two-state IN channel model as explained in Section 6.2 is used. When a pre-processing IN mitigation scheme such as the CN or the RN scheme is used, the threshold setting is: $T_{clip} = 2.2\sigma_S^2$ and $T_{null} = 1.4T_{clip}$ [10]; $T_{rep} = T_{clip}$.

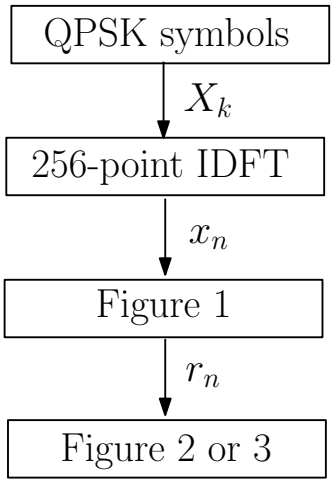

Figure 6.4: Simulation block diagram.

In [22] the threshold used to detect the location of the IN in $n^{(l)}$ is defined as $Thr = c.\sigma_e$, where c is a constant factor and σ_e^2 is the variance of the statistical independent noise caused by wrong decisions made by the detect-operator. However, using a threshold which is a function of *only* the wrong decision variance is not practical, since it requires the knowledge of the transmitted samples (see Section 6.4.2.2). Therefore, in simulations we consider the threshold Thr which is a function of the noise variance in each iteration l, $Thr = c.\sigma_n^{(l)}$, and it can be calculated from the vector $n^{(l)}$. The constant factor $c \geq 1$ itself is a subject to be optimized with the help of a brute-force search with respect to the BER.

6.5.1 Simulation 1: Is the usage of the RN scheme as the pre-processing IN mitigation scheme a good idea ?

This simulation is to show the performance of the Häring-iterative scheme when the output of a pre-processing IN mitigation scheme is used in the zeroth iteration only (Mengi's idea [10]). Two different simple IN mitigation schemes will be considered, the clipping-nulling (CN) scheme (the MH-iterative scheme idea) and the replacement-nulling (RN) scheme (our first idea, see Section 6.4.1).

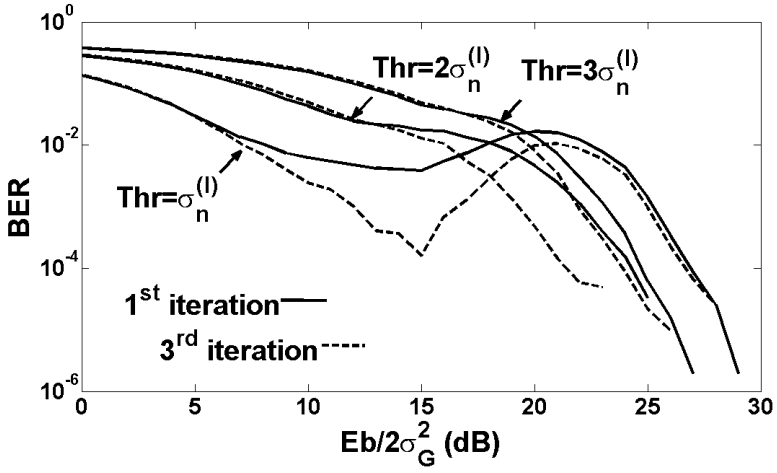

Figure 6.5: Performance of the Häring-iterative scheme with the CN scheme as the pre-processing IN mitigation scheme. Different values of the threshold Thr are considered. The IN parameters are: $A = 0.1, \sigma_I^2 = 100\sigma_G^2$.

The threshold setting for T_{clip}, T_{rep} and T_{null} follows the explanation in Section 6.5. The threshold Thr which is used to detect the location of the IN is optimized with the help of a brute-force search (see Figures 6.5 and 6.6). As it can be seen, regardless the type of pre-processing IN mitigation scheme, $Thr = \sigma_n^{(l)}$ is a good threshold for mitigating the IN.

Another important information that we can see (Fig. 6.7) is that the usage of RN scheme as the pre-processing IN mitigation scheme is a good idea to mitigate the IN. In the high-SNR region, however, due to the usage of the replacement threshold T_{rep} which is not good for high-SNR [7], the RN scheme delivers a worse performance. We will see later (Simulation 6.5.3), that the high-SNR region problem can be eliminated when we apply also our second proposed idea.

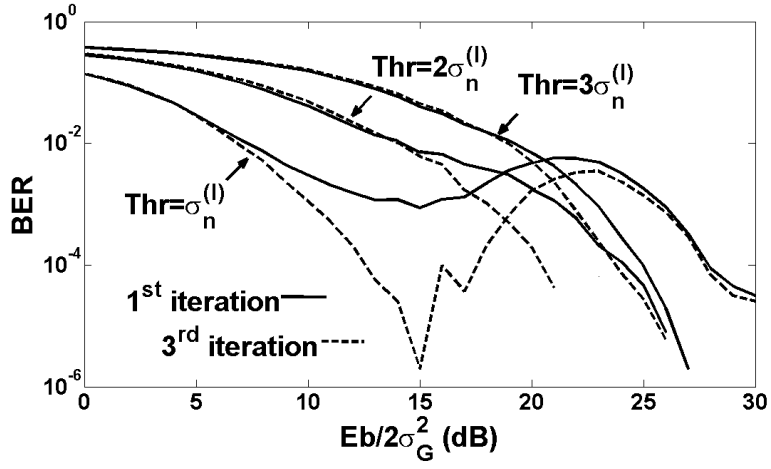

Figure 6.6: Performance of the Häring-iterative scheme with the RN scheme as the pre-processing IN mitigation scheme. Different values of the threshold Thr are considered. The IN parameters are: $A = 0.1, \sigma_I^2 = 100\sigma_G^2$.

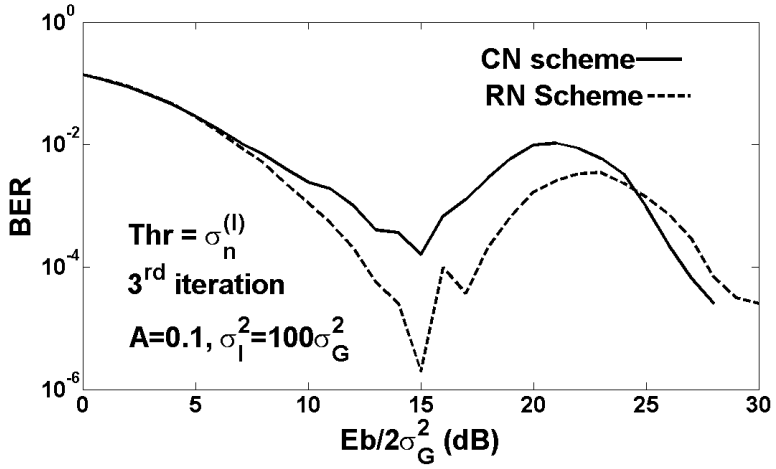

Figure 6.7: Performance comparison of the Häring-iterative scheme when the RN scheme and the CN scheme are used as the pre-processing IN mitigation scheme.

6.5.2 Simulation 2: Is the usage of the output of a pre-processing IN mitigation scheme in all iterations a good idea ?

First of all, we discuss what actually happens when the output of a pre-processing IN mitigation scheme is used only in the zeroth iteration $l = 0$ and when it is used in all iterations $l \geq 0$.

In the MH-iterative scheme, where the output of the CN scheme is used only in the zeroth iteration, the noise variance in each iteration, $\sigma_n^{2(l)}$, depends on the wrong decision variance σ_e^2, the AWGN variance σ_G^2 and the IN variance σ_I^2. In our proposed scheme, however, due to the usage of the output of the pre-processing IN mitigation scheme in all iteration l, the noise variance $\sigma_n^{2(l)}$ depends *mainly* on the wrong decision variance σ_e^2 and the AWGN variance σ_G^2. This can be seen clearly from Fig. 6.8: in the low-SNR region, where the influence of the IN is strong, the average noise variance in the MH-iterative scheme is high, whereas our proposed system produces almost a flat average noise variance.

The benefit of having the flat average noise variance is that the optimized threshold Thr value, which is a function of the noise variance, can work fine for all SNR. The optimization of the threshold Thr value used in the MH-iterative scheme on the other hand, needs an accurate approximation of the SNR: a different SNR needs a different constant factor c. This is a high complexity task and therefore becomes unattractive from a practical point of view.

In this simulation, as it is mentioned in Section 6.5, we use a brute-force search to find a good constant factor c with respect to the BER that will be used in the MH-iterative scheme and our proposed scheme. We find the constant factor $c = 1$ for the MH-iterative scheme while for our proposed scheme, the constant factor $c = 3$. This indicates that the threshold Thr value used in the MH-iterative scheme depends *only* on the noise variance and therefore it leads to the following consequences: in the low-SNR, the threshold Thr value is too high and in the high-SNR it is too low.

When the threshold Thr value is too high in the low-SNR, then we allow more noisy received samples vector r to enter the next iteration. In the high-SNR, on the other hand, when the threshold Thr value is too low then we allow more approximated transmitted samples vector $c^{(l)}$, which might contain decision errors made by the ML estimation, to enter the next iteration. Based on these two consequences, the MH-iterative scheme is expected to be worse in performance compared to the performance of our proposed scheme (Fig. 6.9).

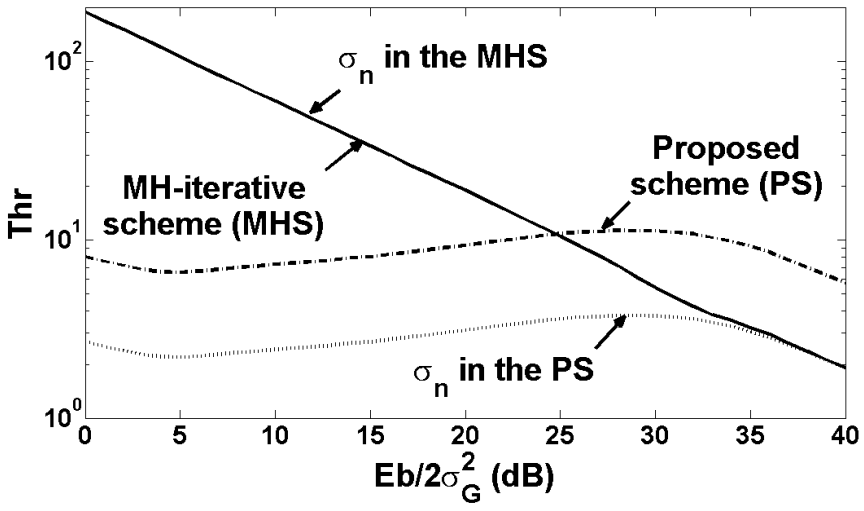

Figure 6.8: The value of the threshold Thr as a function of SNR. The threshold Thr values for the MH-iterative scheme and our proposed scheme are $\sigma_n^{(l)}$, and $3.\sigma_n^{(l)}$, respectively. The depicted noise variance is an average noise variance from iteration 1 to iteration 3. Both systems use the clipping-nulling (CN) scheme as the pre-processing IN mitigation scheme. The IN parameters are: $A = 0.1, \sigma_I^2 = 1000\sigma_G^2$.

6.5.3 Simulation 3: Does the combination of the first and the second proposed ideas bring the best performance ?

In our simulations so far, we looked at the performance brought by our first idea only and second idea only. We see that each idea provides a positive contribution. In this simulation, we provide the performance of our proposed scheme when both ideas are used. By comparing Fig. 6.9, in which only the second idea is used, to Fig. 6.10 where we combine the first and the second ideas, we can see that additional gain can be achieved. We see also that the high-SNR problem introduced by the usage of the RN scheme as the pre-processing IN mitigation scheme (see Simulation 6.5.1) is not noticeable.

Another simulation result that we will discuss is the performance of both schemes when the IN power spectral density (PSD) is reduced: we change the IN PSD from $\sigma_I^2 = 1000\sigma_G^2$ to $\sigma_I^2 = 100\sigma_G^2$. As can be seen in Fig. 6.11, our proposed scheme performance is still better than the MH-iterative scheme in terms of the BER. However, when we compare the performance of our proposed scheme depicted in Figures 6.10 and 6.11, it is interesting to see that for $10 < SNR \leq 20$ – the SNR-region in which the influence of the IN is still strong – the reduction in the IN PSD is not followed by the reduction in the BER. This

is because the number of received samples corrupted by the IN, whose magnitudes are lower than the thresholds used in the pre-processing IN mitigation scheme, increases. As a result, the threshold Thr value used in our proposed scheme is more influenced by the IN variance (see Fig. 6.12). Therefore, the increase in the BER is expected.

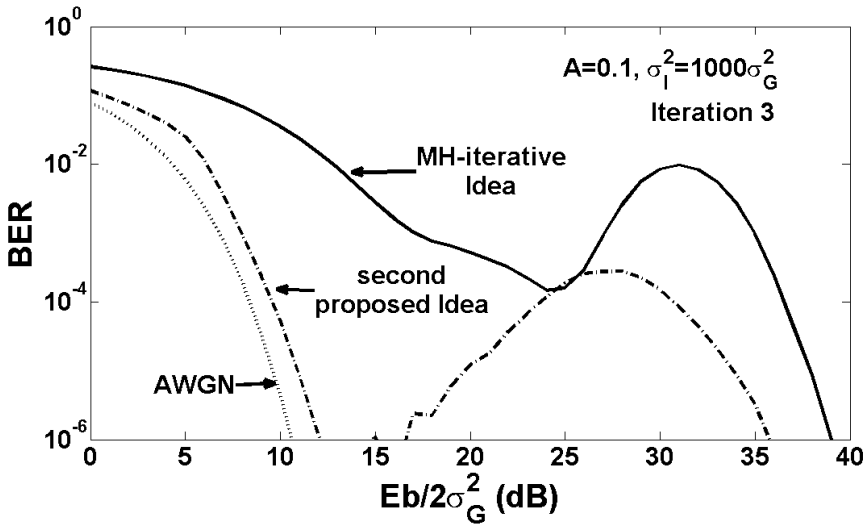

Figure 6.9: Performance comparison between the original MH-iterative scheme and the proposed scheme. Both schemes use the clipping-nulling (CN) scheme as the pre-processing IN mitigation scheme. The IN parameters are: $A = 0.1, \sigma_I^2 = 1000\sigma_G^2$.

6.5.4 Simulation 4: How does the performance of both schemes in a weakly disturbed channel look like ?

In three previous simulations, we discuss the performance of the MH-iterative scheme and our proposed scheme when $A = 0.1$ – the probability of occurrence of IN in a heavily disturbed channel. In this simulation, we look at the performance of both schemes in a weakly disturbed channel ($A = 0.01$).

In a weakly disturbed channel, the received samples in both schemes are mostly corrupted by the AWGN. The IN in this channel is modelled to have a large PSD. Hence we can expect an improved detection for the pre-processing IN mitigation scheme. This condition implies that there is no need to detect the IN further with the help of the threshold Thr. Therefore, the usage of a high threshold Thr value which allows more received samples r_i, instead of the approximated transmitted samples $c_i^{(l)}$, to enter the next

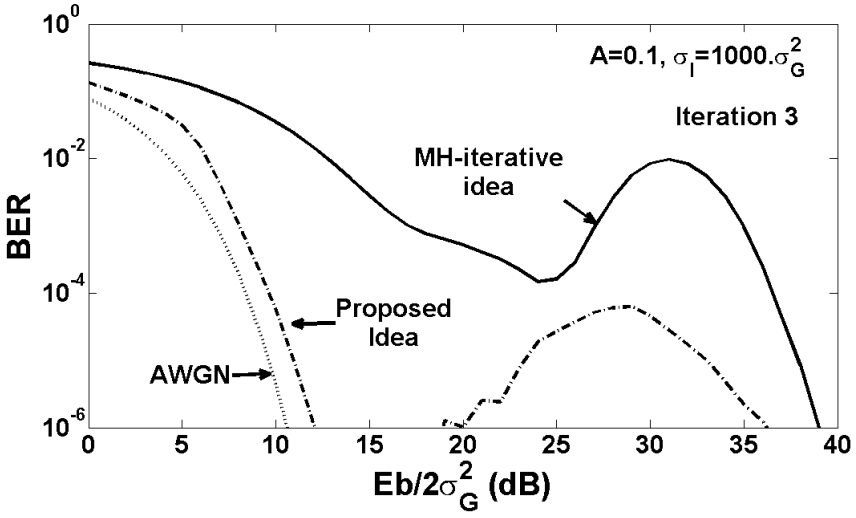

Figure 6.10: Performance comparison between the original MH-iterative scheme and the proposed scheme. The MH-iterative scheme uses the clipping-nulling (CN) scheme as the pre-processing IN mitigation scheme, whereas our proposed scheme uses the replacement-nulling (RN) scheme as the pre-processing IN mitigation scheme. The IN parameters are: $A = 0.1, \sigma_I^2 = 1000\sigma_G^2$.

iteration is preferable. The brute-force search to find a good threshold Thr value used in our proposed scheme confirms this situation: we have to increase the threshold Thr value from $Thr = 3\sigma_n^{(l)}$ to $Thr = 5\sigma_n^{(l)}$ in order to have a better performance (Fig. 6.13). In the MH-iterative scheme, however, it cannot be confirmed. The brute-force search gives the same threshold Thr value, $Thr = \sigma_n^{(l)}$. Fortunately as it is explained in Simulation 6.5.2, in the low-SNR the threshold Thr value used in the MH-iterative scheme is already good – Thr is high. Therefore, we could expect a comparable performance of both schemes in the low-SNR. In the high-SNR, for an almost AWGN channel, we expect that both schemes should also deliver a comparable performance (Fig. 6.14).

6.6 Conclusion

The MH-iterative scheme is an iterative impulsive noise (IN) mitigation scheme for OFDM based transmission which delivers a good performance with a low complexity in the receiver design. In this chapter, we report two ideas to improve its performance. The first idea is to use the replacement-nulling (RN) scheme as the pre-processing IN mitigation scheme instead of the clipping-nulling (CN) scheme. The second idea is to use the output

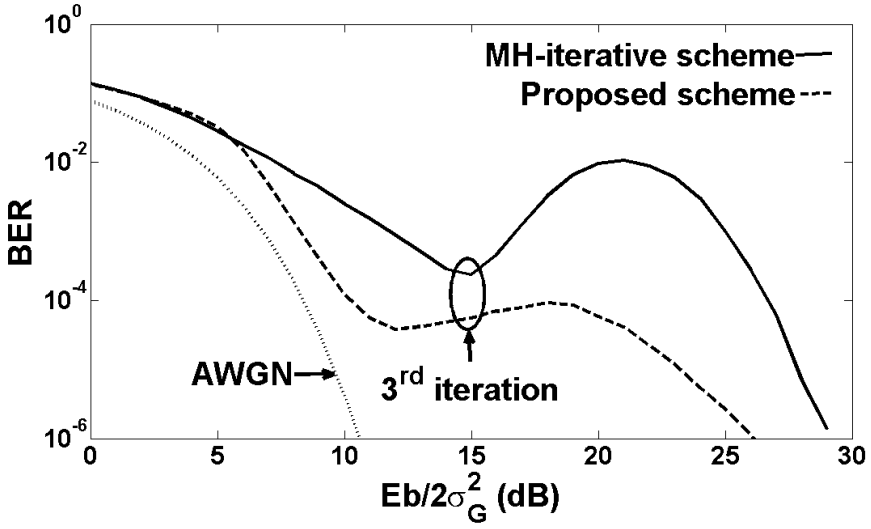

Figure 6.11: Performance comparison between the original MH-iterative scheme and the proposed scheme. The MH-iterative scheme uses the clipping-nulling (CN) scheme as the pre-processing IN mitigation scheme, whereas our proposed scheme uses the replacement-nulling (RN) scheme as the pre-processing IN mitigation scheme. The IN parameters are: $A = 0.1, \sigma_I^2 = 100\sigma_G^2$. The threshold Thr values for the MH-iterative scheme and the proposed scheme are $Thr = \sigma_n^{(l)}$ and $Thr = 3\sigma_n^{(l)}$, respectively.

vector $\widetilde{r}$ of the pre-processing IN mitigation scheme in all iterations instead of only in the zeroth iteration.

The performance comparison in terms of the bit error rate (BER) between the MH-iterative scheme and the proposed scheme is done with the help of simulations of uncoded QPSK-256OFDM transmission in the two-state IN channel model. The results show that the proposed scheme brings better performance than the MH-iterative scheme.

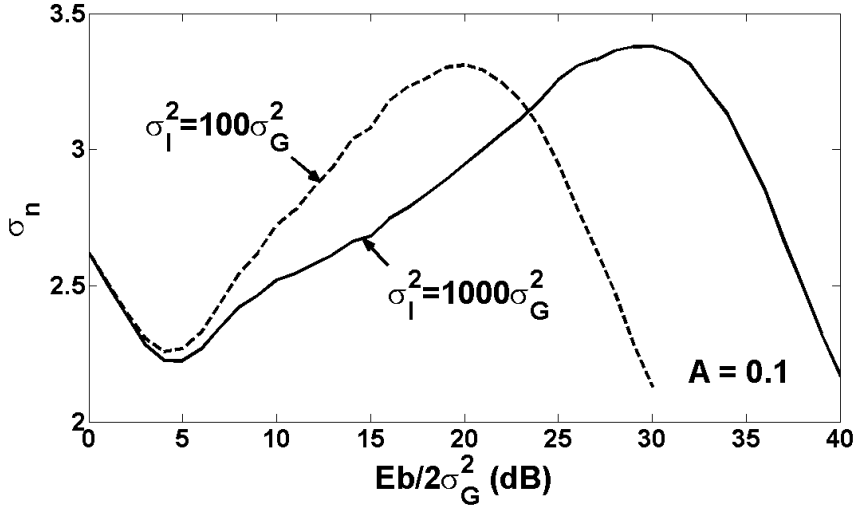

Figure 6.12: Average noise variance from iteration 1 to iteration 3 in the proposed scheme (both proposed ideas are used) as a function of SNR for two different IN variances.

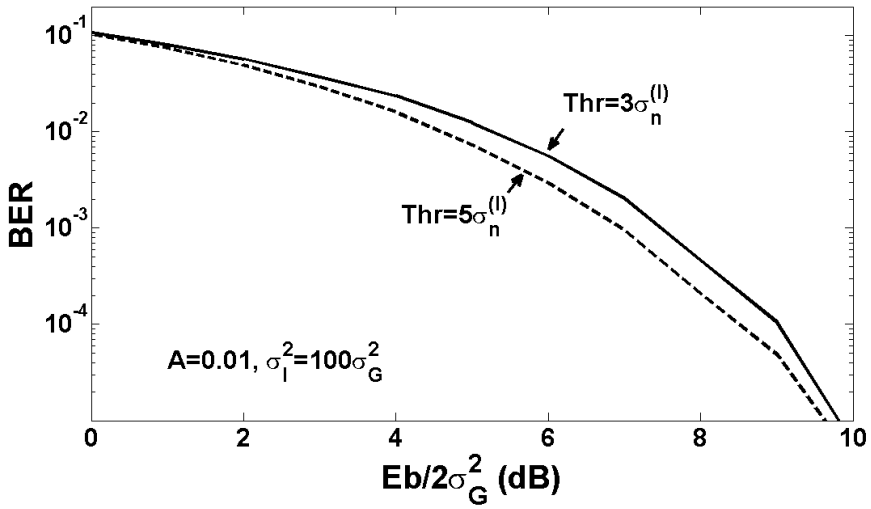

Figure 6.13: Performance of the proposed scheme in a weakly disturbed channel for two different threshold Thr values in the first iteration. The replacement-nulling (RN) scheme is used as the pre-processing IN mitigation scheme. The IN parameters are= $A = 0.01$, $\sigma_I^2 = 100\sigma_G^2$

.

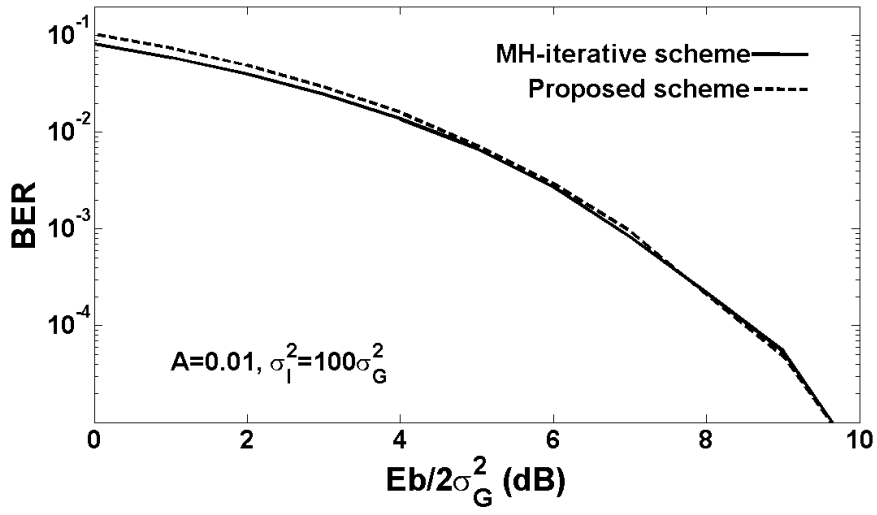

Figure 6.14: First iteration performance comparison between the MH-iterative scheme and the proposed scheme in a weakly disturbed channel. The MH-iterative scheme uses the clipping-nulling (CN) as the pre-processing IN mitigation scheme whereas our proposed scheme uses the replacement-nulling (RN). The threshold Thr values for the MH-iterative scheme and our proposed scheme are: $Thr = \sigma_n^{(l)}$ and $Thr = 5\sigma_n^{(l)}$, respectively. The IN parameters are= $A = 0.01$, $\sigma_I^2 = 100\sigma_G^2$

.

7 G3-PLC throughput based on real measurements and its influencing factors

We discuss the performance (in terms of data throughput) of the G3-PLC technology based on a real measurement in Hamburg-Germany. Three points to be discussed: the influencing factor of near and far transmission throughput, the influence of a repeater on the throughput, and the influence of different UDP packet size on the throughput.

7.1 Introduction

IEEE smart grid section mentions in their website that the next-generation electrical power system is directed not only for power delivery but also for information delivery. This is called a "smart grid". The vision of the smart grid, of course, is a good vision and needs the support of various parties.

The PLC channel as the main channel of the smart grid has been known to have many problems. Impulsive noise (IN), narrow band interferences (NBI), and signal attenuation are examples of problems found in this channel. The IN and NBI introduce errors on the transmitted data. Whereas signal attenuation, which depends on the PLC network topology and the type of devices connected to the PLC, produces packet-loss and, therefore, degrades the achievable throughput performance.

The G3-PLC technology – the technology of interest in this chapter – uses the concatenation of a Reed-Solomon (RS) and a convolution code (CC) to reduce the errors in the transmitted data. To reduce the number of loss-packets, a device can act not only as a transmitter and a receiver but also as a repeater.

This chapter discusses the performance (in terms of data throughput) of the G3-PLC technology which operates in the 150–500 kHz frequency band, measured at Vattenfall Europe's LV Distribution Grid in Germany and its influencing factors. This technology has been standardized by the G3-PLC Alliance and accepted as the ITU-T standard [29].

The rest of this chapter is as follows. In Section 7.2, we explain what has been done during the measurement activities. Then, in Section 7.3, we present the list of the important parameters considered in the analysis and explain their correlation with the throughput. The analysis of the measurement data is given in Section 7.4, and finally the conclusion is presented in Section 7.5.

7.2 Measurement setup

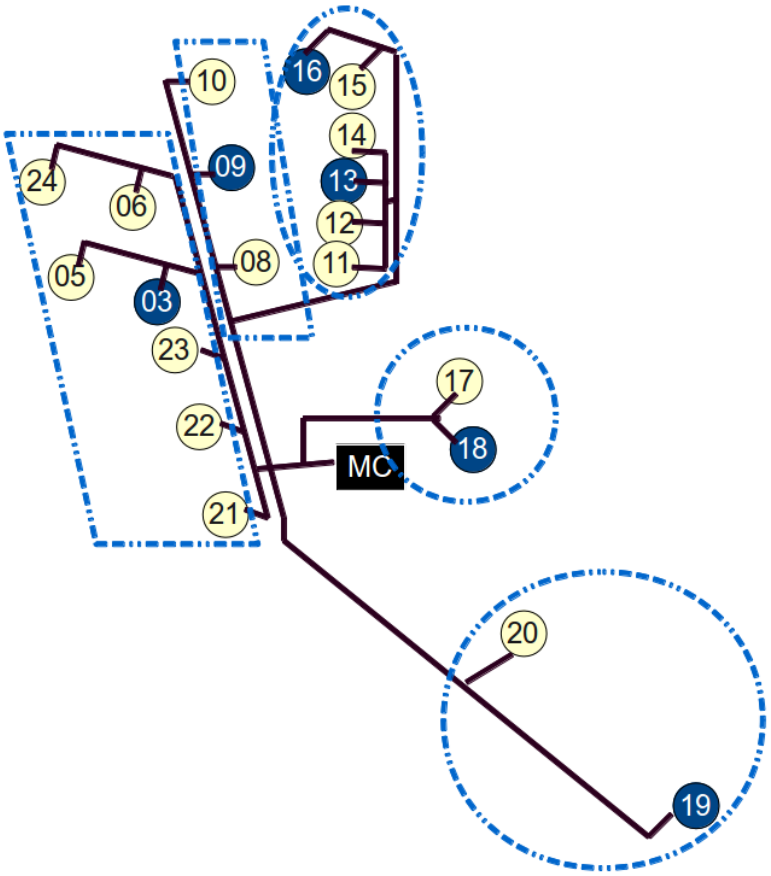

Figure 7.1: Network setup of the field test.

Fig. 7.1 shows the measurement map. During the measurements, the narrow band PLC modems G3-PLC are used.

There are 21 nodes in total. Twenty nodes are called *terminal devices* (TD) and are installed in the test field. A node, which is called *measurement computer* (MC), is a data concentrator and is installed in the transformer station. The MC and the blue TD are equipped with an UMTS communication module. The module is needed to allow a test operator to access a node remotely, in order to control the node.

For testing the power line connection between the nodes, the following tests are performed, the round-trip-time (RTT) delay test and the throughput test. The RTT is measured with the ping command. It defines the time needed to transmit a transport-layer data unit (datagram) from a source to a destination and from the destination to the source. The throughput defines the number of datagram transmitted/received per unit time. In our case, it is measured in terms of bits per second with help of the iperf program.

In addition to the RTT and throughput information, the nodes provide some information about the test conditions such as the topology, the route cost, the modulation, the tone map and the quality indicator. The topology gives the information about the best path which is considered during the transmission from a transmitter to a receiver. From this information, one knows whether a direct connection from the transmitter to the receiver is possible or not. If the direct connection is not possible then in the topology information, one can see that there is another node in between the transmitter node and the receiver node. The route cost (RC) is the cumulative link cost along the route towards the destination. The modulation information gives the information about the type of modulation used during a transmission. Four possible modulation modes are ROBO, BPSK, QPSK, and 8PSK. The number of carrier frequencies is noted on the tone map, whereas the quality indicator is the line quality (LQ) information.

There are two scenarios of measurements: the up-link test and the down-link test. The up-link test measures the throughput for the transmission from a TD node to the MC, whereas in the down-link test the throughput is measured for the transmission from the MC to a TD. For all measurement scenarios, the UDP protocol is used.

7.3 Correlation between throughput and other measurement parameters

In Section 7.2, the list of measurement parameters is given. Here we show the correlation (dependency) between the throughput and other measurement parameters.

7.3.1 Round-trip-time (RTT)

The correlation between the round-trip-time (RTT) delay and the achieved throughput is a negative correlation. This means that if the RTT increases then the throughput decreases, and vice versa. The justification of this correlation is as follows. Let T be a number of bits transmitted per second (bits/s), then in order to receive the same number of bits/s, the required time t for transmitting a single bit is $1/T$. In the real system, there is always a delay during the transmission, thus $t > 1/T$. When t increases, which can be inferred from the RTT, the throughput decreases.

7.3.2 Line quality (LQ)

First of all, we shall explain the definition of the line quality (LQ) and briefly explain how it is calculated. The LQ is a characterization of the quality of the underlying power line channel. It is the average signal-to-noise ratio (SNR), where averaging is done over all active tones and pilot tones, if present, in the received packet. It influences the decision on the type of modulation that can be used. Based on this knowledge, the LQ and the achieved throughput have a positive correlation i.e. when the LQ increases then the throughput also increases. This is due to the fact that in the better LQ a higher-order modulation can be used, resulting in an increase of the throughput. For a low LQ a lower-order modulation is used and as a result, the throughput decreases.

7.3.3 Route cost (RC)

As it was mentioned before, the route cost (RC) is the cumulative link cost along the route towards the destination. The transmitted data is routed in the path with the minimum

RC. A link cost (LC) is calculated as follows,

$$\begin{aligned} LC &= AdpKr \,.\, MOD_{kr} + AdpKm \,.\, MOD_{km} \\ &\quad + AdpKc \,.\, \frac{(T_M - T_A)}{(T_M)} \\ &\quad + AdpKq \,.\, \frac{(Maximum\ LQ - LQ)}{(Maximum\ LQ)} \\ &\quad + AdpKrt \,.\, \frac{R_A}{R_M} \end{aligned} \tag{7.1}$$

where

- T_M and T_A are the maximum number of tones and the number of active tones, respectively,
- R_A is the number of active routes and R_M is the maximum number of active routes,
- MODKr = 1 for robust mode, 0 for other modulations,
- MODKm = 3 for DBPSK or BPSK modulation, 2 for DQPSK or QPSK modulation, and 1 for D8PSK or 8PSK modulation,
- AdpKr, AdpKm, AdpKc, AdpKq, AdpKh, AdpKrt are a weight factor for ROBO, a weight factor for modulation, a weight factor for the number of active tones, a weight factor for the LQ, a weight factor for hop and a weight factor for the number of active routes in the routing table, respectively, to calculate the link cost.

From (7.1), we can infer that in very good channel conditions, the link cost is very low. This is due to the fact that for a very good channel condition, the highest-order modulation, i.e. 8PSK, is used instead of robust mode. The LQI is equal to the maximum LQI, and the number of active routes is very small. All conditions, that are mentioned, obviously produce the improvement on the throughput. However, in practical situations, the very good channel condition does not exist. The channel condition might degrade, resulting in an increase of the link cost, and thus RC. As a result, the throughput decreases. Therefore, the RC has a negative correlation with the throughput.

7.3.4 Quantity of carrier frequencies (QoC)

The quantity of carrier frequencies (QoC) has a positive correlation with the throughput. This is obvious since the higher the number of sub-carriers the higher the number of bits that can be transmitted, and vice versa.

As an additional information, in the technology, there is on-off mechanism on sub-carriers. When a sub-carrier is a subject to narrow band interference, the sub-carrier is turned off and cannot be used in the transmissions.

7.4 Results and analysis

The results are presented in two subsections. The first sub-section gives the results of the up-link test results, whereas the second presents the down-link test result.

7.4.1 Up-link test results

The up-link test is a 24 hours test. A TD node transmits packets to the MC in a duration of 20 minutes. After a transmission finished, there is a duration of at least 10 minutes before the next transmission starts. The transmitter bandwidth is 130 kBit/s and the UDP packet size is 1000 bytes. There are 5 transmitting nodes. Every transmitting node represents a group of the test field area, as it is shown in Fig. 7.1.

Fig. 7.2 shows the throughput of all transmissions from every transmitting node to the MC. To simplify the analysis, we shall state questions of interest and give the answer to every question (Q).

Q_1 : *What is the most influencing factor of a near/far distance transmission ?*

We consider the transmission from the TD18 to the MC as the near transmission. Whereas the transmission from the TD24 to the MC is considered as the far transmission. We choose these two transmissions because we observe an interesting phenomenon. The throughput of the near transmission is in average slightly better than that of the far transmission. But there is a point in time, i.e. during the night-time, where the far

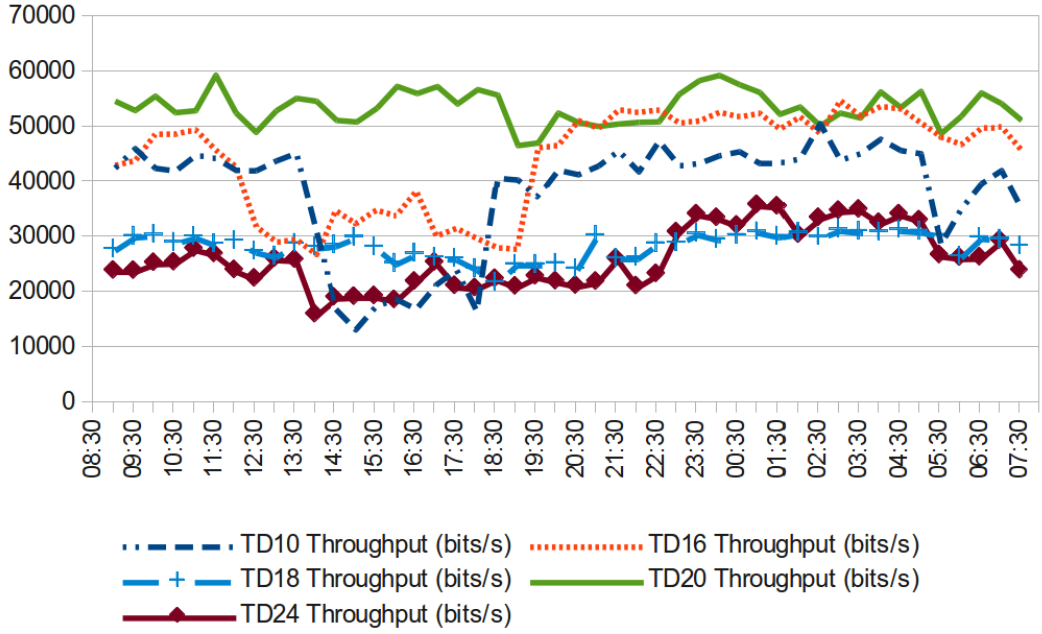

Figure 7.2: Throughput performances in the up-link test.

transmission is slightly better than the near transmission.

To find out the influencing factors of the near and the far distance transmissions, we calculate the correlation between the measurement parameters and the achieved throughput performance. The Pearson product-moment correlation – the linear correlation (dependence) between two variables X and Y, is used. The correlation r can be calculated as follows,

$$r = \frac{\sum(x_i y_i)}{sqrt(\sum((x_i)^2) \ . \ \sum((y_i)^2))}, \tag{7.2}$$

where $x_i = X_i - \bar{X}$ and $y_i = Y_i - \bar{Y}$. X_i and $\bar{X}$ are the value of X on the i^{th} observation and the average value of X, respectively. Y_i and $\bar{Y}$ are the value of Y on the i^{th} observation and the average value of Y, respectively.

Tables 1 and 2 present the correlation results of the near and far distance transmissions, respectively. As it can be seen, the most influencing factor of the near distance transmission is the line quality (LQ), whereas for the far distance transmission it is the route cost (RC). It is also worthwhile to mention that the round-trip-time (RTT) shows a good correlation with the throughput achieved, while the number of carrier frequencies

(QoC) has a weak correlation.

Table 7.1: The correlation between measurement parameters and the achieved throughput for the transmission from the TD18 to the MC.

Parameters	Correlation
RC	−0.05
RTT	−0.35
Qoc	0.06
LQ	0.56

Table 7.2: The correlation between measurement parameters and the achieved throughput for the transmission from the TD24 to the MC.

Parameters	Correlation
RC	−0.76
RTT	−0.73
Qoc	0.09
LQ	0.28

Having the information about the influencing factors of the near and the far transmissions, then the phenomenon of interest – why the throughput of the far distance transmission is better than that of the near distance transmission, can be explained as follows. Fig. 7.3 gives the complete information of our discussed transmissions. As shown, during the night time – the time in which the phenomenon happens – there is actually an improvement in the achieved throughput performance of both transmissions. But the improvement of the far transmission is better than that of the near transmission. The reason is because the values of the RC, and also the RTT, of the far transmission is surprisingly better, i.e. lower, than that of the near transmission. This is somehow not expected, since the near transmission has a better LQ than the far transmission (Fig. 7.3), and from (7.1) we know that a good LQ might result in a lower RC. After investigating the topology of the transmissions, we find that the situation, where the RC of the far transmission is better than that of the near transmission, is a reasonable situation. This is because there is no direct communication from TD18 to MC – TD18 communicates with MC all the time during the day via TD17. Whereas the communication between TD24 and MC is a direct communication. Thus, it is obvious that RC and RTT values of the near transmission are worst.

The use of a repeater in between the transmitter and the receiver in the near transmission, of course, provokes further questions. Later, we shall discuss *why and when is a*

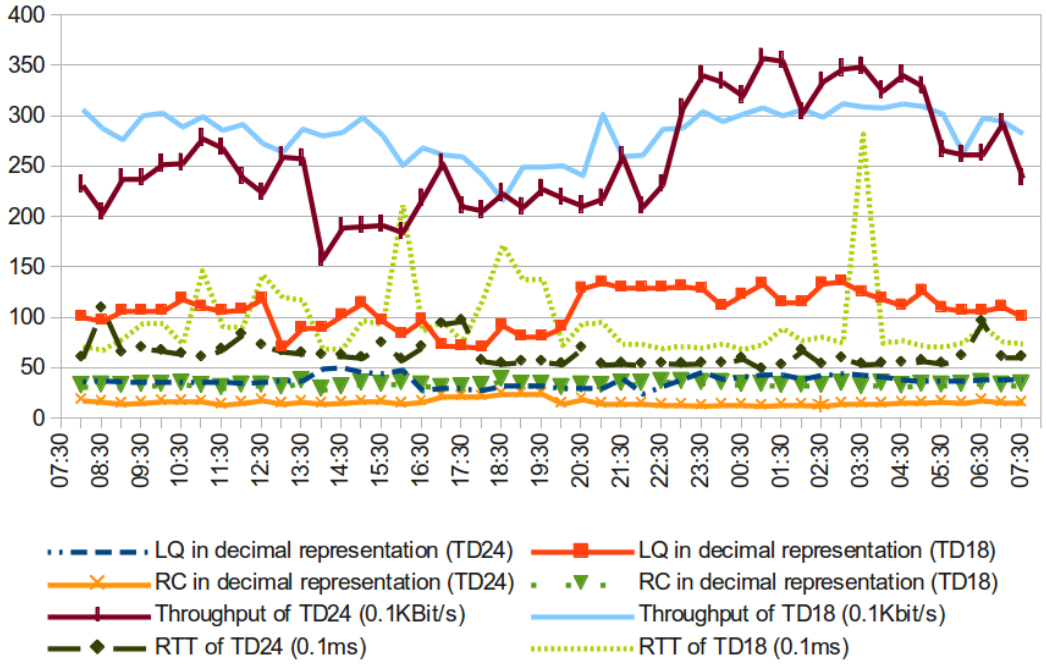

Figure 7.3: The throughput performance and the measurement parameters of the near and far transmissions.

repeater needed ?

Q_2 : *Why is there a noticeable throughput degradation in the time interval between 14 pm and 18 pm ?*

Fig. 7.2 shows that the lowest throughput performance of some transmissions is observable during the time interval between 14 pm and 18 pm. As it can be seen, only the transmissions from TD20 and TD18 to MC produce a stable throughput performance. This means, there must be a common influencing factor that produces this situation.

Based on the measurement data, the common influencing factor is the change on the topology of transmission between the transmitter and the receiver, i.e., from direct to indirect communication. Fig. 7.4 shows the number of the repeaters used during each transmission. As it can be seen, during that time interval, there is the usage of a repeater in almost all transmissions, except the transmission from TD20 to MC and from TD16 to MC. We shall focus only on the transmission from TD16 to MC. As it is mentioned before, during this transmission there is a noticeable degradation of the throughput.

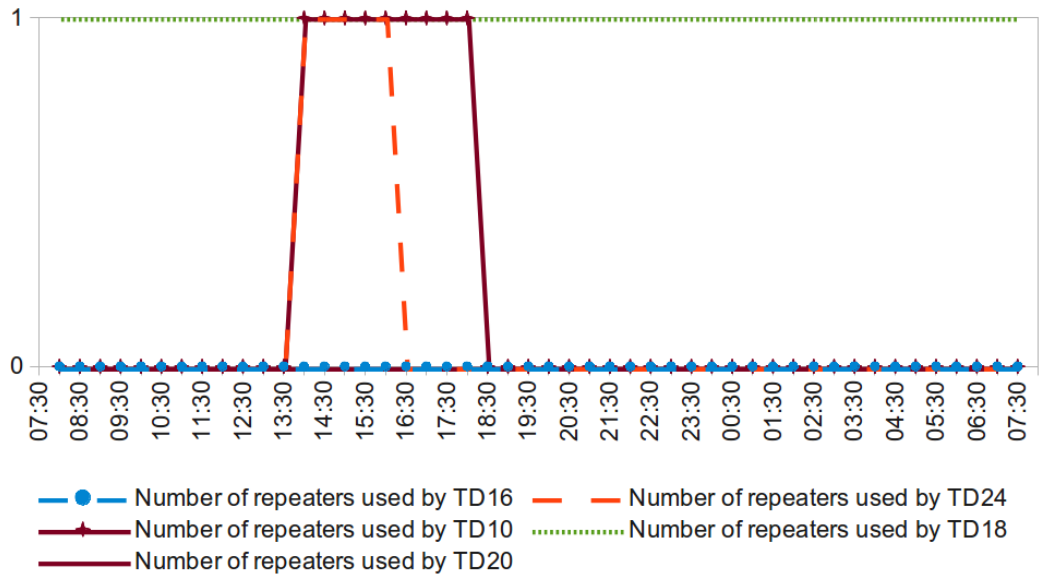

Figure 7.4: The number of repeaters used during the transmission from TD* to MC.

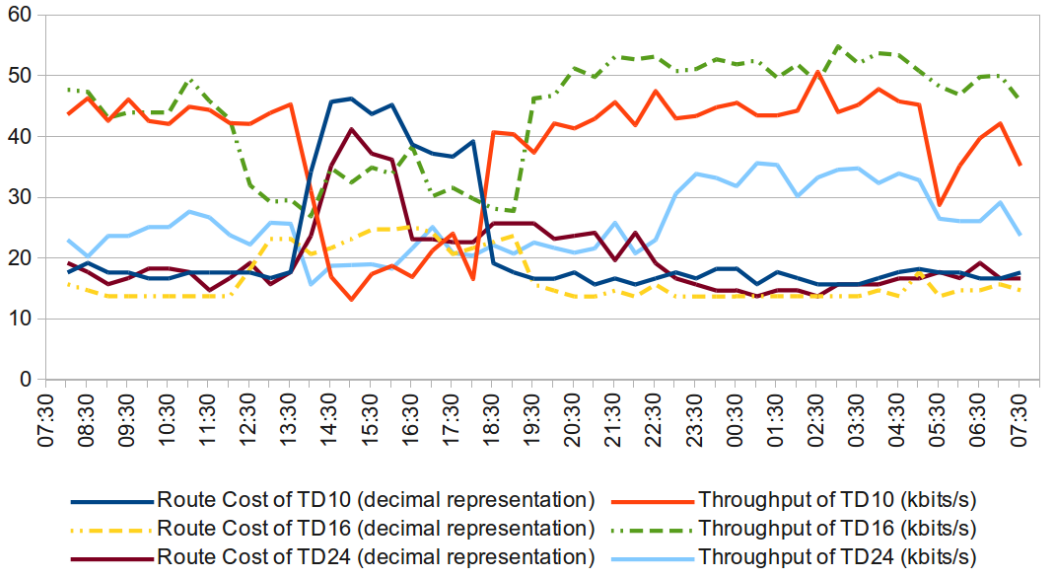

Figure 7.5: The throughput vs. the RC value during the transmissions from TD10, TD16 and TD24 to MC.

In the measurement setup section, we mentioned that the usage of a repeater can be observed from the topology information. This information is collected before and after every throughput test. It means that there is no information about the topology of a transmission that might change, during the throughput test. This might be a reason why the usage of a repeater during TD16 to MC transmission is not recorded in the topology

information. However, the usage of a repeater can also be identified from the RC value. As shown in the last observation – the observation on the near and far transmissions, the RC value increases when a repeater is used. From Fig. 7.5, one can see that there is a noticeable increase of the RC value, in the time interval of interest, during the transmission from TD16 to MC.

Q_3 : Why and when a repeater is needed ?

As it is mentioned before, a device can act as a transceiver and as a repeater. The role of a repeater is important, since it makes sure that the transmitted data from the transmitter is routed in a good path, such that the transmitted data arrives at the receiver. The data-sheet mentions that a node shall repeat the transmitted data from another node, if and only if, it is not a destination node, and its RC to the destination node is less than or equal to the RC expected.

In the previous observations, we see that the usage of a repeater contributes a negative effect on the throughput performance achieved. However, this contribution is the price to achieve a reliable transmission. Unfortunately, there is no measurement parameter that can be used to know the main factor behind the activation of the repeater. The knowledge of this factor might help us designing good locations of nodes such that reliable transmissions can always be achieved.

One of the dominant parameters in PLC is that of attenuation [25]. When the signal attenuation is too high then the transmitted data might not arrive at the receiver. To overcome this problem, the usage of a repeater is needed [14]. Hooijen [30] mentioned that the main parameter determining the level of signal attenuation is the number of houses. This knowledge helps us to find the reason behind the usage of the repeater in the near transmission – the transmission from TD18 to MC. In terms of the number of households, the near distance (approx. 150 m) has a larger number than that of the far distance (approx. 225 m). In this case, the near distance transmission faces the higher attenuation and therefore, a repeater is needed.

Furthermore, as shown in the transmission topology (Fig. 7.4), the near transmission, all the time during the day, involves a repeater. This is a result of the fact that TD17 and TD18 are installed in a high building. The building has 14 floors with approximately 112 apartments. TD18 is installed on the 14th floor and TD17 is installed downstairs. In this

type of building, the network loads can be expected to be high during the day. Therefore, the channel condition remains bad during the day. Thus, TD17 has to become a repeater, in between TD18 and MC, guaranteeing the transmitted data from TD18 to arrive at MC.

Q_4 : *Why the transmission from TD20 to MC is the best ?*

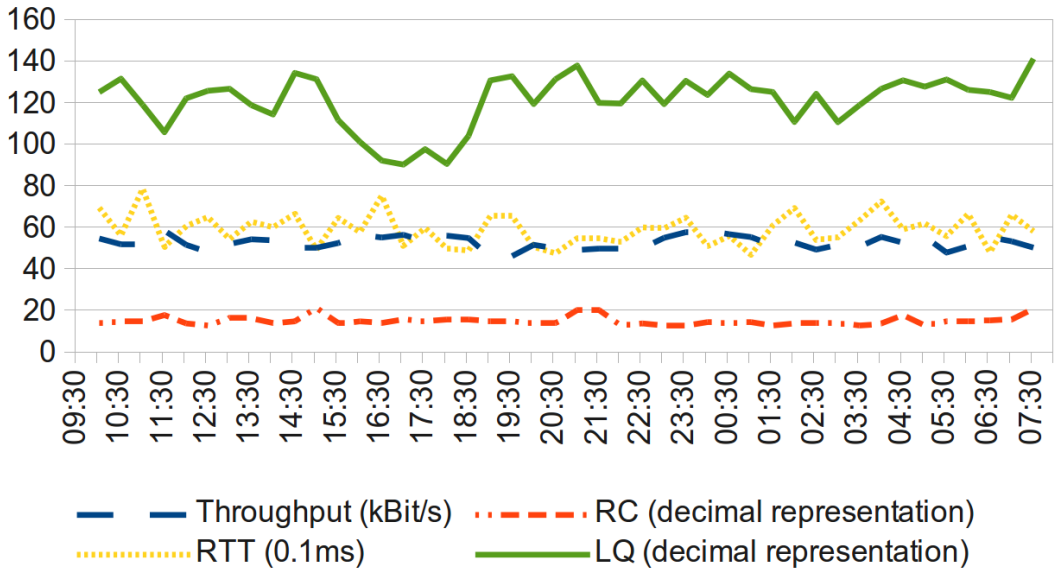

Figure 7.6: The throughput performance and the measurement parameters of the TD20 to MC transmission.

The transmission from the TD20 to the MC produces the best throughput performance due to the fact that:

1. the transmission is a near distance transmission and, at the same time,
2. the number of loads connected between the transmitter (TD20) and the receiver (MC) is very low.

Fig. 7.6 presents some important information about this transmission. As shown, the RTT and the RC show a stable behaviour there is no noticeable change during the transmission. The LQ, on the other hand, shows a noticeable change in the time interval between 15:30pm and 18:30pm. However, this change is not followed by the change in the type of modulation used. Therefore, the impact of the change in the LQ produces no effect on the achieved throughput.

7.4.2 Down-link test results

A down-link test is a test to measure the throughput of the transmission from the MC to a TD. The test is conducted during the night-time and the duration of every transmission is 2 minutes. The transmitter bandwidth used is 130 kBits/s. The special property of this test is there are two UDP packet sizes used: 100 Bytes and 1000 Bytes. So, the basic investigated question in this test is: *what is the influence of the packet size on the throughput achieved ?*

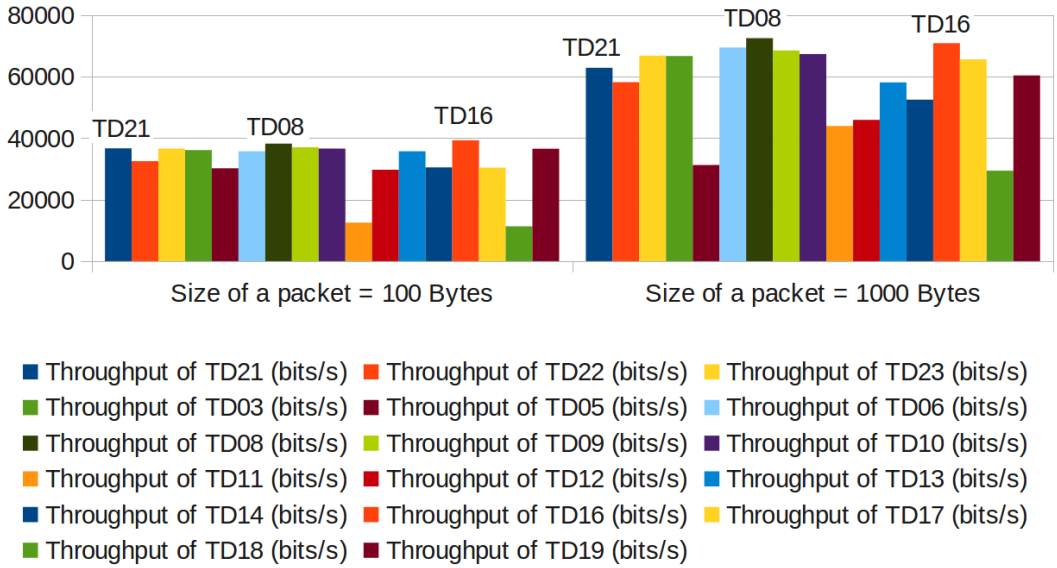

Figure 7.7: Throughput for 100 Bytes and 1000 Bytes packets transmission measured on 07.05.2012.

The measurement results collected in three different days show the same result (Fig. 7.7), i.e. the transmission of 1000 Bytes packets has a better throughput than 100 Bytes packets transmission. This means there must be only a single common reason that can explain the found result.

To find out the common reason, we look at the two main measurement parameters, the RC (Fig. 7.8) and the LQ (Fig. 7.9). If the RC is the common reason, then the expectation is that the RC during 1000 Bytes packets transmission must be always lower (better) than that during 100 Bytes packets transmission. The same direction of thought is applied for the LQ. If it is the common reason, then the LQ during 1000 Bytes packets transmission is expected to be greater (better) than that during 100 Bytes packets transmission. Unfortunately, as it can be seen, none of the parameters is the common

reason.

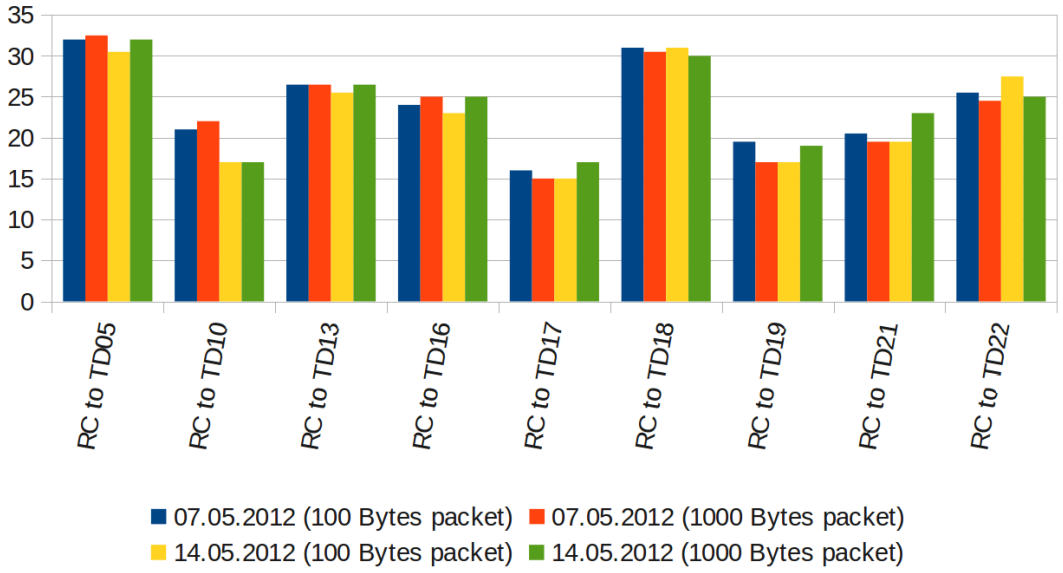

Figure 7.8: Route cost (RC) measured in two different days.

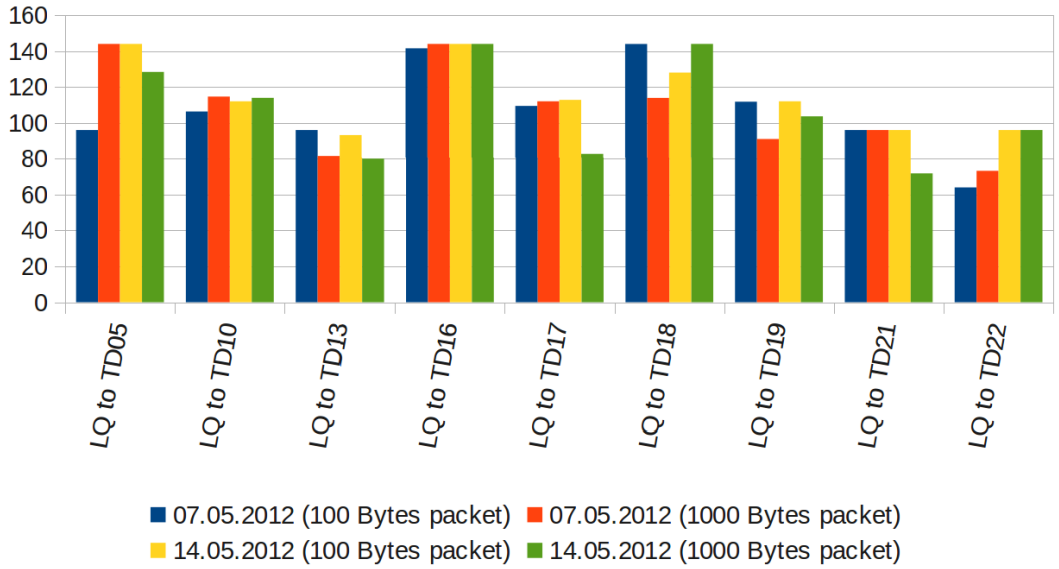

Figure 7.9: Line quality (LQ) measured in two different days.

Fortunately, there are supporting publications. Authors in [31] mentioned that the improvement on the time efficiency T_E for processing a packet brings the improvement on

the throughput. The T_E can be calculated as follows,

$$T_E = \frac{Packet\ size}{Packet\ size + Header\ size}. \tag{7.3}$$

From (7.3), we see that if the header size is fixed and the packet size increases then the T_E improves. In our case, UDP IPv6 transmission is used. The UDP IPv6 header is 48 Bytes regardless the size of the packet (or payload). Therefore, $T_E = 0.68$ for 100 Bytes packets transmission, and it is 0.95 for 1000 Bytes packets transmission. As we can see, there is an improvement on the T_E of 27%.

Another supporting publication is in [32]. In this publication, the authors defined the throughput T_P as the ratio between the transmitted packet size x and the delay the transmitted packet experiences,

$$T_P = \frac{8\ .\ x}{delay(x)}, \tag{7.4}$$

where $delay(x) = a\ .\ x + b$. The variable a defines the time needed for sending 1 data byte, and the variable b defines the time needed for the protocol overhead for sending a packet. Both variables a and b depend on the frequency band we are working in, where the higher the frequency the lower their value. The protocol overhead takes into account the header size. Beside that, in the technology of interest – G3-PLC technology, the protocol overhead also comes from the usage of the carrier sense multiple access / collision avoidance (CSMA/CA) and the automatic repeat request (ARQ) protocols. These two protocols influence obviously the throughput achieved, since both of them produce "wait time" costs. In the CSMA/CA, before sending data, a device must check whether there is another transmission or not. If no, the data is transmitted. If yes, the device backs off once again and so on. In the ARQ, when a packet is corrupted at the receiver, the transmitter has to repeat the transmission of the packet. If the transmission channel is assumed to be perfect, as it is done in [32], and the channel is always idle when the device is ready to transmit data, then the CSMA/CA and the ARQ contribute nothing in the protocol overhead. However, the PLC is not a perfect channel. The transmitted packets might be corrupted at the receiver and therefore the ARQ is needed to guarantee a reliable transmission. In our case, the influence of the CSMA/CA protocol on the throughput achieved is negligible. This is due to the fact that every measurement data is collected only for a single communication, i.e. the communication from the MC to a TD in duration

of 2 minutes.

Having made use of the ARQ protocol as the main factor that influences the throughput achieved then the obtained result can be explained as follows. In our scenario the transmitter bandwidth is constant, i.e. 130 kBits/s. Therefore, in terms of the number of packets being transmitted per second, the 100 Bytes packets transmission is higher than the 1000 Bytes packets transmission. In other words, we can say that the number of headers being transmitted during small packets transmission is larger than that during big size packets transmission. As it is mentioned in the UDP IPv6 specification, the header plays an important role in justifying the correctness of a received packet. If the header is corrupted, then the corresponding received packet is dropped. Therefore, under the assumption that the correctness of the header is the only important information used to trigger the retransmission in the ARQ protocol, then we expect that the probability of retransmission during small packets transmission is high. Thus, the $delay(x)$ for small packets transmission is also high, and as a result, the throughput is lower.

7.5 Conclusion

In this chapter, the G3-PLC throughput based on real measurements in Germany is presented and analysed. There are three main discussion points:

1. first, we discussed the most influencing factor on near transmission and far transmission. We observed that for the near transmission, the line quality (LQ) produces a strong correlation with the throughput achieved, whereas for the far transmission, it is the route cost (RC). We also observed that the round-trip-time (RTT) shows a good correlation with the throughput achieved.

2. Second, we discussed the influence of the usage of a repeater in between a transmitter and a receiver. The measurement data shows that it produces noticeable degradation on the throughput.

3. The last discussion is about the influence of UDP packet size. The results show that big size packets transmission produces better throughput than that of small size packet transmission.

8 Summary and Possible Future Work

In this chapter, we summaries our contributions reported in this thesis and we suggest ideas possible future work. The contributions are related to OFDM based transmissions.

8.1 Contributions related to narrow band interference (NBI)

Our contributions related to NBI were reported in Chapters 1 and 2 and summarized as follows:

1. A proposed frequency-domain NBI model for an OFDM system.
2. A proposed coded modulation for QPSK-OFDM based transmission which can be used for combating NBI.
3. A proposed new simple block code of length $M = 4$ called *permutation code plus* (PC^+).
4. A comparison performance between concatenated Reed-Solomon (RS) code and convolution code (CC), and concatenated RS code and PC^+. The comparison has only focused on hard decision decoding.

8.1.1 Possible future work

As it can be noticed in this work, we only focused on hard decision decoding. Therefore, it is interesting to investigate soft decisions decoding in the future. It is also interesting to investigate the impact of the variation of the PC^+ codeword length M on results for $M > 4$.

8.2 Contributions related to impulsive noise (IN)

Our contributions related to IN were presented in Chapters 3, 4, and 5 and summarized as follows:

1. A proposed way to turn a parametric threshold based IN mitigation scheme into a non-parametric one.

2. A proposed single threshold IN mitigation scheme called *replacement* (R) scheme. Considering this scheme and other simple single threshold IN mitigation schemes discussed in the literature, as the clipping (C) scheme and the nulling (N) scheme, we now have additional *joint* IN mitigation schemes beside the CN scheme: the CR scheme, the RN scheme and the CRN scheme.

3. A new proposed way of combining simple IN mitigation schemes and its optimum selecting algorithm. Contrary to the conventional joint IN mitigation schemes, the proposed combining mechanism with the help of its selecting algorithm allows more flexibility in combining simple IN mitigation schemes. It allows not only the combination between different simple IN mitigation schemes with different threshold values, but also the combination of a simple IN mitigation scheme with different threshold values, and the combination of different IN mitigation schemes with the same threshold value.

4. Improved Mengi-Häring (MH) iterative scheme. We proposed the use of the RN scheme as a pre-processing IN mitigation scheme and the use of the output of the pre-processing IN scheme in all iterations.

8.2.1 Possible future work

1. Our proposed selecting algorithm for the new combining scheme is a frequency-domain algorithm. It is interesting, in the future, to look at the possibility of having a time-domain selecting algorithm. In this way, the selection of the best IN mitigation output can be done only in the time domain. And as a result, the complexity of the proposed combining scheme is reduced.

2. It is possible to investigate furthermore the possibility of improving the MH-iterative scheme by introducing the usage of multi-thresholds. We have done a preliminary investigation on this idea. The result confirms that this is a good direction to go.

8.3 Contributions related to the analysis performance of G3-PLC technology

Our contributions related to analysing the performance of the G3-PLC technology are mainly to explain the factors that influence the performance (in terms of throughput) of the G3-PLC technology. The following is a list of important results we found:

1. The use of a repeater between a transmitter and a receiver is a good idea to achieve a reliable transmission. However, we observe only a drop in performance (in terms of data throughput) when a repeater is used.

2. Large packet size transmission delivers a better data throughput than that of small packet size transmission.

3. Number of loads between a transmitter and a receiver influences the throughput achieved more than the influence of the distance between the transmitter and the receiver.

3. In G3-PLC technology there are modulations of different orders that can be used. The measurement results show that the highest order modulation, i.e. 8PSK, is never used.

References

[1] M. Wetz, W. G. Teich, and J. Lindner, "OFDM-MFSK with differentially encoded phases for robust transmission over fast fading channels," in *11th Int. OFDM-Workshop*, Hamburg, Germany, Aug. 2006.

[2] V. N. Papilaya, T. Shongwe, A. J. H. Vinck, and H. Ferreira, "Selected subcarriers QPSK-OFDM transmission schemes to combat frequency disturbances," in *16th IEEE International Symposium on Power Line Communications and Its Applications (ISPLC)*, Beijing, China, Mar. 27–30, 2012, pp. 200–205.

[3] T. Shongwe, V. N. Papilaya, and A. Vinck, "Narrow-band interference model for OFDM systems for powerline communications," in *17th IEEE International Symposium on Power Line Communications and Its Applications (ISPLC)*, Johannesburg, South Africa, Mar. 24–27, 2013, pp. 268–272.

[4] H. A. Suraweera, C. Chai, J. Shentu, and J. Amstrong, "Analysis of impulse noise mitigation techniques for digital television systems," in *8th Int. OFDM Workshop*, Hamburg, Germany, Sept. 2003, pp. 172–176.

[5] O. P. Haffenden and et al., "Detection and removal of clipping in multicarrier receivers," European patent application EP1 043 874, Oct. 11, 2000, published in Bulletin 2000/41.

[6] N. P. Cowley, A. Payne, and M. Dawkins, "COFDM tuner with impulse noise reduction," European patent application EP1 180 851, Feb. 20, 2002, published in Bulletin 2002/08.

[7] V. N. Papilaya and A. J. H. Vinck, "Investigation on a new combined impulsive noise mitigation scheme for OFDM transmission," in *17th IEEE International Symposium on Power Line Communications and Its Applications (ISPLC)*, Johannesburg, South Africa, Mar. 24–27, 2013, pp. 86–91.

[8] S. Zhidkov, "Analysis and comparison of several simple impulsive noise mitigation schemes for OFDM receivers," *IEEE Transactions on Communications*, vol. 56, no. 1, pp. 5–9, 2008.

[9] N. Pavlidou, A. J. H. Vinck, J. Yazdani, and B. Honary, "Power line communications: state of the art and future trends," *Communications Magazine, IEEE*, vol. 41, no. 4, pp. 34–40, 2003.

[10] A. Mengi, "On combined coding and modulation," Ph.D. dissertation, Institute for Experimental Mathematics of Duisburg-Essen University, Essen, Germany, May 2010.

[11] M. Hoch, "Comparison of PLC G3 and prime," in *15th IEEE International Symposium on Power Line Communications and Its Applications (ISPLC)*, Udine, Italy, Apr. 3–6, 2011, pp. 165–169.

[12] Y.-H. Kim, K.-H. Kim, H.-M. Oh, K.-H. Kim, and S.-C. Kim, "Mitigation of effect of impulsive noise for OFDM systems over power line channels," in *IEEE International Symposium on Power Line Communications and Its Applications (ISPLC)*, Jeju city, Jeju Island, Apr. 2–4, 2008, pp. 386–390.

[13] H.-M. Oh, Y.-J. Park, S. Choi, J.-J. Lee, and K.-C. Whang, "Mitigation of performance degradation by impulsive noise in LDPC coded OFDM system," in *IEEE International Symposium on Power Line Communications and Its Applications (ISPLC)*, Orlando Florida, USA, Mar. 26–29, 2006, pp. 331–336.

[14] H. C. Ferreira, L. Lampe, J. Newbury, and E. T. G. Swart, *Power Line Communications: Theory and Applications for Narrowband and Broadband Communications Over Power Lines*. Chichester, England: John Wiley and Sons, 2010.

[15] C. Snow, L. Lampe, and R. Schober, "Error rate analysis for coded multicarrier systems over quasi-static fading channels," *IEEE Transactions on Communications*, vol. 55, no. 9, pp. 1736–1746, 2007.

[16] S. Haykin, *Communication Systems 4th ed.* New York: John Wiley and Sons, 2001.

[17] B. Sklaar, *Digital Communications: Fundamentals and Applications*. Englewood Cliffs, New Jersey: Simon and Schuster, 1988.

[18] D. Galda and H. Rohling, "Narrow band interference reduction in OFDM-based power line communication systems," in *IEEE Int. Symp. on Power Line Commun. and its Appl. (ISPLC)*, Malmo, Sweden, Apr. 4–6, 2001, pp. 345–351.

[19] R. Nilsson, F. Sjoberg, and J. LeBlanc, "A rank-reduced LMMSE canceller for narrowband interference suppression in OFDM-based systems," *IEEE Transactions on Communications*, vol. 51, no. 12, pp. 2126–2140, 2003.

[20] A. Coulson, "Bit error rate performance of OFDM in narrowband interference with excision filtering," *IEEE Transactions on Wireless Communications*, vol. 5, no. 9, pp. 2484–2492, 2006.

[21] D. Middleton, "Canonical and quasi-canonical probability models of class A interference," *IEEE Transactions on Electromagnetic Compatibility*, vol. EMC-25, no. 2, pp. 76–106, 1983.

[22] J. Haering and A. J. H. Vinck, "OFDM transmission corrupted by impulsive noise," in *Proc. of IEEE Int. Symp. on Power Line Commun. and its Appl. (ISPLC)*, Limeric, Ireland, Apr. 2000, pp. 9–14.

[23] D.-F. Tseng, R.-B. Yang, T.-R. Tsai, Y. Han, and W.-H. Mow, "Efficient clipping for broadband power line systems in impulsive noise environment," in *16th IEEE International Symposium on Power Line Communications and Its Applications (ISPLC)*, Beijing, China, Mar. 27–30, 2012, pp. 362–367.

[24] C. W. Helstrom, *Probability and stochastic processes for engineers (2nd edition)*. New York, USA: Macmillan, 1991.

[25] A. J. H. Vinck, *Coding concepts and Reed-Solomon Codes*. Essen, Germany: Institute for Experimental Mathematics, Duisburg-Essen University, 2013.

[26] E. Alsusa and K. Rabie, "Dynamic peak-based threshold estimation method for mitigating impulsive noise in power-line communication systems," *IEEE Transactions on Power Delivery*, vol. 28, no. 4, pp. 2201–2208, 2013.

[27] J. Lin, M. Nassar, and B. Evans, "Impulsive noise mitigation in powerline communications using sparse bayesian learning," *IEEE Journal on Selected Areas in Communications*, vol. 31, no. 7, pp. 1172–1183, 2013.

[28] E. Biglieri, "Coding and modulation for a horrible channel," *Communications Magazine, IEEE*, vol. 41, no. 5, pp. 92–98, 2003.

[29] ITU-T G.9903, *Narrowband orthogonal frequency division multiplexing power line communication transceivers for G3-PLC networks*, 10/2012.

[30] O. Hooijen, "On the relation between network-topology and power line signal attenuation," in *International Symposium on Power Line Communications and Its Applications (ISPLC)*, Tokyo, Japan, Mar. 1998, pp. 45–55.

[31] D. Murray, T. Koziniec, K. Lee, and M. Dixon, "Large MTUs and internet performance," in *13th IEEE Int. Conf. on High Performance Switching and Routing*, Belgrade, Serbia, Jun. 2012, pp. 82–87.

[32] B. Latre, P. D. Mil, I. Moermana, B. Dhoedt, and P. Demeester, "Throughput and delay analysis of unslotted IEEE 802.15.4," *Journal of networks*, vol. 1, no. 1, pp. 20–28, May 2006.